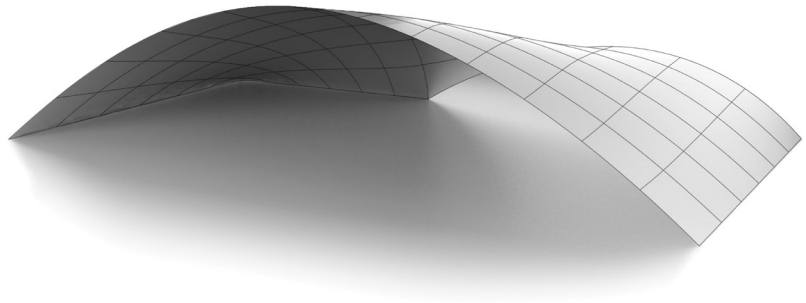




LUND
UNIVERSITY



NUMERICAL METHODS FOR CONCEPTUAL STRUCTURAL DESIGN

VEDAD ALIC

Structural
Mechanics

Licentiate Dissertation

DEPARTMENT OF CONSTRUCTION SCIENCES

DIVISION OF STRUCTURAL MECHANICS

ISRN LUTVDG/TVSM--16/3075--SE (1-107) | ISSN 0281-6679

ISBN 978-91-7623-733-5 (print) | 978-91-7623-734-2 (Pdf)

LICENTIATE DISSERTATION

NUMERICAL METHODS FOR CONCEPTUAL STRUCTURAL DESIGN

VEDAD ALIC

Copyright © 2016 Division of Structural Mechanics
Faculty of Engineering LTH, Lund University, Sweden.

Printed by Media-Tryck LU, Lund, Sweden, April 2016 (*Pl*).

For information, address:

Div. of Structural Mechanics,
Faculty of Engineering LTH, Lund University, Box 118, SE-221 00 Lund, Sweden.

Homepage: www.byggmek.lth.se

Acknowledgements

The work presented in this thesis was done at the Division of Structural Mechanics, Faculty of Engineering at Lund University, Sweden. During the work, Prof. Kent Persson acted as my main supervisor, and Prof. Karl-Gunnar Olsson as my co-supervisor. The financial support was provided by the Swedish strategic research programme eSSSENCE. The support is gratefully acknowledged.

I would like to thank my supervisors, Prof. Kent Persson and Prof. Karl-Gunnar Olsson, without whose support the work would not have been possible. Furthermore, thanks to Prof. Erik Serrano for providing some last-minute feedback. I owe my gratitude to the staff of Construction Sciences for some the friendly discussions, a pleasant work environment, and some nice games of ping pong. Thanks to Mr. Bo Zadig for helping with the design of some graphics for the dissertation.

Finally, I would like to thank my family for their endless support.

Lund, April 2016
Vedad Alic

Abstract

Conceptual design is the first phase in the design process in which all the requirements and design objectives are synthesized into conceptual alternatives. In practice today, major decisions regarding the buildings geometry, massing, and overall form are usually made during the first phase. Considering structural performance requirements during conceptual design enhances interdisciplinary interaction, and creates a visual link between form and numeric performance evaluations, reducing work on poorly performing solutions. To include structural performance in conceptual design requires, amongst other things, the availability of tools such as simulation software, suitable for conceptual studies.

The aim of the research is to develop new efficient methods and procedures for supporting an interactive and iterative design process that includes engineering aspects. By integrating engineering knowledge and physical aspects in the developed tools, a more efficient and better-adapted design process can be obtained. Modeling tools for conceptual studies should encourage creativity and be capable of interactively modifying the model in a sketch-like fashion once it has been created. Supporting an interactive and iterative design process, requires new interaction models and numerical approaches in the tools used.

The research has focused on two different areas, where the first is related to conceptual studies for reducing ground borne wave propagations in an urban scale. A tool is developed for simulating forms with masses placed on top of soil in an urban scale and studying the resulting effect that the forms have on the propagating waves. The tool uses the finite element method and studies the vibration reduction effects in the frequency domain. Paper A presents the tool and draws some conclusions related to the levels of vibration reduction for various patterns, showing that some patterns are effective in mitigating the incoming vibrations. The approach in the tool makes it possible to obtain results in minutes, allowing the user to generate many alternative proposals quickly, and act as an aid in brainstorming sessions.

Papers B and C focus on a recent extension of the finite element method, called isogeometric analysis. The implementation of isogeometric analysis with membrane elements for form finding of efficient shapes for shells is presented. The dynamic relaxation method is used for finding the static solutions. The method is employed directly on design geometry, which is described by non-uniform rational b-splines (NURBS), without the need for any further discretization. Paper B investigates various selections of mass and damping for the dynamic relaxation method with NURBS based membrane elements. The results are used to implement two plug-ins for the computer aided design applications Rhinoceros 3D and Grasshopper 3D, of which the former is presented in paper C. The method describes form found geometries well with very few elements and can be used to explore different efficient shapes for shells very rapidly and directly in design software, and is thus suited for design explorations.

Populärvetenskaplig sammanfattning

Samarbetet mellan ingenjörer och arkitekter förbättras av nya beräkningsmetoder som förenklar stegen från utformning till strukturanalys – vilket leder till bättre design av samhällets byggnader och strukturer.

I byggprocessen handskas arkitekter och ingenjörer med komplexa problem, speciellt vid projektets start råder det många obesvarade frågor. Formgivandet av en ny byggnad brukar börja med att det ges som uppdrag till en grupp bestående av bl.a. ingenjörer och arkitekter som behöver besvara en stor mängd frågeställningar som: Vad byggnaden ska användas till? Var byggnaden ska stå? Hur många människor ska få plats? Krävs det stora spännvidder? Hur är budgeten?

För att lösa alla dessa problem påbörjas en process att börja formge. Genom denna process tydliggörs vilka mål och frågeställningar som är viktiga, och vilka som kan försummas. De första skedena i formgivningsprocessen utförs oftast av arkitekter som koncentrerar sig på byggnadens geometri och övergripande form. Beträktandet av prestandaaspekter som struktur, akustik, och energi brukar senareläggas vilket kan leda till svårigheter när olika konsulter blandas in och resultera i byggnader som inte når upp till sin fulla potential. Detta projekt inriktar sig på utvecklandet av metoder och verktyg riktade till ingenjörer som är involverade i dessa tidiga skeden av formgivningsprocessen. Verktygen ska stödja ett kreativt och interaktivt arbete med nya former och strukturer som ger effektiv prestanda.

Forskningen har behandlat två olika områden. Det första har handlat om att studera möjligheten att placera byggnader mellan tungt trafikerade vägar och vibrationskänsliga anläggningar, för att reducera mängden vibrationer vid anläggningen. För att möjliggöra studien har ett skissverktyg utvecklats där det är möjligt att skissa ut byggnader i form av massor, och studera deras effekt på vibrationers fortplantning i marken. Genom att ha ett enkelt skissverktyg underlättas möjligheterna till att utforma bra stadsplaner som även förbättrar miljön för existerande byggnader runtomkring.

I den andra delen har kombinationen av en ny beräkningsmetod (isogeometrisk analys) med befintliga beräkningstekniker för att hitta effektiva former för strukturer med stora spännvidder studerats. En sådan teknik är simuleringen av hängande modeller. Hängande modeller användes av bland annat Antoni Gaudí när han designade La Sagrada Família i Barcelona. Kombinationen av metoder möjliggör ett interaktivt utforskande av effektiva former för skalstrukturer och valv med stora spännvidder. Den nya beräkningsmetoden gör det möjligt att utföra en simulering direkt på en geometri som är ritad i ett datorprogram. Tidigare metoder har inneburit ett tidskrävande arbete med att konvertera arkitektens ritningar till en beräkningsmodell. Genom att reducera detta tidskrävande steg kan ingenjörer istället fokusera på utformning och analys. Ingenjörens återkoppling till arkitekten kan ske i ett interaktivt samtal, vilket leder till byggnader där strukturella och arkitektoniska intentioner är sammankopplade.

Contents

I	Introduction and overview	xiii
1	Introduction	1
1.1	Aims and objectives	2
1.2	Main contributions from the thesis	2
1.3	Disposition	3
2	Overview	5
2.1	Conceptual design	5
2.1.1	Conceptual design stages	6
2.2	Considering structural performance in conceptual design	6
2.3	Computational tools for conceptual structural design	8
2.4	Computer aided geometric design	8
2.5	Computer aided engineering	10
2.6	Existing computational tools for conceptual structural design	11
2.6.1	Rapid feedback tools	11
2.6.2	Integrated analysis tools in CAGD software	13
2.6.3	Structural optimization	14
2.6.4	Graphical methods	14
2.6.5	Classical form finding	16
2.7	Conclusions and present research	18
3	Theory	21
3.1	Geometric preliminaries	21
3.1.1	B-splines	21
3.1.2	Derivates of B-splines	23
3.1.3	NURBS	24
3.1.4	Special cases of NURBS	24
3.2	The finite element method	25
3.3	NURBS based isogeometric analysis	25
3.3.1	The isoparametric and isogeometric concepts	26
3.3.2	NURBS elements	26
3.3.3	Refinement	26
3.4	Elasticity	27
3.4.1	Strong form of elasticity	28

3.4.2	Weak form and virtual work	28
3.4.3	Linear elasticity	29
3.5	Structural dynamics	29
3.5.1	Steady state dynamics	30
3.5.2	Dynamic model reduction with damping	30
3.5.3	Multi-level sub-structuring	31
3.6	Kirchhoff-Love shell and membrane theory	32
3.6.1	Geometry of curved surfaces and bodies	32
3.6.2	Mechanics	34
3.6.3	Membrane part	35
3.6.4	Finite element implementation	36
3.6.5	The linear elastic NURBS based Kirchhoff-Love shell	38
3.7	Dynamic relaxation	38
4	Applications of form finding	41
4.1	Forms for vibration reduction in an urban scale	41
4.1.1	Max IV	41
4.1.2	Problem statement	42
4.1.3	Earlier studies	42
4.1.4	Computational model	43
4.1.5	Examples	47
4.2	IGA form finding plug-ins	49
4.2.1	Shell structures - context	49
4.2.2	Plug-ins	50
4.2.3	Rhinoceros 3D plug-in	51
4.2.4	Grasshopper 3D plug-in	52
4.2.5	Simple example	53
4.2.6	Multi-patch examples	55
5	Conclusions	57
5.1	Further research	58
6	Summary of appended papers and programs	59
6.1	Appended papers	59
6.2	Developed demonstrator programs	60
	References	61
II	Appended publications	67

Paper A

Form Finding for Ground Vibration Reduction in an Urban Scale.

Vedad Alic and Kent Persson.

Proceedings of IASS-SLTE Symposium 2014: Shells, Membranes and Spatial Structures: Footprints

Paper B

Form Finding with Dynamic Relaxation and Isogeometric Membrane Elements.

Vedad Alic and Kent Persson.

Published in: Computer Methods in Applied Mechanics and Engineering.

doi:10.1016/j.cma.2015.12.009

Paper C

Using isogeometric elements and dynamic relaxation as a form finding technique.

Vedad Alic and Kent Persson.

Proceedings of IASS 2015 Amsterdam Symposium: Future Visions.

Part I

Introduction and overview

1 Introduction

Conceptual design is the first phase in the design process in which all the requirements and design objectives are synthesized into conceptual alternatives. In practice today, major decisions regarding the buildings geometry, massing and overall form are usually made during the first phase. Considering structural performance requirements during conceptual design enhances interdisciplinary interaction and creates a visual link between form and numeric performance evaluations, reducing work on poorly performing solutions.

In most buildings and facilities there are physics and engineering related demands that must be addressed, such as, strength, room acoustics, vibrations, etc. By considering such demands already in conceptual design, better performing and more intriguing buildings can be constructed. The opposite also holds, if only the engineering aspects are focused upon, functional and aesthetical design requirements may not be fulfilled. To include such demands in conceptual design requires close collaboration and communication between architects and experts in different fields as well as the availability of tools such as simulation software, suitable for conceptual studies to support this communication.

Traditionally, structural engineers participating in conceptual design normally have to make analysis based on architect sketches, relying on their long professional experience and hand calculations of simplified equivalent structures to facilitate input and feedback to the architects. Standard finite element analysis (FEA), which is commonly used by engineers at construction companies, requires detailed models of the geometry, long computational times and produce results of a very high precision. However, in conceptual design only qualitative calculations are needed whereas detailed quantitative calculations are only required at the final design stages.

This thesis is about the development of methods and tools for including structural considerations in the conceptual design of the built environment. Modelling tools for conceptual studies must encourage creativity and be capable of interactively modifying the model in a sketch-like fashion once it has been created. This is a fundamental aspect in any design activity, where the designer is constantly going forward and backwards, re-elaborating over some particular aspect of the model, its general layout, or even coming back to a previous solution that had been temporarily abandoned. Supporting an interactive and iterative design process, requires new interaction models and numerical approaches in the tools used.

1.1 AIMS AND OBJECTIVES

The aim of the research is to improve the conceptual design process by including engineering aspects and supporting an interactive and iterative workflow by development of new efficient methods and procedures. Improving the conceptual design process allows designers to explore design alternatives and increases the chances of creating well performing buildings and environments.

In the long-term, the outcome will result in new developed methods and tools that improve the conceptual design process and collaboration between architects and engineers. This enables reduced environmental and construction cost, creates inherent safety in the structures and makes integration of the aesthetic and technical goals possible. Another result by using this integrated approach is that engineers, designers and architects will have a greater awareness and understanding of how engineering and physical aspects affect the design process and how these are expressed in structures.

The objectives presented in this thesis include the following activities:

- Literature studies of methods and tools suitable for conceptual structural design are performed. Possible directions for the research are identified.
- Numerical methods that meet the objectives stated in the literature review are developed.
- Implementation of developed methods in demonstration programs.

1.2 MAIN CONTRIBUTIONS FROM THE THESIS

Most tools for conceptual structural design deal with considerations of statics. The phenomena that the tools consider could be broadened. One of the tools presented here is related to

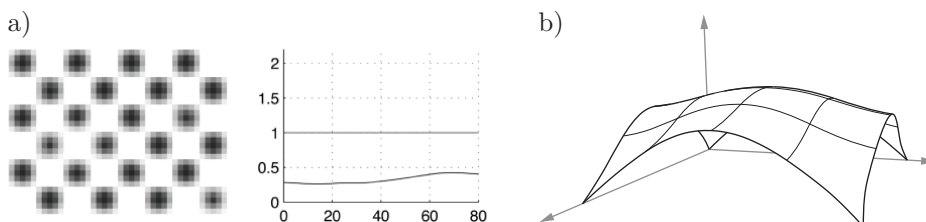


Figure 1.1: The contributions of the thesis are related to two different parts. a) Wave propagation tool for conceptual studies. b) Form finding using Non-Uniform Rational B-Splines (NURBS) elements.

conceptual studies of ground borne wave propagations in an urban scale, where the tool can be used to study the effect of placing forms with masses in an urban scale on top of soil and the resulting effect that the forms have on the propagating waves, see Fig 1.1 a). Such computations require powerful computers and are time consuming. However, the approach in the tool makes it possible to obtain results in minutes, allowing the user to generate many alternative proposals quickly and act as an aid in brain-storming sessions. Moreover, tools such as this could be used as an aid in studying the effects of vibration from road and rail traffic in the densification of cities. The main contributions from this part of the research are:

- A tool for studying vibration reduction by arrangement of masses is developed.
- The vibration reduction effects of masses on soil are shown.
- It is shown that various patterns lead to various levels of reduction, and in some cases amplification.

An other part of the research is related to a recent extension of the finite element method (FEM), isogeometric analysis (IGA), see Fig. 1.1 b). IGA allows for performing finite element analysis directly on a CAD geometry. It is used here with a dynamic relaxation solution technique in a form finding procedure. The thesis applies this to develop form finding plug-ins for Rhinoceros [1] and for Grasshopper [2]. The method allows for exploration of efficient forms for shells under gravity loads to be performed directly within the design application with the design geometry, in or near real-time. The approach allows the user to work seamlessly with design and analysis. The main contributions from this part of the research are:

- Demonstrator tools for form finding with IGA are developed.
- The implementation of NURBS based IGA membrane elements with the dynamic relaxation solver is presented.
- The advantages of using NURBS based IGA rather than classical finite elements for form finding are shown.

1.3 DISPOSITION

The thesis is ordered in the following manner:

- **Chapter 1** gives the introduction to the licentiate thesis. It briefly covers the need for considering structural aspects in the conceptual design of buildings, and presents the main contributions from the thesis.

- **Chapter 2** contains a review of literature related to the design process, and a review of existing tools and methods related to conceptual structural design. It ends with the statement of some identified research objectives.
- **Chapter 3** lists the relevant theories used in the appended papers. This covers Computer Aided Geometric Design (CAGD) technologies, such as B-splines and NURBS. Further it covers theories from computational mechanics, such as the Finite Element Method, Isogeometric Analysis, structural dynamics and wave propagation.
- **Chapter 4** contains examples of the developed software. The wave propagation tool is shown in a brief example, and the two Rhinoceros 3D plug-ins are presented.
- **Chapter 5** concludes the thesis.
- **Chapter 6** summarises the appended papers.
- **Paper A** investigates the search of forms in an urban scale that are effective in reducing vibration propagation from external sources, such as highways, high-speed rail-roads and industrial plants, and describes the related tool.
- **Paper B** describes a form finding techniques using isogeometric membrane elements together with dynamic relaxation.
- **Paper C** describes the implementation of the Rhinoceros 3D plug-in, and possible work-flows using isogeometric membranes for form finding.

2 Overview

In this chapter a review of the need for including structural considerations in conceptual design, and the methods and computer tools available for conceptual structural design, are presented. However, first computer tools commonly used for the design of buildings are briefly described, since most tools for conceptual design are related to them. These fall into two categories, the first is often called Computer Aided Design (CAD), however, since CAD can encompass more than just geometry they are here narrowed to Computer Aided Geometric Design (CAGD). The second category is Computer Aided Engineering (CAE).

2.1 CONCEPTUAL DESIGN

The building design process is divided into several phases, of which the first one is the conceptual design phase. The conceptual design phase is characterized by an ambiguity of design

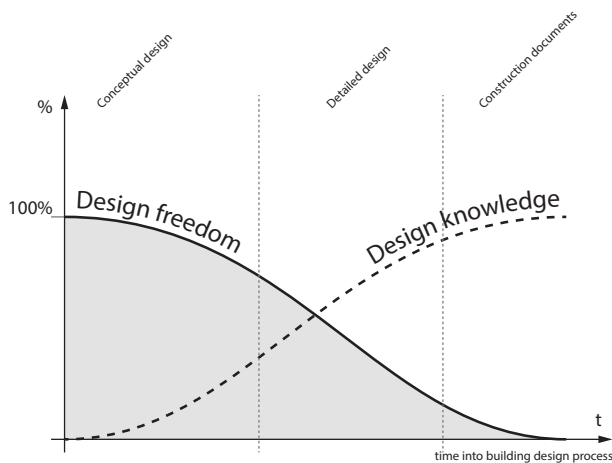


Figure 2.1: Illustration of the design freedom and design knowledge vs. time into design process.

constraints and requirements and a creative work where several alternative variations of a design based on the initial requirements are quickly generated [3]. The process is often creative and iterative. Conceptual design is the most important phase of a design process [4, 5], where the amount of design freedom and impact of design decisions is very high, illustrated in Fig. 2.1. According to [4] it has been estimated that about 75% of the final product cost is accounted for by design decisions.

The earlier stages are generally performed by the architecture team alone, without the expertise of the engineers. The architecture team focuses on the buildings geometry, massing and overall form [6], while postponing the buildings performance aspects, such as structure, acoustics, and energy, to later stages. Engineers are often omitted from the stage where it is most possible to affect the structural performance [7].

2.1.1 Conceptual design stages

The conceptual design phase can be divided into two stages. In the first stage the clients' requirements are mapped to functional specifications [5]. The second stage is where a design team creates alternative solutions which fulfil the specifications, see Fig. 2.2.

The developed tools and methods presented in this thesis, are intended for the later stage of conceptual design after some specifications have been set (the type of structure, or some requirements which are important to consider), see Fig. 2.2.

2.2 CONSIDERING STRUCTURAL PERFORMANCE IN CONCEPTUAL DESIGN

There are several reasons for why it is important to include structural performance considerations early on in the conceptual design stage. The overall form and member topology are generally already determined during conceptual design. Form and member topology are the two most important aspects of structural performance [8]. If their effects on the building as a structure have not been considered it can lead to wasteful and poorly performing solutions, where structural engineers need to make poor design work. If the form of the building is innovative, it can be difficult to realise with a conventional structural system, and a challenging task for the structural engineers to understand the structural behaviour. Results can be wasteful, expensive, and maintenance-intensive, and it can ultimately lead to poor design and even collapse, for example see [8, 9].

However, if the structural design is considered from the beginning of the project, the work load on the structural engineering team is reduced. Structures whose conceptual design is well thought out early in the project, with ideas of load paths and overall structural behaviour included from the start are often easier to deal with in the detailed design and analysis stages

[10]. Moreover, the range of solutions is much larger as no constraints have been set yet, and there are opportunities for better performing solutions, and on occasion, solutions whose quantifiable aspects are integrated into the design.

Well performing structures require less use of material, lead to savings in cost, consume fewer resources, are more sustainable, safer, are more durable and easier to build [8]. For instance, during times when resources were scarce, engineers such as Robert Maillart, Félix Candela, Eladio Dieste and Pier Luigi Nervi were able to win competitions by developing the most cost-effective structures through considerations of good structural form [11].

The consideration of form early on in a design process makes it more likely that the architectural intentions of the project will be realized, since the risk of requiring changes to the design due to structural considerations in later stages are reduced. Early structural considerations can lead to an increased architectural variety. It can also lead to buildings where the aesthetic and technical considerations are in harmony.

In conclusion, considering only parts of the design requirements during conceptual design limits the success of the whole design process and the final proposal. Enlarging the set of requirements assessed at an early stage, enhances interdisciplinary interaction, and creates designs whose performance aspects have greater chances of success. To include engineering related aspects in early-stage design requires close collaboration and communication between architects and experts in different fields of engineering, as well as the availability of tools, such as simulation software suitable for conceptual studies and design.

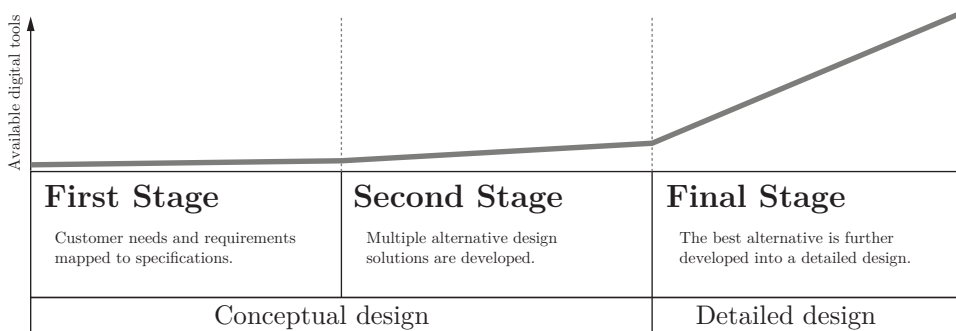


Figure 2.2: Availability of design tools in different design stages [5].

2.3 COMPUTATIONAL TOOLS FOR CONCEPTUAL STRUCTURAL DESIGN

The use of computer tools has become widespread in engineering and in architecture. Fig. 2.2 is an illustration of the available digital tools for the different stages of the design process [5]. Software tools for making design decisions have been developed, however, most of the software available today are applicable to detailed design phases [4, 5]. Poor choices made in the conceptual design phase are difficult to compensate for in the detailed design phase, yet there have been very few computer-tools developed for the conceptual design phase. Partly since the amount of knowledge available in the early phases of a design is limited [4], and early stage design often includes rapid changes in design direction. These factors make it difficult to use computer based tools which often require precise information that is time-consuming to input into the computer.

In [8] an argument is made that current availability of computational tools reflect and strengthen the separation of formal design from structural behaviour, with architectural tools focusing on geometry, independent of performance, and structural tools focusing on analysis of an already established geometry.

However, the time available to create a design proposal is getting increasingly shorter due to increased financial pressure while projects are in general increasing in complexity. In the later design stages computers help produce results faster and manage the complexity better. Developing computer tools for the early design process can help in making better, more informed decisions that include more aspects in the early design, and streamline the later stages of detailed design process. The use of computational tools also has the advantage of being able to store, re-use and share the generated design knowledge, and potentially apply it to other projects.

2.4 COMPUTER AIDED GEOMETRIC DESIGN

Computer Aided Geometric Design (CAGD) tools are used for developing designs, drafting, documentation, and communication of for instance a proposed design or construction documents. One of the first computer tools in the area of CAGD was Sketchpad 1963 [12]. The ancestor to CAGD pioneered the way of human-computer interaction, graphics user interfaces and computer graphics.

In the beginning commercial CAGD tools were used for documentation of designs by use of 2D drafting, and have since been developed to capable 3D software. CAGD tools used in the built environment are categorized as follows:

- Drafting tools: 2D drafting, 3D drafting
- Building information modelling (BIM)
- Design computation

It was simple to introduce 2D drafting into existing design processes as it simply continued the practice of representing buildings as multiple 2D drawings [13]. Some believe that it delayed the use of 3D tools even though they were available [13].

The foundations of BIM were established in the 80s [13]. BIM represents a design as an assembly of objects. BIM workflow forces one to define or use pre-defined objects before the overall form. The object approach limits itself to later stages since it requires detailed information which is missing in the conceptual design. BIM is often criticized for being easy to create the obvious (using common objects) but difficult when one needs to deviate and create design innovations. BIM has good support for collaboration, multiple disciplines can work in a common model.

If drafting and BIM are the first two eras of building related CAGD then design computation is the third (although their developments overlap each other). According to [13] some objectives of design computation are to overcome limitations of BIM (the ability to define own objects and inter-object behaviours) and to move away from manual modelling. In design computation the designer is no longer directly modelling the building: instead time is spent developing a graph or script whose execution generates the model. An apparently minor edit to the graph or script could have a large effect on the generated building, enabling the exploration of a vast array of alternatives. Recently the visual programming environment Grasshopper [2] for the CAGD program Rhinoceros [1] is such a tool that has become very popular, see Fig. 2.3. In Grasshopper the user creates parametric models by connecting consecutive components (creating a graph) which operate on geometry in Rhino. A similar tool to Grasshopper is Autodesk Dynamo [14].

Apart from the mentioned three general categories there are other CAGD tools available. Solid modellers are common as design tools in other industries, but are a rare occurrence in building design, but have occasionally been used, e.g. solid modelling in Digital Project originally developed by Gehry Technologies. General graphics suites (which are also a part of CAGD, but are more of use for visual effects in movies and games, and rely on other technologies) e.g. Maya have been used as conceptual sculpting tools at some architectural studios (e.g. Zaha Hadid Architects) since they are well suited for free form modelling.

CAGD tools are well developed and successfully used in early design stages to explore geometric alternatives. However, they are often limited to geometric considerations and do not consider structure or other performance based aspects of buildings.

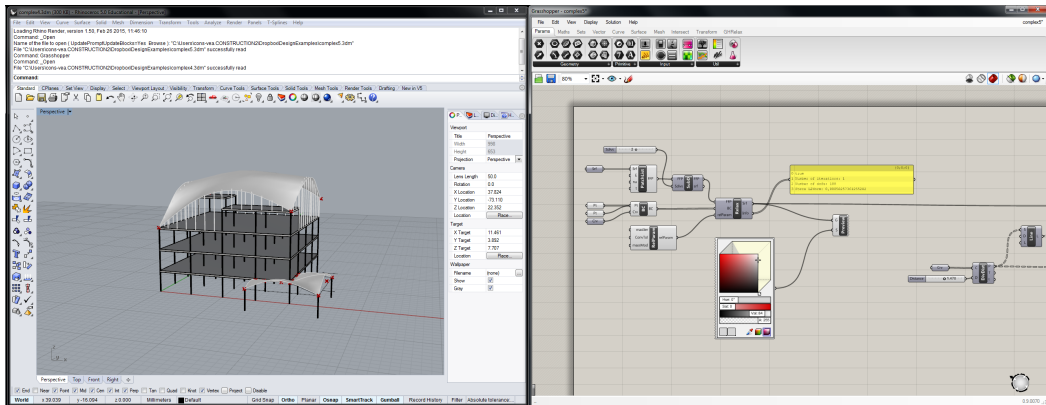


Figure 2.3: The GUI of Rhinoceros V.5 (left) and Grasshopper V.0.9 (right).

2.5 COMPUTER AIDED ENGINEERING

Software tools that support engineering tasks are termed CAE, and include finite element analysis (FEA), computational fluid dynamics (CFD), multi-body dynamics (MBD) and optimization. In this thesis, the finite element method (FEM) is used.

FEM is a technique to find approximate solutions to boundary value problems (BVPs), i.e. a set of differential equations with additional boundary conditions which are known *a priori*. It is applicable to many fields of engineering, physics and mathematics, since many of the underlying physical problems may be expressed as differential equations.

Finite element programs offer capabilities to get a detailed analysis of a structure, including stresses and displacements, but also nonlinear effects such as plasticity, fracture, and buckling. Although being very powerful and able to handle complex geometries, finite element programs require the definition of a pre-set geometry, selected materials, application of forces and defined support conditions in order to provide a solution. The amount of information required for a typical finite element program limits their use in conceptual design. Further, traditional FEM tools produce results with very high precision, however, in conceptual simulations only qualitative results are required. Attempts have been made to adapt the FEM to conceptual structural design, some of these are part of the literature review in the following section.

A promising recent development of finite element analysis is isogeometric analysis [15], where basis functions from CAGD (e.g. b-splines, NURBS, subdivision surfaces) are used instead of the standard Lagrange polynomial basis functions for the finite element approximations. Using the same geometry for both FEM and CAGD makes it easier to use in an iterative process. Isogeometric analysis is covered in the theory part of this thesis.

2.6 EXISTING COMPUTATIONAL TOOLS FOR CONCEPTUAL STRUCTURAL DESIGN

Research of conceptual structural design tools is an emerging field where researchers have taken several different directions, the literature review in the following chapter and [8, 16] give a brief overview. Although there has been some research done, there is a need for development of methods and tools to be used in conceptual structural design.

In [8], two categories of conceptual structural design tools are identified; feedback tools and guidance tools. Feedback tools use existing analysis and verification methods but rely on real-time or near real-time structural analysis integrated into design tools in an interactive experience. The aim is to provide rapid feedback about the structural performance in order to aid in exploring different structural solutions for the design. Guidance tools use optimization techniques in order to suggest new design alternatives based on structural performance. Both types of tools are limited by the performance of the computer, and they have been implemented both in research and in production environments, some of which are covered in this review.

Tools have different approaches for their type of aid in conceptual structural design and are divided into the following types:

- Real time or rapid feedback numerical tools
- Integrated numerical analysis for CAGD tools
- Structural optimization tools
- Graphical methods and tools
- Form finding tools

Some of the tools from the categories are reviewed below. Note that some of the tools may be classified as belonging to more than one category.

2.6.1 Rapid feedback tools

The advantage of rapid feedback numerical tools is that results can be pruced very quickly. Several tools of this type based on the finite element method have been developed at the Division of Structural Mechanics, Lund University. These are ForcePAD [17], ObjectiveFrame [18], and Sketch a Frame [19]. Finite element based rapid feedback tools are adapted to conceptual design by removing time consuming aspects such as precise geometry, material specification, and meshing. The approach doesn't necessarily provide results of high precision, but gives insight and allows for qualitative studies of structural behaviour.

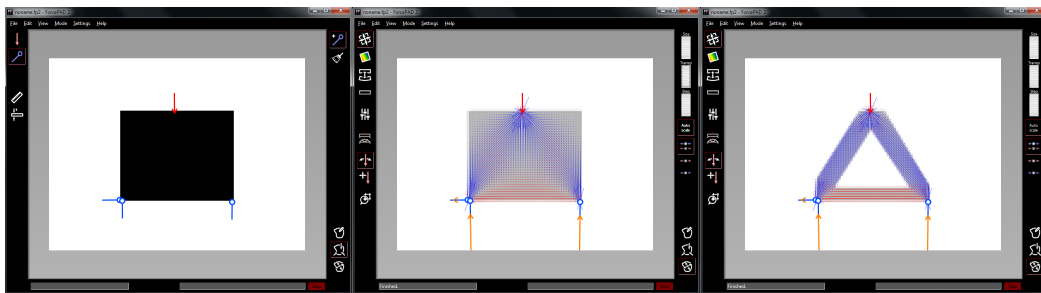


Figure 2.4: The GUI of ForcePAD showing a simply supported block: (left) Physics mode, (middle) Action mode showing the principal stresses, blue is compression and red is tension, (right) Action mode with modified structure, where low stress parts are removed, resulting in a truss.

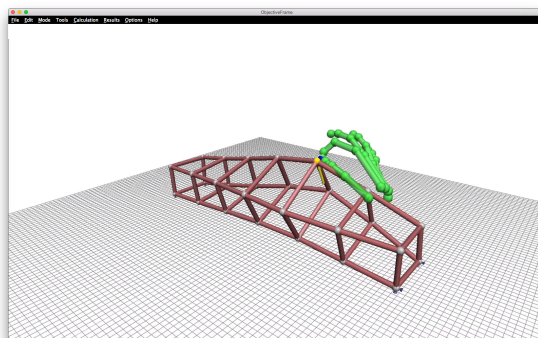


Figure 2.5: The GUI of ObjectiveFrame, showing a deformed model and the hand input.

The key idea behind ForcePAD is that it employs metaphors similar to those of image editing applications. In the application one paints a structure where the stiffness of different parts is controlled by the grayscale, where white is no stiffness, and black is maximal stiffness. The method allows for quick sketching of structures and to make changes to them.

ObjectiveFrame provides real time deformation feedback of loads applied to frame structures, as an idea to imitate the learning of structures through physical models. There has been some recent development of ObjectiveFrame by use of the Leap Motion controller, which allows the user to interact with structural models by using their hands to apply forces, see Fig. 2.5.

Sketch a Frame is a tablet computer application for conceptual design of trusses and frames, developed for use on the iPad. It allows the user to directly manipulate structures and loads through a multi-touch interface. Providing real time feedback it allows for exploration of form. See Fig. 2.6 for an example. The tool is able to show normalized static redundancy factors,

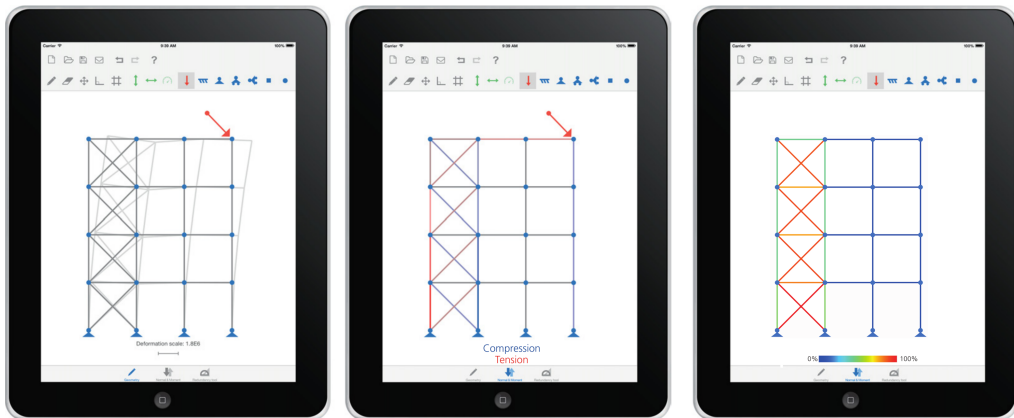


Figure 2.6: The GUI of Sketch a Frame, showing (left to right) deformation, normal forces, and normalized static redundancy factors.

allowing the user to identify members that can be removed from a statically indeterminate structure.

Other academic and commercial applications of real time numerical tools have also been developed, such as the Model-Alive feature of SAP2000 [20], Force Effect [21], PointSketch2D [22], and Dr. Frame 3D.

The real time capabilities of these tools are limited by the computational power available. This limits the complexity of the structures if they are to be analysed in real time.

2.6.2 Integrated analysis tools in CAGD software

Recently, a number of tools have been developed with the intention to include structural considerations into CAGD software. Their approach is to integrate structural analysis modules into CAD software and allow for a smooth workflow, allowing the user to make changes to a design and immediately perform an analysis. Through iterations, it becomes apparent how design changes affect the performance. The tools can make analysis directly for the available geometry in the main software, however, additional discretizations of the geometry is necessary after changes in the geometry, before the numerical analysis is performed. It is not always possible to automate the discretization, and the design geometry can have many details that are unnecessary in the analysis and may make it time consuming. The tools are often limited to a single CAD application, or a combination of a CAD and FE-program.

Some popular examples of such tools are Geometry Gym for Rhinoceros (Mirtschin, 2011), Karamba [23] for Rhinoceros, Kangaroo Physics [24] for Rhinoceros and Robot [25] for Revit. Karamba provides the ability to set up structural models in the visual programming en-

vironment (also called parametric environment) Grasshopper for Rhino. Geometry Gym also interacts with Grasshopper and connects the parametric models to popular BIM or structural analysis software.

2.6.3 Structural optimization

Optimization in structural design combines techniques from CAGD (model description), non-linear mathematical programming (the optimization), and computational mechanics (the structural response) [26]. The methods optimize some objective function f (for instance the weight, stiffness, or strain energy) with respect to some design variables \mathbf{x} (i.e. geometry parameters). Normally constraints and variable bounds on \mathbf{x} need to be satisfied as well.

There are three common types of structural optimization: size optimization, shape optimization and topology optimization. Optimization tools are able to change the geometry to better suit the objective, and can act as guidance tools by suggesting geometry changes.

For shape optimization problems the state of the art approach is to describe the geometry and design variables using NURBS patches. This is done to avoid mesh distortion which is common if the coordinates of the finite element nodes are used as design variables directly [26]. Further, by using NURBS patches there is an advantage that the number of design variables are reduced.

Traditional optimization has the limitation that it converges to one optimal solution, this is not well suited for conceptual design where the designer wants to generate multiple solutions and where some goals can be of a qualitative type. By using heuristic optimisation methods, such as genetic algorithms, multiple well performing designs can be generated. These can be better suited from other design objectives which can be difficult to describe numerically in an objective function, but which the designer can in other ways identify as important [27] (i.e. non performance oriented objectives). Grasshopper has built-in support for genetic algorithms. Mueller [8] has proposed methods for allowing the user to interact with an optimization algorithm, [28], being able to generate several design proposals with good performance but not necessarily the optimal, which are instead selected out of other aspects. See for instance the online tool structureFIT [29].

A challenge for optimization tools is that the computations grow exponentially with the number of design variables and sometimes make the methods unsuited for problems that are more complex.

2.6.4 Graphical methods

Graphic statics is a graphical method for determining the forces in an assembly of axially loaded members, such as trusses, cables, and arches. The first comprehensive presentation of graphical

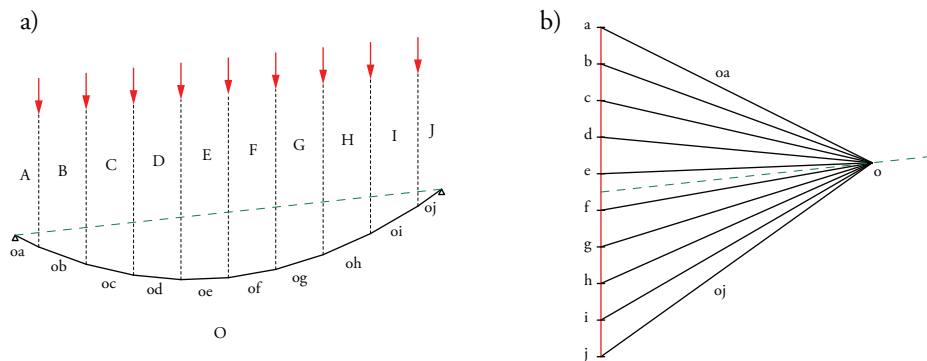


Figure 2.7: Graphic statics solution for a cable with a uniformly distributed load. a) Form diagram. b) Force diagram.

techniques was done by Culmann [30], who is considered the father of graphic statics. Other important contributors to graphic statics were Maxwell, Cremona, and Bow. Graphic statics have been used to design structures by amongst others Maurice Koechlin (co-designer of the Eiffel Tower) and Robert Maillart [11].

It is based on construction of two reciprocal diagrams: the form diagram representing the actual geometry of the structure, and the force diagram that represents the internal forces through vectors. Changes in the geometry are reflected in the force diagram, providing a visual relationship between the two. Because forces are graphically represented using vectors, no numerical analysis is required to calculate the forces. Fig. 2.7 shows an example solution for a cable using graphic statics.

Several computer tools using graphic statics have been developed. One such tool is Active Statics, an on-line tool intended for educational use, where some predefined problems are solved with graphic statics. Users are able to manipulate structures and see how the internal forces change. Another on-line tool is eEQUILIBRIUM, containing some further examples. RhinoStatics is a plug-in which can be used for graphic statics in Rhinoceros 3D and is not limited to some pre-defined examples. Recently there has been a prototype tool developed for Grasshopper [31].

Graphic statics can only provide unique solutions to statically determinate structures, for which the equations of equilibrium can be solved without the addition of further constraints (considering for instance elasticity or relative stiffness of members). A further requirement is that all the loads and members must be co-planar, limiting the use of graphic statics to two-dimensional problems. Graphic statics solutions to simple structures, such as the one in Fig. 2.7 are elegant and clear, however, for more complex structures the force diagrams can quickly become difficult to read.

The indeterminacy of graphic statics is exploited in the theory of thrust network analysis, which

extends the method to three dimensions and generates compression only vaulted surfaces and networks under gravitational loading. Graphic statics and related methods are used for the assessment of the safety of historic masonry [32], and for the form finding and design of new vaulted structures.

2.6.5 Classical form finding

There have been several definitions of classical form finding, one is [33] “form finding is a forward process in which parameters are explicitly/directly controlled to find an ‘optimal’ geometry of a structure which is in static equilibrium with a design loading.”. Some recent definitions of form finding are much broader, [34] “finding an appropriate architectural and structural shape”, allowing for additional constraints and performance criteria. In [35], the different types of definitions are separated into classical and modern form finding.

Regardless of which definition is used, it is known that geometry has a key role on structural performance related goals in buildings. Geometry is also important for other performance related aspects, such as energy, whose relationship to geometry has in the last decade seen an increase in studies [36].

Classical form finding methods are used to find efficient shapes for arches, shells and membranes under certain loads, such as the self-weight or pre-stress. The methods are a type of optimization, but do not rely on general mathematical optimization techniques, but rather on finding states of equilibrium for a prescribed load or stress. The methods can be divided into two types. The first is related to pre-stressed structures, whose shapes are analogous to minimal surfaces. The second is related to the hanging chain and its inverse, an arch.

Pre-stressed structures carry applied loads through tension and are stiffened by the pre-stressing. These can be cable nets or fabric membranes. These structures are some of the most efficient in terms of dead-load to span ratio. The aim of the form finding for pre-stressed structures is to find a shape that is in equilibrium for the prescribed pre-stress. One approach to do this physically is to use soap films which almost assume the shapes of minimal surfaces, see Fig. 2.8, bounded by rigid steel wires. Frei Otto [37] at the Institute for Lightweight Structures (IL) was one of the early adopters of such methods. The shapes from soap film experiments are related to isotropic pre-stress states, however, for fabrics the material properties in the directions of the warp and weft can vary, and it is possible to prescribe an anisotropic pre-stress.

The idea of the hanging chain and its inverse is well known. As the hanging chain cannot take any bending stresses the resultant shape will be in pure tension, which is generally a much more efficient use of material than in bending. A physical form finding model with hanging chains is shown in Fig. 2.8. Inverting the shape creates an arch in pure compression. The method can be extended to membranes which are physically form-found using hanging cloths, which when inverted give the shape of a vault in compression (for simple geometries). For shapes that are more complex the process of finding shapes by use of hanging cloths becomes difficult

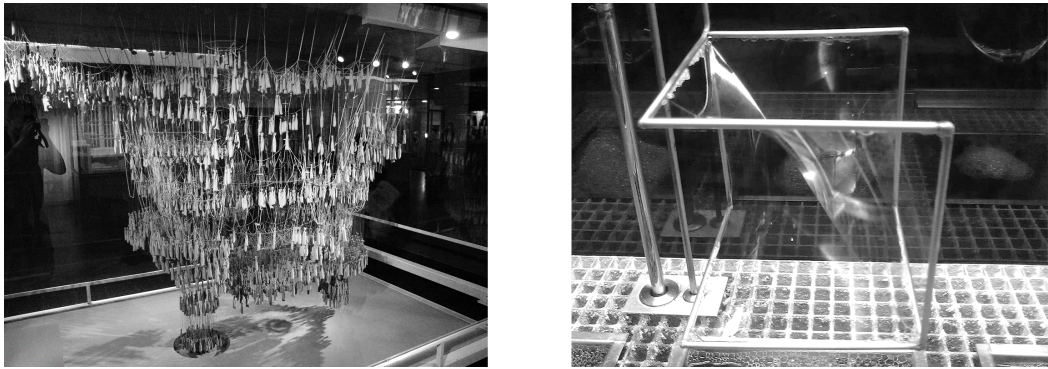


Figure 2.8: Hanging model and soap film model, from Wikimedia Commons.

due to wrinkling from in-plane compressive forces. Heinz Isler [38] pioneered the use of cloths for form finding both as conceptual models and for precise measurements. Using these techniques in physical models required knowledge about the cloths anisotropic properties, the cutting pattern, as well as good structural intuition and patience. Generally, care must be taken when designing compressive structures, such as vaults and arches since buckling may occur.

There is a wide range of numerical methods for form finding, most of which were initially developed for the form finding of pre-stressed structures. For the form finding of pre-stressed structures, pre-stress is prescribed to an initial form which deforms until it settles in an equilibrium state. During the process only geometric stiffness is accounted for, which causes singularities in the tangential mesh direction (nodes are allowed to move freely on the surface). In form finding of hanging models with membrane elements, another type of singularity arises in the surface normal direction, since the elements only provide stiffness in the surface directions. This can for very fine meshes lead to mesh dependent, artificial wrinkling patterns. Different approaches for dealing with the mentioned singularities have been studied and can be divided into three different types [35]:

- *Dynamic methods* solve for the static equilibrium by the use of a fictitious dynamic simulation. The addition of inertia avoids the difficulties of the singular stiffness matrices. A popular method in this category is dynamic relaxation [39, 40]. For the pre-stress type of singularity fictitious forces tangent to the surface may be needed.
- *Geometric stiffness methods*, such as the force density method [41], used for the form finding of cable nets. The cable force is replaced by a force density, which is the ratio of cable force to cable element length. The replacement makes the equations of equilibrium linear.
- *Stiffness matrix methods* rely on adding penalty stiffness to the stiffness matrix to prevent or control singularities. See, for instance [42, 43].

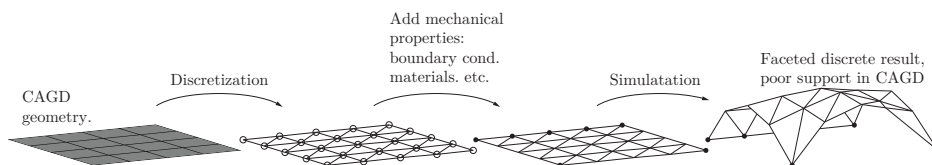


Figure 2.9: Traditional work flow for form finding, starting with a CAGD geometry and ending with a FE-solution with discrete geometry.

Form finding usually requires several iterations, where the designer alternates between specifying mechanical requirements and performing form finding and evaluating the shapes with respect to other design criteria. If it is necessary, changes are made to some mechanical conditions (boundary, initial geometry, material parameters) until a form that fulfils the design requirements is found. Mechanical considerations and design aspects are closely connected and require good communication between FEM and CAGD tools. There are many tools developed which simplify this connection. The tools exist both as standalone tools, such as CADenary [44], one of the first tools for interactively exploring hanging models, and, as plug-ins to CAGD software: Kangaroo [24], Karamba [23], SmartForm [45], Rhinomembrane [46], RhinoVault [47].

All of the developed methods and tools require the discretization of some initial geometry into finite elements. Because of the discretization, it is difficult to continue changing the geometry of a model after the form finding process, since common CAGD tools have poor support for FE type of geometries. Often the employed elements in the FE simulation are flat and lead to faceted geometries, while shells and membranes are curved and smooth, see Fig. 2.9.

2.7 CONCLUSIONS AND PRESENT RESEARCH

During the last decades, there has been an extraordinary development of computer-based tools intended for presenting or communicating the results of architectural projects. However, the tools primarily focus on the geometric aspects of the design. The literature review has covered suitable methods and tools intended to assist in conceptual design studies to generate architectural forms that in a simple and interactive way also consider engineering aspects. However, there is still a need for further development. This thesis has studied two methods for form finding in conceptual design.

The tools that have been reviewed in the literature study have a few different approaches to providing support in conceptual design phases. One approach is to reduce the amount of information that is generally required for a FE analysis (ForcePAD, SketchAFrame, PointSketch) while simultaneously providing real time feedback. Another is to integrate analysis methods

into design software, like for instance GeometryGym and Karamba. One drawback of the latter is that the geometry in the design software still needs to be translated (meshed) to be used. The same is true of form finding tools that are integrated into design tools - for which the initial geometries need to be discretized into finite elements in order to work.

Conceptual tools for vibration reduction in an urban scale

Most of the tools that have been developed for conceptual structural design are intended for the static design of structures. Other structural considerations may be important to include in the early design phases. In the research a tool for studying vibration reduction by the placement of masses on ground in an urban scale was developed. A case study was also made related to the development of a new synchrotron research facility, which is very sensitive to vibrations and was sited close to two roads with dense traffic. Similar tools could be of use for the urban planning and densification of our cities, to decrease vibrations from road and train traffic.

Form finding with NURBS based finite elements

The different tools mentioned in the literature study aimed at bridging the gap of moving the model between CAGD software and CAE. Here, a recent development, isogeometric analysis (IGA), aiming at removing this gap in geometry types by using the same geometric model for both, is studied. The suitability of NURBS based IGA for conceptual structural design tools is investigated, specifically for form finding tools for hanging models together with the dynamic relaxation method. The motivation for this research is:

- There is no need to discretize the NURBS geometry.
- NURBS are particularly well suited for curved geometries.
- It allows for form finding directly in the CAD software and in the architectural context.
- Conceptual design is an iterative procedure, and performing form finding often requires several iterations in order to get satisfactory results, this approach may simplify iterations.
- CAGD programs are in general better at treating complex geometries and modifying them, compared to FE programs. The initial geometries used for the form finding procedure can at times be rather complex.
- NURBS patches are already successfully used for structural shape optimization.
- Recently, other authors have studied similar approaches, see [48, 49].
- Implementing the form finding directly into CAGD software can lead to an interactive and iterative design process.

3 Theory

The theory presented in this chapter relates to Computer Aided Geometric Design (CAGD), the Finite Element Method (FEM), Isogeometric Analysis (IGA), structural dynamics, Kirchhoff-Love shell and membrane theory, and the method of dynamic relaxation, all of which have been used in the present research.

3.1 GEOMETRIC PRELIMINARIES

In the appended papers B and C use is made of NURBS based IGA. In order to explain IGA the necessary B-spline and NURBS theory which is commonly used in CAGD is briefly presented. For further reading, see for instance [50–52].

3.1.1 B-splines

B-splines are non-interpolating, piecewise polynomial curves. A B-spline curve $\mathbf{C}(\xi)$ is defined by its polynomial degree p , a knot vector $\Xi = \{\xi_1, \xi_2, \dots, \xi_{n+p+1}\}$, and a set of n control points $\mathbf{B}_i = (x_i, y_i, z_i)$. The knot vector contains non decreasing values and divides the parametric space into intervals known as knot spans, the first and last values in the knot vector are repeated $p + 1$ times. If an internal knot is repeated r times it is said to have a multiplicity of r . The curve is computed by a summation of the B-spline basis functions multiplied by the control points

$$\mathbf{C}(\xi) = \sum_{i=1}^n N_{i,p}(\xi) \mathbf{B}_i \quad (3.1)$$

where the i :th basis function $N_{i,p}$ is constructed recursively, using the Cox-de Boor formula [53, 54], for $p = 0$

$$N_{i,0}(\xi) = \begin{cases} 1 & \text{if } \xi_i \leq \xi < \xi_{i+1} \\ 0 & \text{otherwise.} \end{cases} \quad (3.2)$$

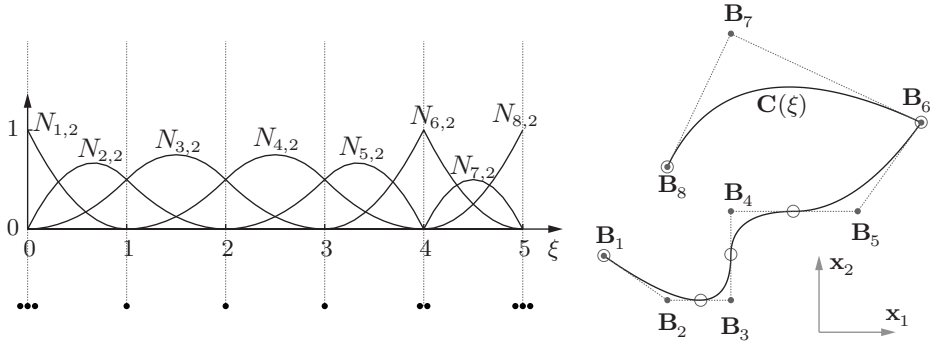


Figure 3.1: Basis functions for a quadratic B-spline and a curve generated with the basis functions.

For $p = 1, 2, 3, \dots$, recursively

$$N_{i,p}(\xi) = \frac{\xi - \xi_i}{\xi_{i+p} - \xi_i} N_{i,p-1}(\xi) + \frac{\xi_{i+p+1} - \xi}{\xi_{i+p+1} - \xi_i} N_{i+1,p-1}(\xi) \quad (3.3)$$

for which implementations can be found in [51]. The continuity of the basis functions at a repeated knot is C^{p-r} , meaning that it is $p-r$ times continuously differentiable. All derivatives exist in the interior of a knot span. Each control point, \mathbf{B}_i , has an associated basis function which is non-zero in $p+1$ knot spans in the half open interval $[\xi_i, \xi_{i+p+1})$, which is known as local support. The local support of the NURBS basis, makes them highly intuitive and predictable for geometrical modelling. The basis functions are only interpolatory at the ends of the knot vector, and at knots with multiplicity $r = p$, leading to C^0 continuity, for an example, see the knot at $\xi = 4$ in Fig. 3.1, where a quadratic B-spline basis with the knot vector $\Xi = \{0, 0, 0, 1, 2, 3, 4, 4, 5, 5, 5\}$ is shown. The division of the parameter space into knot-intervals is indicated by the dashed vertical lines, and the multiplicity of the knots is shown with the dots below the basis functions. The curve on the right in Fig. 3.1 is generated using the basis functions and the 8 control points \mathbf{B}_i , the dashed lines between the control points form the control point polygon. The knot positions in the physical space are indicated with circles.

In general, the number of knots does not coincide with the number of control points or basis functions. The denominators in the quotients in Eq. (3.3) can become zero, but the quotients are in those cases defined as zero [51]. The control polygon is tangent to the endpoints of a B-spline curve.

There are several important properties of the basis functions, such as that they form a partition of unity,

$$\sum_{i=1}^n N_{i,p}(\xi) = 1 \quad \forall \xi \in [\xi_1, \xi_{n+p+1}) \quad (3.4)$$

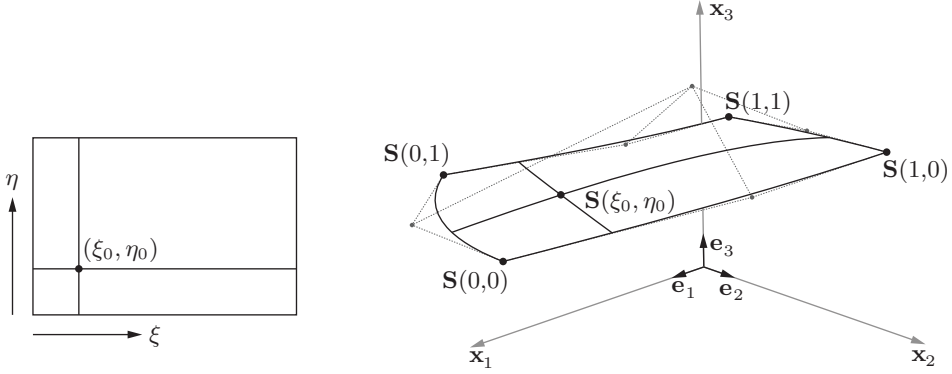


Figure 3.2: A bi-quadratic B-spline surface and its parametric space.

and are by definition non-negative

$$N_{i,p}(\xi) \geq 0 \quad \forall \xi. \quad (3.5)$$

A B-spline surface is defined using the tensor product approach, where another set of univariate basis functions $M_{j,q}(\eta)$ of degree q , with the knot vector $\mathbf{H} = \{\eta_1, \eta_2, \dots, \eta_{m+q+1}\}$, with m control points in the second direction and the control point net $\mathbf{B}_{i,j}$ is used

$$\mathbf{S}(\xi, \eta) = \sum_{i=1}^n \sum_{j=1}^m N_{i,p}(\xi) M_{j,q}(\eta) \mathbf{B}_{i,j} \quad (3.6)$$

and by adding a third direction one can in a similar fashion generate B-spline solids. B-spline surfaces and solids constructed by the tensor product approach are also referred to as patches. In Fig. 3.2 a bi-quadratic B-spline surface and its parametric space are shown, with $\xi, \eta \in [0, 1]$. The control point net is visible with dashed lines, containing the 9 control points $\mathbf{B}_{i,j}$ with $i, j = 1, 2, 3$. The point (ξ_0, η_0) in parametric space is mapped to $\mathbf{S}(\xi_0, \eta_0)$ in three-dimensional Euclidean space.

3.1.2 Derivates of B-splines

The derivates of B-splines are given as

$$\frac{d}{d\xi} N_{i,p}(\xi) = \frac{p}{\xi_{i+p} - \xi_i} N_{i,p-1}(\xi) - \frac{p}{\xi_{i+p+1} - \xi_{i+1}} N_{i+1,p-1}(\xi) \quad (3.7)$$

and are straightforward to generalize for higher order derivatives.

3.1.3 NURBS

NURBS have the ability to represent any conical shapes such as a circle exactly. NURBS can represent both analytic shapes (cones, cubes, etc) and free form surfaces using the same method [50].

A B-spline curve is extended to a NURBS by adding a weight to each control point

$$\mathbf{C}(\xi) = \frac{\sum_{i=1}^n N_{i,p}(\xi) \omega_i \mathbf{B}_i}{\sum_{k=1}^n N_{k,p}(\xi) \omega_k} = \frac{\sum_{i=1}^n N_{i,p}(\xi) \omega_i \mathbf{B}_i}{W(\xi)} = \sum_{i=1}^n R_{i,p}(\xi) \mathbf{B}_i \quad (3.8)$$

where $R_{i,p}$ are the rational NURBS basis functions.

Differentiating the NURBS basis functions results in

$$\frac{d}{d\xi} R_{i,p}(\xi) = \omega_i \frac{W(\xi) N'_{i,p}(\xi) - W'(\xi) N_{i,p}(\xi)}{(W(\xi))^2} \quad (3.9)$$

where the quotient rule has been applied and the prime denotes the derivative with respect to ξ . There are efficient algorithms to compute the derivatives of the B-spline basis [51], these are used in practice together with the quotient rule to compute the NURBS derivatives.

Similarly for surfaces each control point in the control point mesh is extended with a weight, $\mathbf{B}_{i,j} = (x_{i,j}, y_{i,j}, z_{i,j}, \omega_{i,j})$ and the NURBS surface is given by

$$\mathbf{S}(\xi, \eta) = \frac{\sum_{i=1}^n \sum_{j=1}^m N_{i,p}(\xi) M_{j,q}(\eta) \omega_{i,j} \mathbf{B}_{i,j}}{\sum_{k=1}^n \sum_{l=1}^m N_{k,p}(\xi) M_{l,q}(\eta) \omega_{k,l}}. \quad (3.10)$$

A geometrical interpretation of a NURBS is that a NURBS surface in \mathbb{R}^3 is obtained by a projective transformation of a B-Spline surface in \mathbb{R}^4 . In practice the geometric interpretation is important in that algorithms developed for B-splines can be applied to NURBS by treating the NURBS as a B-spline in a higher dimension.

3.1.4 Special cases of NURBS

If all weights are equal the NURBS basis is reduced to a B-Spline basis

$$R_{i,p}(\xi) = N_{i,p}(\xi) \quad \text{if} \quad \omega_k = c \quad \forall k \quad (3.11)$$

and if the knot vector only contains end knots with multiplicity $p + 1$ the B-spline basis is reduced to the Bernstein polynomials

$$N_{i,p}(\xi) = B_{i,p}(\xi) \quad \text{if} \quad \Xi = \{0, 0, \dots, 0, 1, \dots, 1, 1\}. \quad (3.12)$$

3.2 THE FINITE ELEMENT METHOD

The finite element method is based on dividing a region governed by physical phenomena into a set of smaller regions, or finite elements. Simpler approximations are assumed over the elements which approximate the original complex equations. Even though the physical phenomena may vary in a highly non-linear fashion over the whole region the simpler linear or quadratic approximation may hold over the element, provided the element is small enough. The approximations are some kind of interpolation over the element where it is assumed that the values are known at some certain *nodal* points, which are usually located at the boundary of each element. The second step consists of generating a global set of equations from the local by a co-ordinate transformation from the sub-domains' local co-ordinate systems and nodes to the domains' global co-ordinate system and nodes.

The finite element method is numerically stable, meaning that errors from input and intermediate calculations do not grow and cause inaccuracies which make the results meaningless. To minimize the errors from the approximations (or increase precision) a finer mesh with smaller elements or elements with a higher order of basis functions (e.g. going from linear to quadratic elements) may be used, at the expense of computational cost.

3.3 NURBS BASED ISOGEOMETRIC ANALYSIS

The term isogeometric analysis was coined by Hughes, [55], however, approaches for carrying out computation on design geometry were attempted before, by for instance Cirak et al. on thin-shell elements for subdivision surfaces [56]. There were other earlier precedents as well [57–59].

Finite element implementations using NURBS based IGA have much in common with classical FEA, though there are some points on which they differ. One important aspect is that *control points* in IGA are in general not interpolated like *nodal points* in classical FEA, resulting in for instance that if essential boundary conditions are strongly imposed (at non-interpolated control points) they may become slightly smeared. Further, degrees of freedom in IGA are related to control points, and can not be directly interpreted in the same way as degrees of freedom are related to a node in classical FEA. However, most of these types of differences can be treated by the use of proper pre- and post-processing.

For more information on the topic of IGA, and the theory recited here, see [15] or [55].

3.3.1 The isoparametric and isogeometric concepts

In finite element analysis the use of the isoparametric concept is common. The basic idea is that the basis functions which are used to approximate the unknown field are also used to describe (approximately) the geometry. Moreover the basis functions are described in some parent coordinates, $\tilde{\xi}, \tilde{\eta}, \tilde{\zeta} \in [-1, 1]$, [60].

Two general requirements on finite elements are that they must be compatible and complete. If both requirements are fulfilled monotonic convergence of the approximated field to the exact one when elements are made smaller is ensured, [60].

Isoparametric elements fulfil the completeness requirement if their basis functions are a partition of unity. For solid elements it is sufficient to require C^0 continuity between element borders and C^1 on the element interiors in order to fulfil the compatibility requirement, [15].

The isogeometric concept requires that the basis functions which are capable of representing the geometry *exactly* are also used to approximate the unknown field. The basic convergence requirements stated in the earlier paragraphs are not restricted to classical Lagrangian finite elements with polynomial bases, but hold for any reasonably smooth isoparametric basis which is also a partition of unity, e.g. the NURBS basis functions used in this work, [15].

The strength of the isogeometric approach is that it builds upon the already well developed FE- and CAGD theories, without breaking backward compatibility.

3.3.2 NURBS elements

In here an element is defined as an interval in the knot vector. The divisions are marked in Fig. 3.1 for one-dimensional (line and curve) elements. In the figure it is apparent that the basis functions span over several elements, and that the basis functions allow for higher than C^0 continuity between elements.

The use of a parent element requires two separate mappings in NURBS based isogeometric analysis. A first mapping from the parent element coordinates $(\tilde{\xi}, \tilde{\eta})$ to the NURBS parametric coordinates (ξ, η) , and a second mapping from the NURBS parametric coordinates to the physical coordinates (x, y, z) . Fig. 3.3 shows an example of the mappings for a surface consisting of 9 elements. Every element in the parametric and global domains is mapped from the same parent domain. The middle element of the surface is marked with diagonal lines.

3.3.3 Refinement

An attractive property of B-Splines for design and analysis is that the represented geometry is invariant during refinements and is represented exactly irrespective of the mesh being coarse or

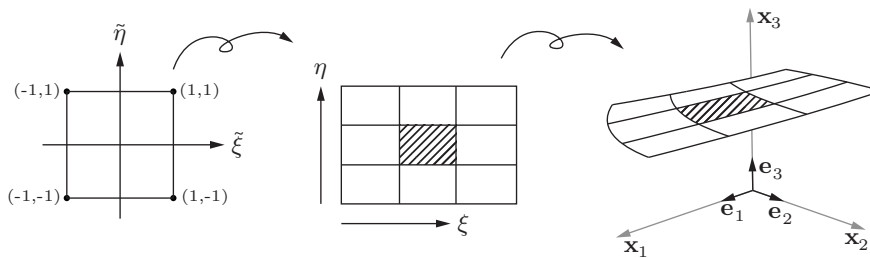


Figure 3.3: A B-spline surface patch consisting of 9 elements. The parent domain, parametric domain and physical surface are shown.

refined. There are three types of refinements possible for B-Splines/NURBS based IGA. The first is the same as for finite elements, namely making the elements smaller (h-refinement), which is done by performing so called knot insertion, whereby new knot values are inserted into the knot vector without affecting the geometry. The elements in NURBS based IGA are defined by the knot spans, and thus by introducing new knots one also introduces new elements. As for finite elements it is possible to increase the degree of the basis functions (p-refinement). Another type of refinement is possible with B-splines/NURBS where if the degree is first raised and the elements are made smaller (k-refinement) it is possible to obtain basis functions with continuous derivatives across element borders. The refinement possibilities make NURBS suitable for form finding where a coarse mesh can be used initially to explore shapes in near real time and a finer one can be used afterward to obtain a more accurate solution.

The tensor product nature of NURBS surfaces, as may be seen in Eq. (3.6), constrains standard isogeometric analysis with NURBS to 4-sided surfaces. However, by use of T-Splines [61], or trimmed NURBS [62] more complex forms may be constructed.

3.4 ELASTICITY

In the derivations operators beginning with capitals are related to material coordinates, and those beginning with lower case relate to spatial coordinates. For instance

$$\text{Div}(\mathbf{A}) = \frac{\partial A_{ij}}{\partial X^j} \mathbf{e}_i; \quad \text{div}(\mathbf{A}) = \frac{\partial A_{ij}}{\partial x^j} \mathbf{e}_i \quad (3.13)$$

where X^j are material coordinates and x^j are spatial and \mathbf{e}_i are unit basis vectors pointing in the axes of a Cartesian reference frame. Summation of repeated indices is implied. Roman indices range from 1 to 3, and Greek indices range from 1 to 2.

3.4.1 Strong form of elasticity

For the subsequent finite element discretizations the material description of the principle of virtual work is used, however we will start out with the spatial description of the strong form since the symmetry of the Cauchy stress tensor simplifies the derivations.

The equation of motion along with the necessary boundary conditions in the spatial description is [63]

$$\left. \begin{aligned} \operatorname{div}(\boldsymbol{\sigma}) + \mathbf{b} &= \rho \ddot{\mathbf{u}} \\ \mathbf{u} = \bar{\mathbf{u}} &\text{ on } \partial v_u \\ \mathbf{t} = \boldsymbol{\sigma} \mathbf{n} = \bar{\mathbf{t}} &\text{ on } \partial v_\sigma \end{aligned} \right\} \quad (3.14)$$

where $\boldsymbol{\sigma}$ is the Cauchy stress tensor, \mathbf{b} is the current body force per unit current volume and $\rho \ddot{\mathbf{u}}$ is the inertia force per unit current volume. The displacements $\mathbf{u} = \mathbf{u}(\mathbf{x}, t)$ are prescribed on ∂v_u and the traction $\mathbf{t} = \mathbf{t}(\mathbf{x}, t, \mathbf{n})$ is prescribed on ∂v_σ . The boundary to the body v is the surface $\partial v = \partial v_u \cup \partial v_\sigma$. \mathbf{n} is the unit outward normal to the surface. The prescribed displacements and tractions must be supplied for $t = 0$.

3.4.2 Weak form and virtual work

For the finite element implementations the weak or virtual work form of Eq. (3.14) is used. The derivations are common and the reader is referred to for instance [63].

To obtain the principle of virtual work in the spatial description we multiply Eq. (3.14) with an arbitrary vector valued weight function $\mathbf{v} = \mathbf{v}(\mathbf{x})$ and integrate over the volume v . After some manipulations and the application of the divergence theorem we first obtain the weak form of Eq. (3.14)

$$f(\mathbf{u}, \mathbf{v}) = \int_v [\boldsymbol{\sigma} : \operatorname{grad}(\mathbf{v}) - (\mathbf{b} - \rho \ddot{\mathbf{u}}) \cdot \mathbf{v}] dv - \int_{\partial v_\sigma} \boldsymbol{\sigma} \mathbf{v} \cdot \mathbf{n} ds = 0 \quad (3.15)$$

\mathbf{v} vanishes over the part of the surface where \mathbf{u} is prescribed, meaning that the boundary only needs to be integrated over ∂v_σ . The weak form needs to be supplied with initial values of the essential boundary conditions at $t = 0$.

If the weight functions \mathbf{v} are considered to be the virtual displacements $\delta \mathbf{u}$ then the weak form leads to the principle of virtual work in spatial description

$$f(\mathbf{u}, \delta \mathbf{u}) = \int_v [\boldsymbol{\sigma} : \operatorname{grad}(\delta \mathbf{u}) - (\mathbf{b} - \rho \ddot{\mathbf{u}}) \cdot \delta \mathbf{u}] dv - \int_{\partial v_\sigma} \bar{\mathbf{t}} \cdot \delta \mathbf{u} ds = 0 \quad (3.16)$$

which can be separated into the internal and external virtual work

$$\delta W_{\text{int}}(\mathbf{u}, \delta \mathbf{u}) = \int_v \boldsymbol{\sigma} : \operatorname{grad}(\delta \mathbf{u}) dv \quad (3.17)$$

$$\delta W_{\text{ext}}(\mathbf{u}, \delta \mathbf{u}) = \int_v \mathbf{b} \cdot \delta \mathbf{u} dv + \int_{\partial v_\sigma} \bar{\mathbf{t}} \cdot \delta \mathbf{u} ds \quad (3.18)$$

where the inertia terms have been neglected and the equilibrium condition is $\delta W_{\text{int}} - \delta W_{\text{ext}} = 0$, valid for any virtual displacements $\delta \mathbf{u}$.

The equations are written in material coordinates using pull-back operations [63], and the internal virtual work is now written as

$$\delta W_{\text{int}}(\mathbf{u}, \delta \mathbf{u}) = \int_V \mathbf{P} : \text{Grad}(\delta \mathbf{u}) dV = \int_V \mathbf{S} : (\delta \mathbf{E}) dV \quad (3.19)$$

where \mathbf{P} is the first Piola-Kirchhoff stress tensor and \mathbf{S} is the second Piola-Kirchhoff stress tensor. \mathbf{E} is the Green-Lagrange strain tensor, and its variation is $\delta \mathbf{E}$. The external virtual work in material coordinates is

$$\delta W_{\text{ext}}(\mathbf{u}, \delta \mathbf{u}) = \int_V \mathbf{B} \cdot \delta \mathbf{u} dV + \int_{\partial V_\sigma} \bar{\mathbf{T}} \cdot \delta \mathbf{u} dS \quad (3.20)$$

where \mathbf{B} is the body force per unit reference volume and which is related to \mathbf{b} through $\mathbf{b} = J^{-1} \mathbf{B}$ (and the volume change $dv = J dV$), and $\bar{\mathbf{T}} dS = \bar{\mathbf{t}} ds$. J is the determinant of the deformation gradient \mathbf{F} . Lastly the integral for the inertia terms is related by $\rho_0 dV = \rho dv$.

3.4.3 Linear elasticity

In paper A the assumptions of linear elasticity and small displacements are employed, i.e. the displacements are assumed to be infinitesimally small, and a linear elastic material law is used. Under these assumptions the equilibrium of a body can be established in the undeformed configuration and the equation of virtual work is simplified to

$$\delta W = \int_V [\boldsymbol{\sigma} : (\delta \boldsymbol{\epsilon}) - (\mathbf{b} - \rho \ddot{\mathbf{u}}) \cdot \delta \mathbf{u}] dV - \int_{\partial V_\sigma} \bar{\mathbf{t}} \cdot \delta \mathbf{u} dS = 0 \quad (3.21)$$

where $\delta \boldsymbol{\epsilon}$ is the variation of the engineering strain, and $\boldsymbol{\sigma}$ is the engineering stress [64].

3.5 STRUCTURAL DYNAMICS

The equation of motion (EOM) for a multi degree of freedom (MDOF) system can from Eq. (3.21) be formulated by use of the FE-method, and with the addition of damping it is given by

$$\mathbf{M} \ddot{\mathbf{u}} + \mathbf{C} \dot{\mathbf{u}} + \mathbf{K} \mathbf{u} = \mathbf{f} \quad \forall t \in (0, T) \quad (3.22)$$

with $\mathbf{u}(t = 0) = \mathbf{u}_0$ and $\dot{\mathbf{u}}(t = 0) = \dot{\mathbf{u}}_0$, where \mathbf{M} is the mass matrix, \mathbf{C} is the damping matrix, \mathbf{K} is the stiffness matrix, \mathbf{u} is the nodal displacements vector and \mathbf{f} is the force vector. \mathbf{M} , \mathbf{C} , and \mathbf{K} are sparse, symmetric and positive-definite matrices. In Paper A, the steady state vibrations of a soil-mass system are studied, and the following subsection will briefly go through the corresponding theory.

3.5.1 Steady state dynamics

Assuming steady state harmonic behaviour with common time factor $e^{i\omega t}$, the equation of motion for a discretized MDOF system can be written using complex arithmetic

$$\mathbf{M}\ddot{\bar{\mathbf{u}}} + \mathbf{C}\dot{\bar{\mathbf{u}}} + \mathbf{K}\bar{\mathbf{u}} = \bar{\mathbf{p}} = \mathbf{p}_0 e^{i\omega t}; \quad \bar{\mathbf{u}}(t) = \bar{\mathbf{U}} e^{i\omega t} \quad (3.23)$$

with the complex response

$$\bar{\mathbf{u}} = \mathbf{u}_\Re + i\mathbf{u}_\Im \quad (3.24)$$

where it is understood that the actual steady-state motion is given by either the real or imaginary part depending on the nature of the excitation (i.e. sin or cos). By rewriting Eq. (3.23) and omitting the common time factor we get

$$(-\omega^2 \mathbf{M} + i\omega \mathbf{C} + \mathbf{K})\bar{\mathbf{U}} = \mathbf{p}_0 \quad (3.25)$$

or

$$\mathbf{D}(\omega)\bar{\mathbf{U}} = \mathbf{p}_0 \quad (3.26)$$

where $\mathbf{D}(\omega)$ is the dynamic stiffness matrix, dependent on the angular frequency ω

$$\mathbf{D}(\omega) = -\omega^2 \mathbf{M} + i\omega \mathbf{C} + \mathbf{K} \quad (3.27)$$

which may be used to calculate the complex amplitude $\bar{\mathbf{U}}$, which in turn can be used to determine the amplitude and phase of the steady-state response. The damping can be introduced by, for instance, computing the damping matrix by use of Rayleigh damping or by computing a structural damping matrix by use of a loss factor, [65]. Note that in the next section and in Paper A the overbar and uppercase are dropped and the complex amplitude is simply referred to as \mathbf{u} . For more information the reader is referred to [65].

3.5.2 Dynamic model reduction with damping

Model reduction methods within engineering are used to lessen computational costs of an analysis. One of the most common reduction method is referred to as Guyan reduction. A set of active "master" coordinates, and a set of dependent "slave" coordinates which may be reduced are chosen. The matrices are then re-ordered and partitioned into separate parts relating to the master and slave degrees of freedom. If no forces are applied to the slave degrees of freedom and the damping is neglectable the equation of motion for the system can be written as (with subscripts m and s for master and slave degrees of freedom, no summations on repeated indices are implied in this subsection)

$$\begin{bmatrix} \mathbf{M}_{mm} & \mathbf{M}_{ms} \\ \mathbf{M}_{sm} & \mathbf{M}_{ss} \end{bmatrix} \begin{Bmatrix} \ddot{\mathbf{u}}_m \\ \ddot{\mathbf{u}}_s \end{Bmatrix} + \begin{bmatrix} \mathbf{K}_{mm} & \mathbf{K}_{ms} \\ \mathbf{K}_{sm} & \mathbf{K}_{ss} \end{bmatrix} \begin{Bmatrix} \mathbf{u}_m \\ \mathbf{u}_s \end{Bmatrix} = \begin{Bmatrix} \mathbf{f}_m \\ 0 \end{Bmatrix} \quad (3.28)$$

by neglecting the inertia terms in Equation 3.28 the transformation matrix \mathbf{T} may be written as

$$\begin{Bmatrix} \mathbf{u}_m \\ \mathbf{u}_s \end{Bmatrix} = \begin{bmatrix} \mathbf{I} \\ -\mathbf{K}_{ss}^{-1}\mathbf{K}_{sm} \end{bmatrix} \mathbf{u}_m = \mathbf{T}\mathbf{u}_m \quad (3.29)$$

the reduced mass and stiffness matrices can then be given as

$$\begin{aligned} \mathbf{K}_r &= \mathbf{T}^T\mathbf{K}\mathbf{T} \\ \mathbf{M}_r &= \mathbf{T}^T\mathbf{M}\mathbf{T} \end{aligned} \quad (3.30)$$

The method is exact at frequency zero and approximate at all other frequencies as the inertia terms have been neglected. Guyan reduction may be extended to Dynamic reduction at steady state harmonic conditions by using the dynamic stiffness matrix

$$(\mathbf{K} - \omega^2\mathbf{M})\mathbf{u} = \mathbf{f} \quad (3.31)$$

or expressed in terms of re-ordered master and slave degrees of freedom

$$\begin{bmatrix} \mathbf{K}_{mm} - \omega^2\mathbf{M}_{mm} & \mathbf{K}_{ms} - \omega^2\mathbf{K}_{ms} \\ \mathbf{K}_{sm} - \omega^2\mathbf{M}_{sm} & \mathbf{K}_{ss} - \omega^2\mathbf{K}_{ss} \end{bmatrix} \begin{Bmatrix} \mathbf{u}_m \\ \mathbf{u}_s \end{Bmatrix} = \begin{Bmatrix} \mathbf{f}_m \\ 0 \end{Bmatrix} \quad (3.32)$$

from which we get the transformation matrix \mathbf{T}

$$\begin{Bmatrix} \mathbf{u}_m \\ \mathbf{u}_s \end{Bmatrix} = \begin{bmatrix} \mathbf{I} \\ -(\mathbf{K}_{ss} - \omega^2\mathbf{M}_{ss})^{-1}(\mathbf{K}_{sm} - \omega^2\mathbf{M}_{sm}) \end{bmatrix} \mathbf{u}_m = \mathbf{T}\mathbf{u}_m \quad (3.33)$$

which can once again be used in Eq. (3.30) to obtain the reduced system matrices. This method is exact at frequency ω for undamped systems and works well for systems with low damping. If there is significant damping in the system one needs to use the full dynamic matrix

$$(\mathbf{K} + i\omega\mathbf{C} - \omega^2\mathbf{M})\mathbf{u} = \mathbf{f} \quad (3.34)$$

and using Equation 3.34 one gets the transformation matrix

$$\begin{Bmatrix} \mathbf{u}_m \\ \mathbf{u}_s \end{Bmatrix} = \begin{bmatrix} \mathbf{I} \\ -(\mathbf{K}_{ss} + i\omega\mathbf{C}_{ss} - \omega^2\mathbf{M}_{ss})^{-1}(\mathbf{K}_{sm} + i\omega\mathbf{C}_{sm} - \omega^2\mathbf{M}_{sm}) \end{bmatrix} \mathbf{u}_m = \mathbf{T}\mathbf{u}_m \quad (3.35)$$

which once again can be used in Eq. (3.30) to obtain the reduced system matrices, where \mathbf{C}_r follows in the same procedure. As no error is introduced in the transformation matrix this method is exact at frequency ω but the resulting reduced system matrices \mathbf{M}_r , \mathbf{C}_r and \mathbf{K}_r are complex [66]. It should be noted that the reduced system matrices produced by these methods are no longer sparse and require a rather large reduction of degrees of freedom in order to be of computational benefit.

3.5.3 Multi-level sub-structuring

In Paper A multi-level sub-structuring has been used to decrease the computational cost and time of the dynamic reduction, where the dynamic reduction has been applied to each sub-structure level starting at the bottom of the substructure tree, see Fig. 3.4 (d), and only keeping the interface and master degrees of freedom.

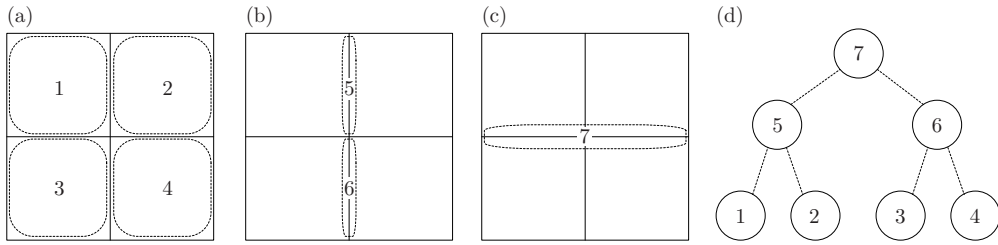


Figure 3.4: (a) bottom level substructures and internal dofs. (b) higher level substructures and interface dofs for the bottom level substructures (dashed area). (c) highest level substructure with interface dofs between substructures 5 and 6. (d) substructure tree.

3.6 KIRCHHOFF-LOVE SHELL AND MEMBRANE THEORY

In Papers B and C geometrically non-linear isogeometric membrane elements are used for the form finding and linear elastic Kirchhoff-Love shell theory is used for analysis on the form found geometry. The following sections contain the theory and the finite element discretization.

The Kirchhoff-Love shell theory requires C^1 continuity of the displacement field to fulfil the compatibility requirements, which is impossible to achieve with traditional Lagrange-type basis functions. NURBS allow for a higher order continuity and their use for Kirchhoff-Love shell elements fulfils the continuity requirement without the need for any rotational degrees of freedom. It was first presented in [67].

3.6.1 Geometry of curved surfaces and bodies

Shells and membranes are characterized by being much thinner in one of their dimensions than the other two, and are often curved. It is natural to describe them using a mid-surface description together with a thickness parameter t . Any point $\mathbf{r}(\xi^1, \xi^2)$ in three-dimensional physical space lying on the mid-surface can be described using only two parameters, (ξ^1, ξ^2) . On each point on the mid-surface in the current configuration a set of covariant base vectors is defined

$$\mathbf{a}_\alpha = \mathbf{r}_{,\alpha} = \frac{\partial \mathbf{r}}{\partial \xi^\alpha}; \quad \alpha = 1, 2. \quad (3.36)$$

Indices following a comma denote differentiation with respect to the parametric coordinates, unless otherwise stated. A third covariant base vector perpendicular to the surface is defined as

$$\mathbf{a}_3 = \frac{\mathbf{a}_1 \times \mathbf{a}_2}{|\mathbf{a}_1 \times \mathbf{a}_2|}. \quad (3.37)$$

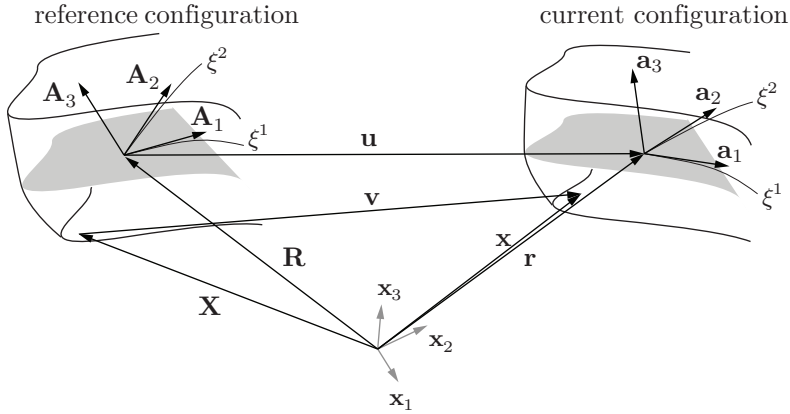


Figure 3.5: Shell geometry in reference and current configurations.

Contravariant base vectors are related to the covariant [68] by

$$\mathbf{a}_i \cdot \mathbf{a}^j = \delta_i^j; \quad i, j = 1, 2, 3 \quad (3.38)$$

where δ_i^j is 1 if $i = j$, 0 otherwise. Since \mathbf{a}^α lie in the tangent plane to the surface spanned by \mathbf{a}_α , it follows that

$$\mathbf{a}_3 = \mathbf{a}^3. \quad (3.39)$$

The metric tensor on the tangent plane, also called the first fundamental form of the surface is

$$a_{\alpha\beta} = \mathbf{a}_\alpha \cdot \mathbf{a}_\beta \quad (3.40)$$

or in contravariant or mixed form

$$a^{\alpha\beta} = \mathbf{a}^\alpha \cdot \mathbf{a}^\beta; \quad a_{\cdot\beta}^\alpha = a_\beta^{\cdot\alpha} = \delta_\beta^\alpha. \quad (3.41)$$

Equivalent equations can be formed in the reference configuration using the undeformed base vectors, \mathbf{A}_i .

Similarly, for points in the reference and current shell body the covariant base vectors are

$$\mathbf{g}_i = \mathbf{x}_{,i}; \quad \mathbf{G}_i = \mathbf{X}_{,i} \quad (3.42)$$

and the metric components for the body are

$$g_{ij} = \mathbf{g}_i \cdot \mathbf{g}_j; \quad G_{ij} = \mathbf{G}_i \cdot \mathbf{G}_j. \quad (3.43)$$

3.6.2 Mechanics

The deformation gradient \mathbf{F} maps a line element $d\mathbf{X}$ into $d\mathbf{x}$, and can be expressed by the base vectors of the reference and current configurations, see [69],

$$\mathbf{F} = \mathbf{g}_k \otimes \mathbf{G}^k. \quad (3.44)$$

The Green-Lagrange strain tensor is

$$\mathbf{E} = \frac{1}{2}(\mathbf{F}^T \mathbf{F} - \mathbf{I}) \quad (3.45)$$

and the Green-Lagrange strain components can be written in terms of the shell body metrics, for details, see [69],

$$E_{ij} = \frac{1}{2}(g_{ij} - G_{ij}). \quad (3.46)$$

The Kirchhoff-Love shell theory is applicable to thin and moderately thin shell structures where the thickness is assumed to be less than $1/20$ of the shells radius of curvature. The theory assumes that lines normal to the middle surface before deformation remain straight, unstretched and normal to that surface after deformation. Cross-sections are assumed to remain straight, corresponding to a linear strain distribution in the thickness direction. For simplicity, the shell thickness is assumed to be constant with ξ^α [69]. The shell can be completely represented by its mid-surface. The assumptions imply that transverse normal and shear strains are neglected, reducing the strain components to

$$E_{\alpha\beta} = \frac{1}{2}(g_{\alpha\beta} - G_{\alpha\beta}). \quad (3.47)$$

The basic kinematic assumption describes the position vector \mathbf{x} in the shell body by use of the shell mid-surface \mathbf{r} and the shell director, which coincides with the normal, \mathbf{a}_3

$$\mathbf{x} = \mathbf{r} + \xi^3 \mathbf{a}_3; \quad \xi^3 \in [-t/2, t/2] \quad (3.48)$$

and gives the body covariant base vectors in terms of the mid-surface base vectors

$$\mathbf{g}_\alpha = \mathbf{a}_\alpha + \xi^3 \mathbf{a}_{3,\alpha}. \quad (3.49)$$

Using Eq. (3.49) in Eq. (3.43)

$$g_{\alpha\beta} = (\mathbf{a}_\alpha + \xi^3 \mathbf{a}_{3,\alpha}) \cdot (\mathbf{a}_\beta + \xi^3 \mathbf{a}_{3,\beta}) = a_{\alpha\beta} - 2\xi^3 b_{\alpha\beta} + (\xi^3)^2 \mathbf{a}_{3,\alpha} \cdot \mathbf{a}_{3,\beta} \quad (3.50)$$

in which the quadratic term $(\xi^3)^2$ is neglected for very thin shells and

$$b_{\alpha\beta} = -\mathbf{a}_\alpha \cdot \mathbf{a}_{3,\beta} = \mathbf{a}_{\alpha,\beta} \cdot \mathbf{a}_3 \quad (3.51)$$

are the covariant components of the second fundamental form of the surface.

The results from Eq. (3.50) are used to split the strain components in membrane and bending parts

$$E_{\alpha\beta} = \epsilon_{\alpha\beta} + \xi^3 \kappa_{\alpha\beta} \quad (3.52)$$

where the membrane strains are

$$\epsilon_{\alpha\beta} = \frac{1}{2}(a_{\alpha\beta} - A_{\alpha\beta}) \quad (3.53)$$

and the bending strains, which represent the change in curvature are

$$\kappa_{\alpha\beta} = B_{\alpha\beta} - b_{\alpha\beta}. \quad (3.54)$$

3.6.3 Membrane part

For the form finding in this thesis we neglect the bending part, and focus on the membrane strains.

The components of the membrane strains are expressed in the base vectors of the reference configuration and displacements using $\mathbf{r} = \mathbf{R} + \mathbf{u}$, see Fig. 3.5,

$$\epsilon_{\alpha\beta} = \frac{1}{2}(\mathbf{A}_\alpha \cdot \mathbf{u}_{,\beta} + \mathbf{A}_\beta \cdot \mathbf{u}_{,\alpha} + \mathbf{u}_{,\alpha} \cdot \mathbf{u}_{,\beta}). \quad (3.55)$$

The components of the membrane stress resultant can be computed by integration of the 2nd Piola-Kirchhoff stress over the thickness, which for a homogeneous linear elastic material becomes

$$n^{\alpha\beta} = \int_{-t/2}^{t/2} S^{\alpha\beta} d\xi^3 = t S^{\alpha\beta} = \frac{Et}{1-\nu^2} C^{\alpha\beta\gamma\delta} \epsilon_{\gamma\delta} \quad (3.56)$$

where

$$C^{\alpha\beta\gamma\delta} = \nu A^{\alpha\beta} A^{\gamma\delta} + \frac{1}{2}(1-\nu)(A^{\alpha\gamma} A^{\beta\delta} + A^{\alpha\delta} A^{\beta\gamma}) \quad (3.57)$$

and ν is Poisson's ratio, and E is Young's modulus.

The internal virtual work in Eq. (3.19) is used and by neglecting the bending part we obtain

$$\delta W_{\text{int}} = \int_V \mathbf{S} : \delta \mathbf{E} dV = \int_A \mathbf{n} : \delta \boldsymbol{\epsilon} dA \quad (3.58)$$

and performing the double contraction gives

$$\delta W_{\text{int}} = \int_A n^{\alpha\beta} \delta \epsilon_{\alpha\beta} dA. \quad (3.59)$$

3.6.4 Finite element implementation

The following section explains the finite element discretization using NURBS based IGA of the internal and external virtual work for the membranes described in the previous section. For books on FEM see for instance Ottosen and Petersson [60] or Bathe [64], and on IGA, see Hughes et al. [55].

From the internal and external virtual work the internal and external forces can be derived

$$\delta W_{\text{int}} = \delta \mathbf{u}^T \mathbf{f}^{\text{int}}; \quad \delta W_{\text{ext}} = \delta \mathbf{u}^T \mathbf{f} \quad (3.60)$$

where

$$\delta \mathbf{u} = \begin{bmatrix} \delta \hat{\mathbf{u}}_1 \\ \vdots \\ \delta \hat{\mathbf{u}}_A \\ \vdots \\ \delta \hat{\mathbf{u}}_{nm} \end{bmatrix}; \quad \mathbf{f}^{\text{int}} = \begin{bmatrix} \mathbf{f}_1^{\text{int}} \\ \vdots \\ \mathbf{f}_A^{\text{int}} \\ \vdots \\ \mathbf{f}_{nm}^{\text{int}} \end{bmatrix}; \quad \mathbf{f} = \begin{bmatrix} \mathbf{f}_1 \\ \vdots \\ \mathbf{f}_A \\ \vdots \\ \mathbf{f}_{nm} \end{bmatrix} \quad (3.61)$$

where $\delta \hat{\mathbf{u}}_A$ is the variation of the control point displacement vector for the A :th control point, $\mathbf{f}_A^{\text{int}}$ is the internal force vector for the A :th control point, and \mathbf{f}_A is the external force vector for the A :th control point. The column matrices \mathbf{f} and \mathbf{f}^{int} contain the internal and external force vectors, respectively.

The equilibrium condition $\delta W_{\text{int}} - \delta W_{\text{ext}} = 0$ should hold for any virtual displacements and can thus be written as

$$\mathbf{f}^{\text{int}} - \mathbf{f} = 0. \quad (3.62)$$

To reach that expression the following FE discretizations are used for the displacements and virtual displacements, where the Galerkin method is adopted

$$\mathbf{u} = \sum_{A=1}^{nm} \tilde{N}_A \hat{\mathbf{u}}_A; \quad \delta \mathbf{u} = \sum_{A=1}^{nm} \tilde{N}_A \delta \hat{\mathbf{u}}_A \quad (3.63)$$

where $\hat{\mathbf{u}}_A$ is the control point displacement vector for the A :th control point, $\delta \hat{\mathbf{u}}_A$ is the variation of the control point displacement vector for the A :th control point and \tilde{N}_A is the A :th bi-variate NURBS basis function

$$\tilde{N}_A(\xi, \eta) = \frac{N_{i,p}(\xi)M_{j,q}(\eta)\omega_{i,j}}{\sum_{k=1}^n \sum_{l=1}^m N_{k,p}(\xi)M_{l,q}(\eta)\omega_{k,l}} = \frac{N_{i,p}(\xi)M_{j,q}(\eta)\omega_{i,j}}{W(\xi, \eta)} \quad (3.64)$$

where the tilde on the left hand side has been dropped for convenience in subsequent equations. No summations are implied on the right hand side in Eq. (3.64), and the commas do not denote differentiation with respect to the parametric coordinates. The global bivariate basis number A is related to i, j through

$$A = n(j - 1) + i \quad (3.65)$$

where n is the number of control points in the first direction of the control point net.

The internal virtual work from Eq. (3.59) is for convenience rewritten in matrix notation as

$$\delta W_{\text{int}} = \int_{\Omega_0} (\delta \boldsymbol{\epsilon})^T \mathbf{n} dA; \quad \delta \boldsymbol{\epsilon} = \begin{bmatrix} \delta \epsilon_{11} \\ \delta \epsilon_{22} \\ 2\delta \epsilon_{12} \end{bmatrix}; \quad \mathbf{n} = \begin{bmatrix} n^{11} \\ n^{22} \\ n^{12} \end{bmatrix}. \quad (3.66)$$

To introduce the discretization the virtual strains are written explicitly

$$\delta \boldsymbol{\epsilon} = \begin{bmatrix} \delta \epsilon_{11} \\ \delta \epsilon_{22} \\ 2\delta \epsilon_{12} \end{bmatrix} = \begin{bmatrix} \mathbf{A}_1 \cdot \delta \mathbf{u}_1 + \mathbf{u}_1 \cdot \delta \mathbf{u}_1 \\ \mathbf{A}_2 \cdot \delta \mathbf{u}_2 + \mathbf{u}_2 \cdot \delta \mathbf{u}_2 \\ \mathbf{A}_1 \cdot \delta \mathbf{u}_2 + \mathbf{A}_2 \cdot \delta \mathbf{u}_1 + \mathbf{u}_2 \cdot \delta \mathbf{u}_1 + \mathbf{u}_1 \cdot \delta \mathbf{u}_2 \end{bmatrix} \quad (3.67)$$

after the discretization the virtual strain is

$$\delta \boldsymbol{\epsilon} = \begin{bmatrix} \mathbf{A}_1 \cdot (N_{A,1} \delta \hat{\mathbf{u}}_A) + \mathbf{u}_1 \cdot (N_{A,1} \delta \hat{\mathbf{u}}_A) \\ \mathbf{A}_2 \cdot (N_{A,2} \delta \hat{\mathbf{u}}_A) + \mathbf{u}_2 \cdot (N_{A,2} \delta \hat{\mathbf{u}}_A) \\ \mathbf{A}_1 \cdot (N_{A,2} \delta \hat{\mathbf{u}}_A) + \mathbf{A}_2 \cdot (N_{A,1} \delta \hat{\mathbf{u}}_A) + \mathbf{u}_2 \cdot (N_{A,1} \delta \hat{\mathbf{u}}_A) + \mathbf{u}_1 \cdot (N_{A,2} \delta \hat{\mathbf{u}}_A) \end{bmatrix} \quad (3.68)$$

where summation over the repeated index A is implied, the equations are re-written as

$$\delta \boldsymbol{\epsilon} = \begin{bmatrix} N_{A,1} \mathbf{a}_1 \cdot \mathbf{e}_1 & N_{A,1} \mathbf{a}_1 \cdot \mathbf{e}_2 & N_{A,1} \mathbf{a}_1 \cdot \mathbf{e}_3 \\ N_{A,2} \mathbf{a}_2 \cdot \mathbf{e}_1 & N_{A,2} \mathbf{a}_2 \cdot \mathbf{e}_2 & N_{A,2} \mathbf{a}_2 \cdot \mathbf{e}_3 \\ \mathbf{b}_3 \cdot \mathbf{e}_1 & \mathbf{b}_3 \cdot \mathbf{e}_2 & \mathbf{b}_3 \cdot \mathbf{e}_3 \end{bmatrix} \delta \hat{\mathbf{u}}_A = \mathbf{B}_A \delta \hat{\mathbf{u}}_A \quad (3.69)$$

where

$$\begin{aligned} \mathbf{a}_1 &= \mathbf{A}_1 + \mathbf{u}_1 \\ \mathbf{a}_2 &= \mathbf{A}_2 + \mathbf{u}_2 \\ \mathbf{b}_3 &= N_{A,2} \mathbf{a}_1 + N_{A,1} \mathbf{a}_2 \end{aligned} \quad (3.70)$$

and the discrete forms of the covariant base vectors and displacement vector derivatives are

$$\mathbf{A}_\alpha = \sum_{A=1}^{nm} N_{A,\alpha} \mathbf{R}_A; \quad \mathbf{u}_{,\alpha} = \sum_{A=1}^{nm} N_{A,\alpha} \hat{\mathbf{u}}_A. \quad (3.71)$$

For computer implementation the virtual strain is rewritten as

$$\delta \boldsymbol{\epsilon} = \begin{bmatrix} \mathbf{B}_1 & \cdots & \mathbf{B}_A & \cdots & \mathbf{B}_{nm} \end{bmatrix} \delta \mathbf{u} = \mathbf{B} \delta \mathbf{u} \quad (3.72)$$

from which we get the discretized internal forces

$$\delta W_{\text{int}} = \delta \mathbf{u}^T \mathbf{f}^{\text{int}} = \delta \mathbf{u}^T \int_A \mathbf{B}^T \mathbf{n} dA \quad (3.73)$$

where \mathbf{n} is from Eq. (3.66).

The components of the discrete membrane stress resultants in matrix notation are computed as

$$\mathbf{n} = \frac{Et}{1 - \nu^2} \mathbf{C} \boldsymbol{\epsilon} \quad (3.74)$$

where the covariant strain components are

$$\boldsymbol{\epsilon} = \begin{bmatrix} \epsilon_{11} \\ \epsilon_{22} \\ 2\epsilon_{12} \end{bmatrix} = \begin{bmatrix} \mathbf{A}_1 \cdot \mathbf{u}_1 + \frac{1}{2} \mathbf{u}_1 \cdot \mathbf{u}_1 \\ \mathbf{A}_2 \cdot \mathbf{u}_2 + \frac{1}{2} \mathbf{u}_2 \cdot \mathbf{u}_2 \\ [\mathbf{A}_1 \cdot \mathbf{u}_2 + \mathbf{A}_2 \cdot \mathbf{u}_1 + \mathbf{u}_2 \cdot \mathbf{u}_1] \end{bmatrix} \quad (3.75)$$

and the matrix \mathbf{C} by use of Eq. (3.57) becomes

$$\mathbf{C} = \begin{bmatrix} (A^{11})^2 & \nu A^{11} A^{22} + (1 - \nu)(A^{12})^2 & A^{11} A^{12} \\ \text{sym.} & (A^{22})^2 & A^{22} A^{12} \\ & & \frac{1}{2} [(1 - \nu) A^{11} A^{22} + (1 + \nu)(A^{12})^2] \end{bmatrix}. \quad (3.76)$$

The equations are implemented in an element form and integrated numerically using Gaussian quadrature over a parent element.

3.6.5 The linear elastic NURBS based Kirchhoff-Love shell

To perform verification studies after the form finding has been performed, a small displacements, linear elastic NURBS based Kirchhoff-Love shell is implemented. To describe the strains up to first order in \mathbf{u} , the quadratic terms of the membrane strains are neglected, leading to

$$\epsilon_{\alpha\beta} = \frac{1}{2} (\mathbf{A}_\alpha \cdot \mathbf{u}_{,\beta} + \mathbf{A}_\beta \cdot \mathbf{u}_{,\alpha}) \quad (3.77)$$

which is supplemented with the linearized bending strains

$$\kappa_{\alpha\beta} = -\mathbf{A}_{\alpha,\beta} \cdot \Delta \mathbf{a}_3 - \mathbf{u}_{\alpha,\beta} \cdot \mathbf{A}_3 \quad (3.78)$$

with

$$\Delta \mathbf{a}_3 = \mathbf{a}_3 - \mathbf{A}_3 = -\frac{1}{|\mathbf{A}_1 \times \mathbf{A}_2|} \{ \mathbf{A}_3 \times [\mathbf{A}_3 \times (\mathbf{u}_1 \times \mathbf{A}_2 + \mathbf{A}_1 \times \mathbf{u}_2)] \} \quad (3.79)$$

approximated to the first order in \mathbf{u} . For detailed derivations and the corresponding strain-displacement matrices for FE-implementation, see [70].

3.7 DYNAMIC RELAXATION

Dynamic relaxation was first suggested by Day [39] and further adopted to form finding of lightweight and large span tension structures by Barnes [40,71]. For a thorough discussion on

dynamic relaxation, see [72] and [73]. There are several reasons for using dynamic relaxation for the form finding. It is a vectorized method, for which the cost of each iteration is cheap, resulting in that rapid results can be obtained. It is possible for the user to interact with the relaxation process, since the result from the last iteration can be used as an initial guess for a new problem, where for instance, the material properties or initial geometry is slightly modified. Since it is a dynamic method the presence of a mass matrix makes it possible to handle singularities of the stiffness matrix in the direction perpendicular to the surface of the membranes. The method is suitable for parallelization and has shown good performance on GPUs [74].

The dynamic relaxation method solves static problems by adding fictitious masses, fictitious damping and by using explicit time integration. The equation of motion (EOM) is given by

$$\mathbf{M}\ddot{\mathbf{u}} + \mathbf{C}\dot{\mathbf{u}} + \mathbf{f}^{\text{int}} = \mathbf{f} \quad (3.80)$$

where \mathbf{f}^{int} is the column matrix of internal forces, \mathbf{f} is the column matrix of external forces, \mathbf{M} is the mass matrix, \mathbf{C} is the damping matrix, and \mathbf{u} contains the unknown displacements. Since only the static solution is of interest only \mathbf{f} and \mathbf{f}^{int} must represent the physical problem, all other parameters can be chosen freely. To obtain the motion in time the EOM is integrated using the central difference integration scheme

$$\dot{\mathbf{u}}^{t_n-h/2} = (\mathbf{u}^{t_n} - \mathbf{u}^{t_n-h})/h; \quad \ddot{\mathbf{u}}^{t_n} = (\dot{\mathbf{u}}^{t_n+h/2} - \dot{\mathbf{u}}^{t_n-h/2})/h \quad (3.81)$$

$$\dot{\mathbf{u}}^n = \frac{1}{2}(\dot{\mathbf{u}}^{n-h/2} + \dot{\mathbf{u}}^{n+h/2}) \quad (3.82)$$

which applied to Eq. (3.80) gives a set of equations that update the velocities and displacements as

$$\dot{\mathbf{u}}^{t_n+h/2} = \frac{(2 - ch)}{(2 + ch)} \dot{\mathbf{u}}^{t_n-h/2} + 2h\mathbf{M}^{-1} \frac{(\mathbf{f} - \mathbf{f}^{\text{int}})}{(2 + ch)} \quad (3.83)$$

$$\mathbf{u}^{t_n+h} = \mathbf{u}^{t_n} + h\dot{\mathbf{u}}^{t_n+h/2} \quad (3.84)$$

where \mathbf{M} must be diagonal to preserve the explicit form of the central difference integrator, [73]. \mathbf{C} is chosen as being mass proportional, $\mathbf{C} = c\mathbf{M}$, where c is a damping coefficient for the structure, h is the time step. In the first iteration, $t = 0$ and \mathbf{u}^0 is known, then

$$\dot{\mathbf{u}}^{0+h/2} = h\mathbf{M}^{-1}(\mathbf{f} - \mathbf{f}^{\text{int}})/2. \quad (3.85)$$

Critical damping There are two common alternatives for choosing \mathbf{M} and \mathbf{C} . The first is to use critical damping. To ensure numerical stability and optimal convergence rate the diagonal entries of \mathbf{M} are chosen as suggested in [73] by

$$M_{ii} = \frac{1}{4} \hat{h}^2 \sum_j |K_{ij}|; \quad \text{no sum on } i \quad (3.86)$$

where $\hat{h} = 1.1h$ and the elements of the stiffness matrix K_{ij} are either computed by numerical differentiation of the internal force vector, [73], or derived analytically. The damping coefficient c is chosen to critically damp the lowest eigenmode

$$c = 2\omega_{\min} \quad (3.87)$$

which is estimated by use of Rayleigh's principle

$$\omega_{\min}^2 = \frac{\mathbf{u}^T \mathbf{K} \mathbf{u}}{\mathbf{u}^T \mathbf{M} \mathbf{u}}. \quad (3.88)$$

The stop criterion of the dynamic relaxation process is when the norm of the residual is smaller than a chosen value, as $\|\mathbf{f} - \mathbf{f}^{\text{int}}\|_2 < \epsilon_{\text{err}}$, where $\|\bullet\|_2$ is the Euclidean norm.

Kinetic damping An alternative to viscous damping is to use kinetic damping, [71], where the total kinetic energy of the system is traced through the motion in time and once a peak is detected the current velocities are set to zero, see Fig. 3.6. The EOM for kinetic damping is

$$\mathbf{M} \ddot{\mathbf{u}} + \mathbf{f}^{\text{int}} = \mathbf{f} \quad (3.89)$$

and the set of equations to update the velocities and displacements are simplified

$$\dot{\mathbf{u}}^{t_n+h/2} = \dot{\mathbf{u}}^{t_n-h/2} + h\mathbf{M}^{-1}(\mathbf{f} - \mathbf{f}^{\text{int}}) \quad (3.90)$$

$$\mathbf{u}^{t_n+h} = \mathbf{u}^{t_n} + h\dot{\mathbf{u}}^{t_n+h/2}. \quad (3.91)$$

While kinetic damping typically requires more iterations to converge than the critically damped system, it is cheaper per iteration since it is not necessary to formulate \mathbf{K} or update \mathbf{M} . On the other hand it requires a user selection of \mathbf{M} that is problem dependent.

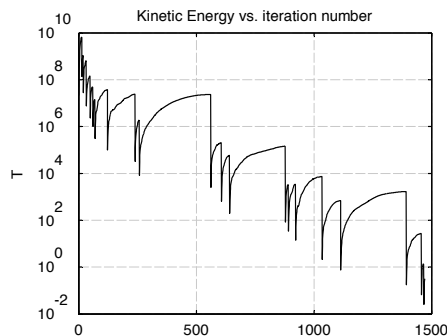


Figure 3.6: Example of kinetic damping. The kinetic energy is reset each time a peak is detected.

4 Applications of form finding

In this thesis, not only classical form finding was studied and applied as in the IGA form finding plugins but also form finding in a broader sense was used for finding of forms for vibration reduction. For the latter it is not about finding an equilibrium shape for a certain stress state, but about finding shapes of masses which reduce incoming vibrations at a sensitive facility and where again the geometry plays a vital part. Perhaps a fitting definition of form finding in this case could be: *to derive geometric shapes which positively influence mechanical or other performance based aspects, and which can support architectural design.*

This chapter presents applications of form finding developed in this research and some results of their use.

4.1 FORMS FOR VIBRATION REDUCTION IN AN URBAN SCALE

Most existing tools for conceptual structural computations focus on problems related to statics. However, on some occasions it is important to consider dynamic effects in the conceptual design phase. As our cities continue to grow and get denser, noise and vibration pollution will be important to consider. In the prototype tool presented here a method proposes how to place masses or buildings to reduce vibrations nearby a high-tech facility which is sensitive to vibrations.

4.1.1 Max IV

MAX-lab (Synchrotron light source) is a national laboratory in Lund, which is operated jointly by the Swedish Research Council (VR) and Lund University.

MAX-IV consists of an electron pre-accelerator, a 250 meter long linear accelerator, and two storage rings with 96 and 528 meters circumference, respectively. The facility is located north-

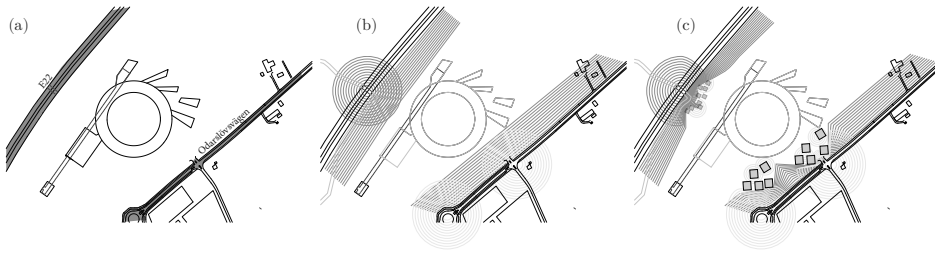


Figure 4.1: Research idea: (a) roads close to facility (b) vibrations from roads (c) reduced by masses of buildings placed in patterns.

east of Lund, at the outskirts of a new area, Lund North-East, roughly 100 meters southeast of the highway E-22, see Fig. 4.1 (a).

4.1.2 Problem statement

The instruments that are operating on nano-level scale at MAX-IV are sensitive to vibrations, where a vertical displacement requirement of 20-30nm RMS during one second for frequencies above 5Hz and below 100Hz has been set in order to ensure good quality of the measurements. With the facility located closely to the highway, vibration reduction measures have been taken to ensure good operation of the facility. The measures include stabilization of the soil underneath the facility to a depth of 4m (stiffening), and the shaping of the ground topography around the facility in a way that will reduce vibrations, see [75]. Other more conventional methods for vibration reduction have also been studied, such as open and in-filled trenches.

Placing out patterns of heavy masses or buildings on the soil surface between the external sources and the facility, see Fig. 4.1(c), could be seen as a cost effective and maintenance free solution, and as one that is more appropriate in an urban situation than more traditional methods such as trenches. As such, it is of interest to find out if it is a possible method of vibration mitigation, and which configurations are most effective.

4.1.3 Earlier studies

Prior experience has shown that separation of functions in urban planning may not be such a great idea. Mixed use zoning has once again become popular due to benefits such as reduced distances between housing, workplaces and retail, more compact development, and a more lively urban fabric. As the office sleeps the living room is awake meaning the mixed used zone has more potential as an active place. Prior to this research an Architectural thesis was done at Chalmers University of Technology, at the department of Architecture [76]. In that thesis

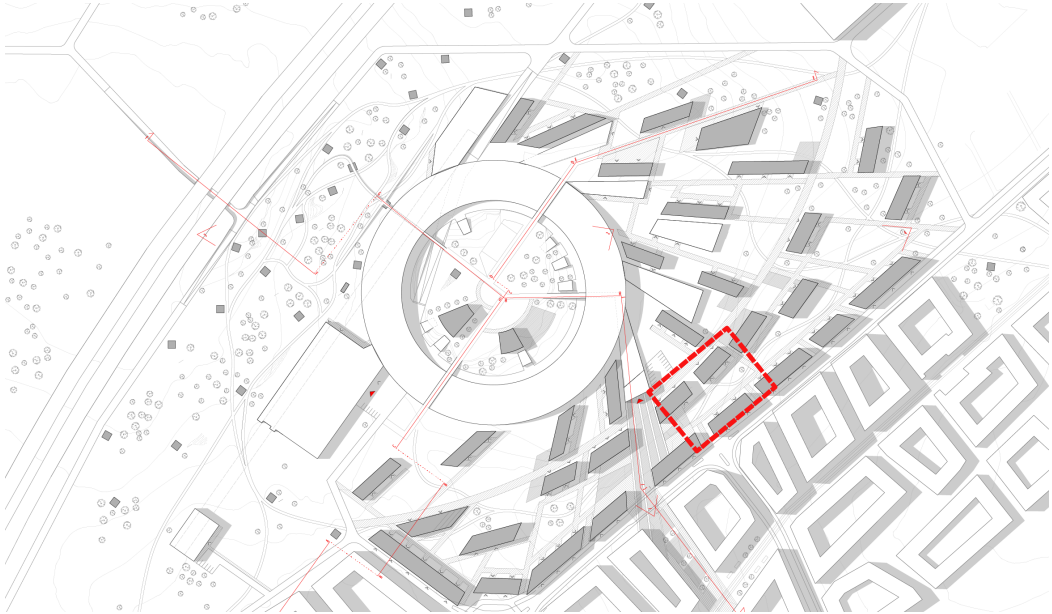


Figure 4.2: Plan from architectural master’s thesis, 80 by 60 meter part that was used in Fig. 4.7 marked in red, [76].

the area around the new research facility Max-IV, was studied and a proposal was done with the ambition to incorporate Max-IV closer into the city of Lund. Building a bit on the mixed use idea the citizens of Lund living nearby MAX-IV would be exposed to a pool of knowledge, but the question to answer was in what way could MAX-IV benefit from the proximity? One idea during the Architectural thesis was that placing the buildings in specific patterns could potentially reduce the incoming vibrations from surrounding traffic.

The architectural thesis built up an urban design, see Fig. 4.2, from solutions that worked well in a digital Ripple Tank Simulator, as well as, physical experiments with scale models using JELL-O as soil and placing out masses on top as buildings. The research presented here was done later to provide a conceptual tool which simulates the wave propagation phenomena. From the conceptual tool vibration reduction by placing different patterns of masses on the ground was investigated.

4.1.4 Computational model

A full 3-D model was created with the aim to study the vibration reduction effects of masses. Pre-processing was carried out in *ABAQUS* and the global system matrices \mathbf{K} , \mathbf{C} , and \mathbf{M} were exported into *MATLAB* where a dynamic model reduction was performed in order to reduce the number of degrees of freedom and speed up the analysis. The dynamic reduction was computationally intensive requiring too much memory on the full 3D model. This was

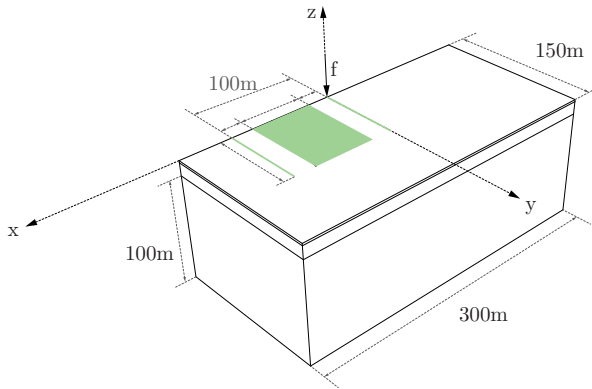


Figure 4.3: 3D model with the retained dofs in the reduced model marked in green.

instead solved by dividing the model into substructures and performing the reduction in several iterations, see the following section or Section 3.5.3. Different organizations of masses were finally assembled on the green area, see Fig. 4.3, and a frequency sweep analysis in steady state was performed, ranging from 5 to 29Hz with 2Hz steps and unit loading applied at the origin. The results were evaluated in terms of the root mean square value (RMS) of the vertical displacement magnitudes, along the green line at a distance of 100m from the load. For the material parameters and details, see Paper A.

Substructuring and dynamic reduction of soil model

Fig. 4.3 shows the final dimensions of the model and the master degrees of freedom from the soil model which were retained after reduction of the system. The reduced system matrices from the dynamic reduction method are frequency dependent and only give exact solutions at a certain frequency meaning that a reduced system was constructed for each frequency that was part of the steady state analysis. As the largest displacements were in the 5-30Hz range and the number of samples had to be kept low, the frequencies studied ranged from 5-29Hz with steps of 2Hz.

Since the whole model had 2 620 860 complex degrees of freedom, performing a dynamic reduction directly proved to be computationally difficult. The structure was then divided into 25 substructures by simply slicing the model into pieces from the top view as indicated by Fig. 4.4 (a). The top view was used because it offered simplicity to the sub-structuring script. In addition, the bedrock elements were much longer in z -direction and using the top-view meant that the number of nodes in all three directions of the substructure would be fairly even providing a favourable ratio between internal and interface degrees of freedom. Each substructure contained about 100 000 degrees of freedom. Out of the 25 substructures only nine unique instances were identified, as indicated by the first digit in Fig. 4.4. Only nine

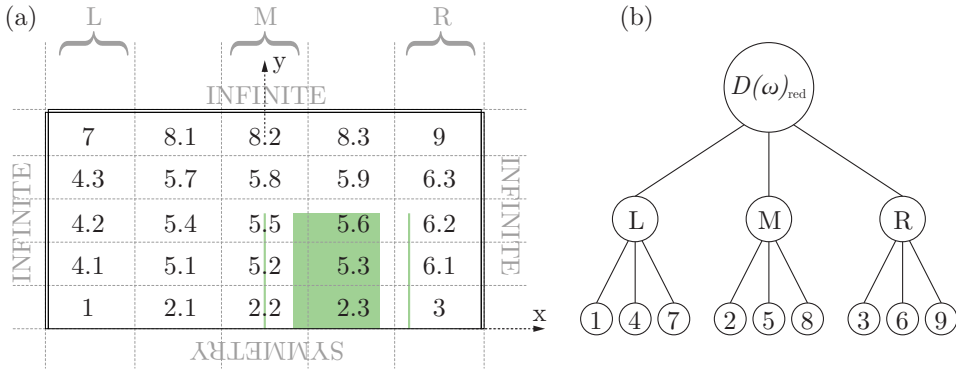


Figure 4.4: (a) Top view of model with substructures (b) Substructure assembly order.

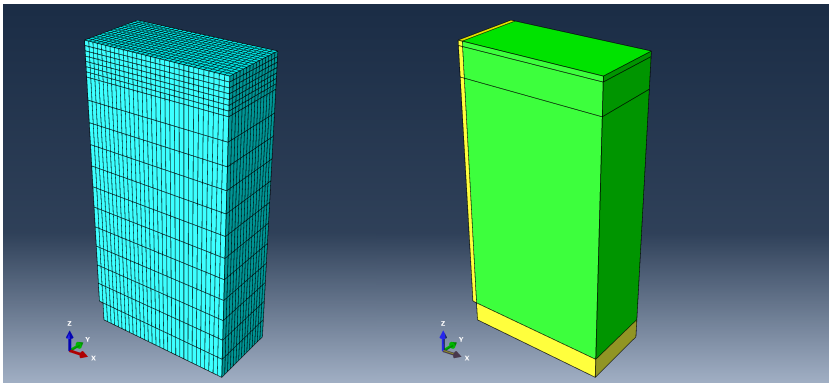


Figure 4.5: (left) Mesh of substructure 1 (right) Material layers of substructure 1, infinite layers are marked in yellow.

of the substructures were thus needed to build the final model. Fig. 4.5 shows the mesh and layers of substructure 1.

For each substructure the degrees of freedom to be retained, to be reduced and to be used as interfaces between structures were identified. In the first sub-structuring step shown in the bottom of Fig. 4.4 (b), the interior degrees of freedom were reduced in all nine substructures. In step two the *Left*, *Middle* and *Right* parts consisting of (1 - 4.1 - 4.2 - 4.3 - 7), (2.2 - 5.2 - 5.5 - 5.8 - 8.2) and (3 - 6.1 - 6.2 - 6.3 - 9), respectively were assembled to three separate structures. A new set of degrees of freedom could be identified to be retained and to be reduced at the next substructure level. Finally, in the third step the *Left*, 3 of the *Middle*, and *Right* parts were assembled and a third reduction was to form the final reduced matrix $\mathbf{D}(\omega)_{red}$ for each frequency.

The final reduced system then contained the dofs at the marked area in Fig. 4.3, the load dofs and the evaluation dofs. In the study different patterns of volumes with point masses were

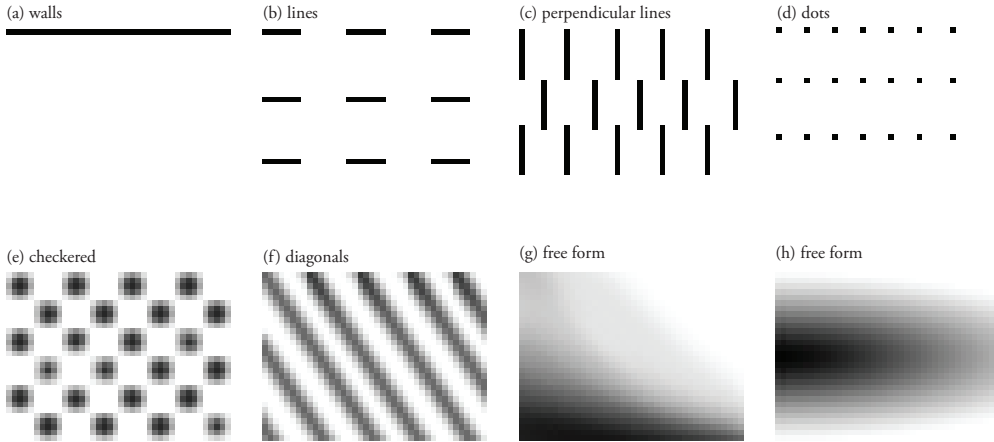


Figure 4.6: Different types of patterns used in 3D simulations.

assembled to the reduced model. Initially it was planned to use the whole soil area between the load and evaluation point for placement of masses. However, since the reduced soil system consisted of full and complex matrices it was important to keep down the number of degrees of freedom as much as possible (and 2D results showed that locating masses too close to the load was unfavourable). The final reduced soil model consisted of 11646 degrees of freedom, taking up about 2.5Gb of memory per matrix. To further keep down the memory only the dynamic matrices $\mathbf{D}(\omega) = \mathbf{K} + i\omega\mathbf{C} - \omega^2\mathbf{M}$ were kept. The reduced model usually took between 10-20 minutes to run, depending on the amount of masses assembled on top, while the large FE-model took days.

Patterns

The final reduced model consisted of an area to place masses that was between $x \in [20 : 80]$, $y \in [0 : 80]$. With a mesh size of two by two meters, the total number of possible positions for placing a mass was $30 \cdot 40 = 1200$. A function was written to read grey-scale images of 30×40 pixels, where each pixel was a possible position for a mass and the value of the pixel was used for the mass density, white meant no density (no mass assembled at the position) and black meant the largest density, $\rho = 8271 \text{kg/m}^3$ unless otherwise stated. The same type of 20-node quadratic brick elements *C3D20R* were used for the masses as for the soil. No material damping was applied to the masses, and Young's modulus was set to $E = 215 \text{MPa}$, and Poisson's ratio $\nu = 0.48$, which was the same as the properties for the upper soil layer.

The model allowed for any configuration of masses to be investigated. Fig. 4.6 shows some examples of the different types of patterns. The patterns that were studied were classified into the following types:

Walls were made of a line, or a set of lines that were parallel to the y -axis, that is perpendicular to the main wave-propagation direction from the source to the evaluation points, like a barrier.

Lines were similar to the walls, but did not span the whole distance along the y -axis, and if there were more rows of them they were allowed to be shifted in relation to each other.

Perpedicular lines were lines that were ordered to go in the main direction of the wave propagation.

Dots and checkered patterns were tried out both with individual masses (dots) placed in an ordered fashion, and also with larger sets of masses ordered in a checkered pattern.

Diagonals with many masses of varying density were tested.

Free form patterns were painted out in some different manners to see if anything out of the ordinary might happen.

Buildings. Some organizations of masses that were more in the scale of buildings were also tried out, for all of these the Young's modulus was set to $E = 30\text{GPa}$. Some parts of the buildings of the architectural thesis proposal were also tried as patterns.

4.1.5 Examples

Some results of using the tool are shown in Paper A. The tool is able to identify several important effects. Masses applied continuously over the whole area can lead to both reduction as well as amplification compared to having no masses. Amplification was obtained due to lensing as shown in Fig. 4.6 (h), or acting as wave guides, Fig. 4.6 (f), however, all patterns with discrete masses show reductions in vibrations; Small masses applied with large spacing are ineffective, Fig. 4.6 (d); Straight open paths from the load to the evaluation point lead to little reduction, Fig. 4.6 (b); Density variation for the different masses has a larger effect on vibration reductions than their position. The results concluded here are shown in Paper A.

In Figs. 4.7 and 4.8 simulations with a part of the building plan from the architectural thesis, are shown. A few different parts of the urban plan were studied, but the 3D steady-state model was too small to study the whole plan at once. No parts of those that were tried showed an increase in RMS of vertical displacement magnitude.

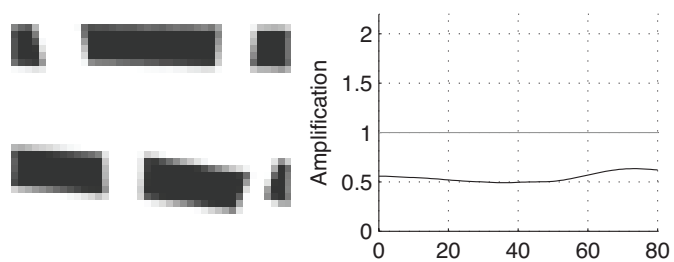


Figure 4.7: Part of pattern from Architectural Thesis, see Fig. 4.2.

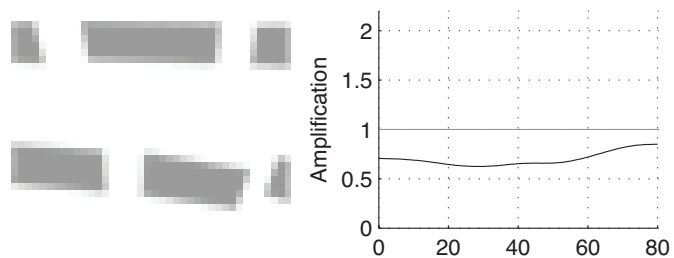


Figure 4.8: Part of pattern from Architectural Thesis, lower density.



Figure 4.9: Top left: Munich Olympic stadium (F. Otto). Top right: Concrete dome (H. Isler), image from Chriusha, Wikimedia Commons. Bottom left: L'Oceanogràfic (Félix Candela). Bottom right: Mannheim Multihalle (F. Otto/B. Happold).

4.2 IGA FORM FINDING PLUG-INS

4.2.1 Shell structures - context

Shells are efficient structures. They can resist bending, but in order to be efficient they should carry load primarily by in plane membrane stress (normal and shear stress in the tangent directions to the shell surface). If the dominant load of the shell is the self-weight then a shell which is given shape by a form finding process will carry that load efficiently. Other loads, such as, asymmetric snow and wind are then resisted through the shells bending capacity. If the shell is designed to be very efficient for carrying the dead load then it can become sensitive to imperfections and buckling, since thin shells have little bending resistance.

Modern thin concrete shells began to appear in the 1920s. Torroja and Nervi designed very expressive shell structures. Heinz Isler and Félix Candela pioneered the use of physical hanging models under gravity load for generating efficient forms for shell structures. In Fig. 4.9 a few examples are shown, including some projects by Frei Otto; the Olympic Stadium in Munich, and the Mannheim Multihalle.

Concrete shells are seldom built today, instead it is more common to use cable nets, textile membranes or steel grids. The structural difference of nets and membranes from shells is

that they are form-active systems without flexural stiffness and change their shape to carry the applied load. Shells are form-passive and do not adjust their shape to the loading conditions. Membranes and nets can be stiffened by prestress and then must be anticlastic (saddle-like) with a negative Gaussian curvature. A challenge shell structures face today is that building the form work is expensive, however new fabrication techniques such as 3d printing or pneumatic form works could improve on this.

4.2.2 Plug-ins

Conceptual design is an iterative procedure, and performing form finding often requires several iterations in order to get satisfactory results. To simplify this work flow, it is favorable to be able to perform the form finding in design software. Using design software can simplify the modeling of the related parameters, such as the initial geometry, the boundary conditions, material parameters etc. Buildings are generally designed in CAD software, and it is of interest to include form finding into CAD. In order to study the possibilities of performing form finding directly in CAD software using NURBS which are well supported by the CAD software two demonstrator plug-ins for form finding with dynamic relaxation on NURBS elements were developed.

The results from Papers B and C was used for developing two demonstrator plug-ins for Rhinoceros 3D and for Grasshopper. Rhinoceros 3D is a popular NURBS modeller commonly used in practice by architects and engineers. Grasshopper is a plug-in for Rhinoceros 3D which provides users with a visual programming environment (VPE), allowing users who are otherwise unfamiliar with programming to develop scripts and parametric models.

The plug-ins developed here have been written using RhinoCommon, which is a .NET plug-in Software Development Kit (SDK) available for Rhinoceros and Grasshopper.

A .NET library for FEA with support for IGA was implemented prior to the development of the plug-ins that acts as the back-end and runs the simulations independent of Rhino/Grasshopper. For the implemented library, the package Math.NET Numerics was used for the necessary linear algebra, together with Intel Math Kernel Library. Fig. 4.10 shows the different classes developed and how they relate to each other.

The general limitations of the plug-ins are that the plug-ins currently support form-finding with multiple patches, but there is no support for trimmed patches. There are, however, formulations of IGA with support for trimmed patches, but they have not been implemented here. The boundaries between adjoining patches need to be compatible, meaning that edges of bordering patches have to be compatible in their discretizations, i.e. exactly the same locations for control points, orders of interpolating functions, and the same knot vectors. The tools currently support uniformly applied loads to the initial geometry.

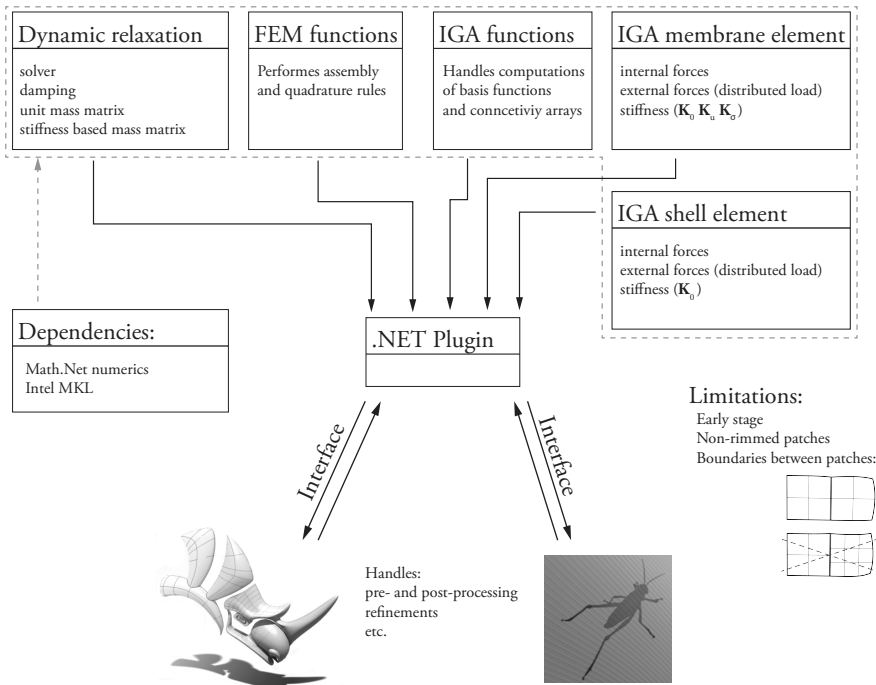


Figure 4.10: Schematic overview of plug-in parts.

4.2.3 Rhinoceros 3D plug-in

The first plug-in interfaces directly with Rhinoceros 3D, and provides form finding capabilities through a simple tabbed computer interface which many users are accustomed to. By filling out the different tabs a form finding can be performed in Rhino.

The interface of the Rhinoceros 3D plug-in is developed using Windows Presentation Foundation (WPF). The interface consists of a tabbed docking panel where initial geometries, materials, and boundary conditions can be set up. The form finding can be performed by filling in the tabs and interactively running the application. Fig. 4.11 shows the four tabs of the Rhinoceros plug-in UI. The first tab handles the initial geometry and the material parameters. The second one is for applying boundary conditions. The third panel is for applying uniformly distributed loads to the initial geometry. The last one controls the dynamic relaxation procedure and the relaxation parameters.

By first modelling the coarsest possible geometry the refinements to smaller elements can be handled by built in function in Rhinoceros. The limitations must be kept in mind while modelling the initial geometry, for instance, modelling a hole requires “patch” modelling techniques.

Using a CAD environment simplifies the modelling of the initial geometry compared to using a

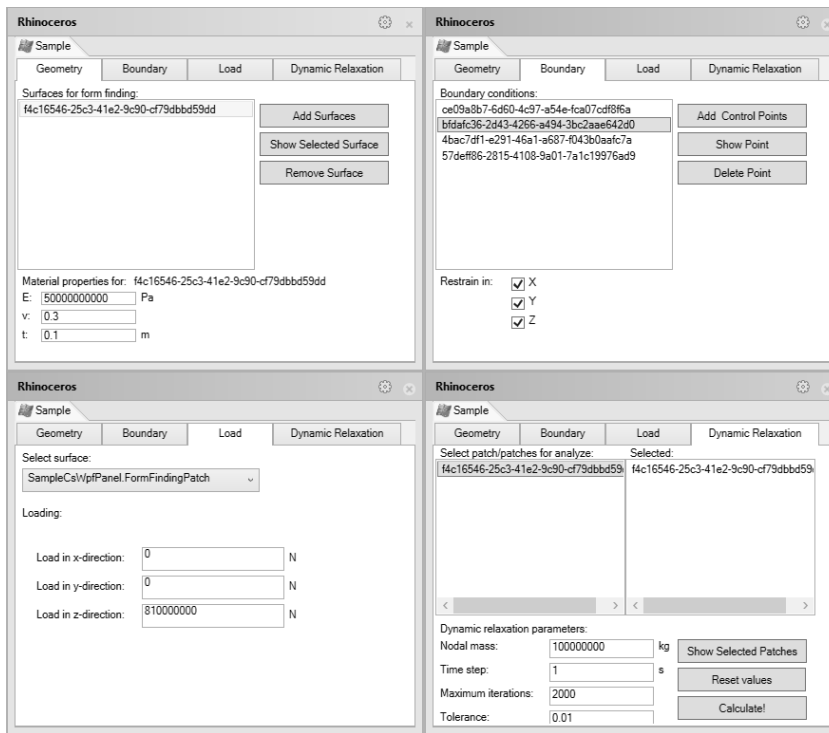


Figure 4.11: The four tabs of the Rhinoceros plug-in UI.

general finite element software. The form finding process typically requires several iterations to fulfil both architectural design and engineering criteria. This requires iterative modifications to the initial geometry which is simple to perform in a CAD software such as Rhinoceros, where unlike traditional FE-software an iterative workflow is important.

4.2.4 Grasshopper 3D plug-in

The second plug-in provides form finding capabilities through the Grasshopper VPE. The interface to the form finding is done through the use of custom Grasshopper components. The inclusion of form finding into Grasshopper makes it possible to create parametric architectural models, where the form finding is a part of the parametric model. Since the form finding is performed using NURBS all of the existing components and functions in Grasshopper can be applied after the form finding process.

The custom components for the Grasshopper VPE were developed using the Grasshopper SDK, and RhinoCommon.

A Grasshopper component can be regarded as a black-box function with a set of custom inputs

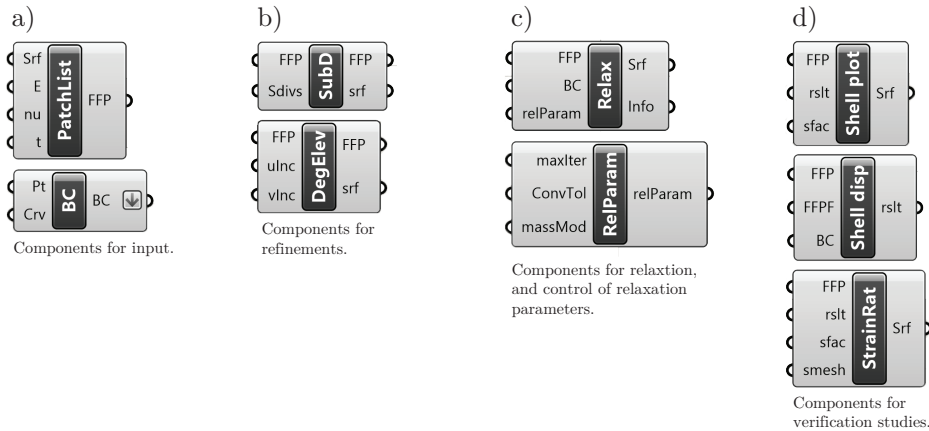


Figure 4.12: The developed grasshopper components, split into four categories: a) references to geometry, material, and boundary conditions. b) components for refinements. c) the dynamic relaxation and control. d) linear elastic small displacements Kirchhoff-Love shell components for studying the form found shape.

and outputs. Fig. 4.12 shows the developed Grasshopper components which are divided into four categories, components for input, components for refinements, components for the relaxation and finally components for verification studies.

4.2.5 Simple example

The capabilities of the two plug-ins are very similar, but since the UI of the second one, the Grasshopper plug-in, is not included in any of the appended papers its capability is shown in the following examples.

The ability to perform form finding with very few elements is favourable in design situations as it allows the designer to quickly explore alternative shapes. In the form finding exploration the first step is to define an initial shape, boundary conditions, material parameters and applied loads (typically the self-weight). Once this is done the the dynamic relaxation is run with a coarse mesh and the form found shape is computed. Some different shapes which were computed in virtually real-time using coarse meshes are shown in Paper C.

The purpose of this example is to show of the advantages of using NURBS elements to integrate the form finding in CAD. The example is intended for showing the design process a roof for a building. Fig. 4.13 shows the setup in Grasshopper for a simple form finding with an initial geometry with a single patch, consisting of one element which is subdivided twice into 4 X 4 NURBS elements with quadratic basis functions. The top left component in the figure (denoted Srf) refers to the initial geometry in Rhino. The bottom left component (denoted Pt)

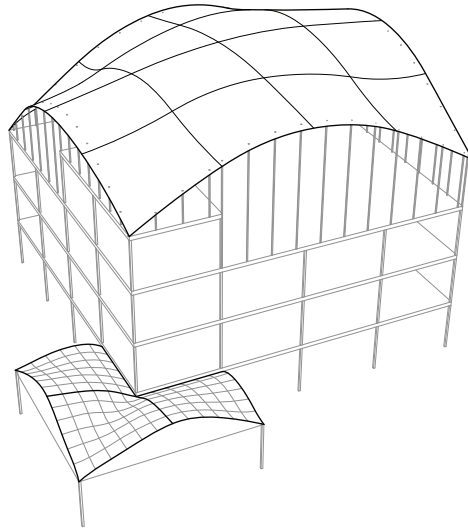


Figure 4.15: Building with added entrance, consisting of three patches.

refined and ran through the form finding process once again, in order to obtain a more optimal shape. This is shown in Paper C.

Integrating the process into Rhinoceros simplifies several parts which are often included in the design process. The form finding can be performed within the architectural context, and thus simplifies considerations related to the surrounding buildings, such as e.g. shading and reflections.

Since the form found shapes is in the design software and being represented by the complete curved geometry description it is easy to do architectural renderings to present to clients. Further detailing operations in CAGD be performed after the form finding since the geometry is still NURBS, and is well supported by the software. Another advantage of CAD tools is that they often include geometry diagnostics tools, such as curvature and edge analysis.

4.2.6 Multi-patch examples

For cases when more complex geometries than simple quadrilaterals are required, multiple patches can be studied. For the current example, if for instance an entrance would be designed at one of the corners of the building multiple patches are required for the geometry and the form finding, see Fig. 4.15.

If a rectangle is divided into multiple patches where the stiffness or boundary conditions are varied, various forms for the same initial surface can be explored, see Fig. 4.16.

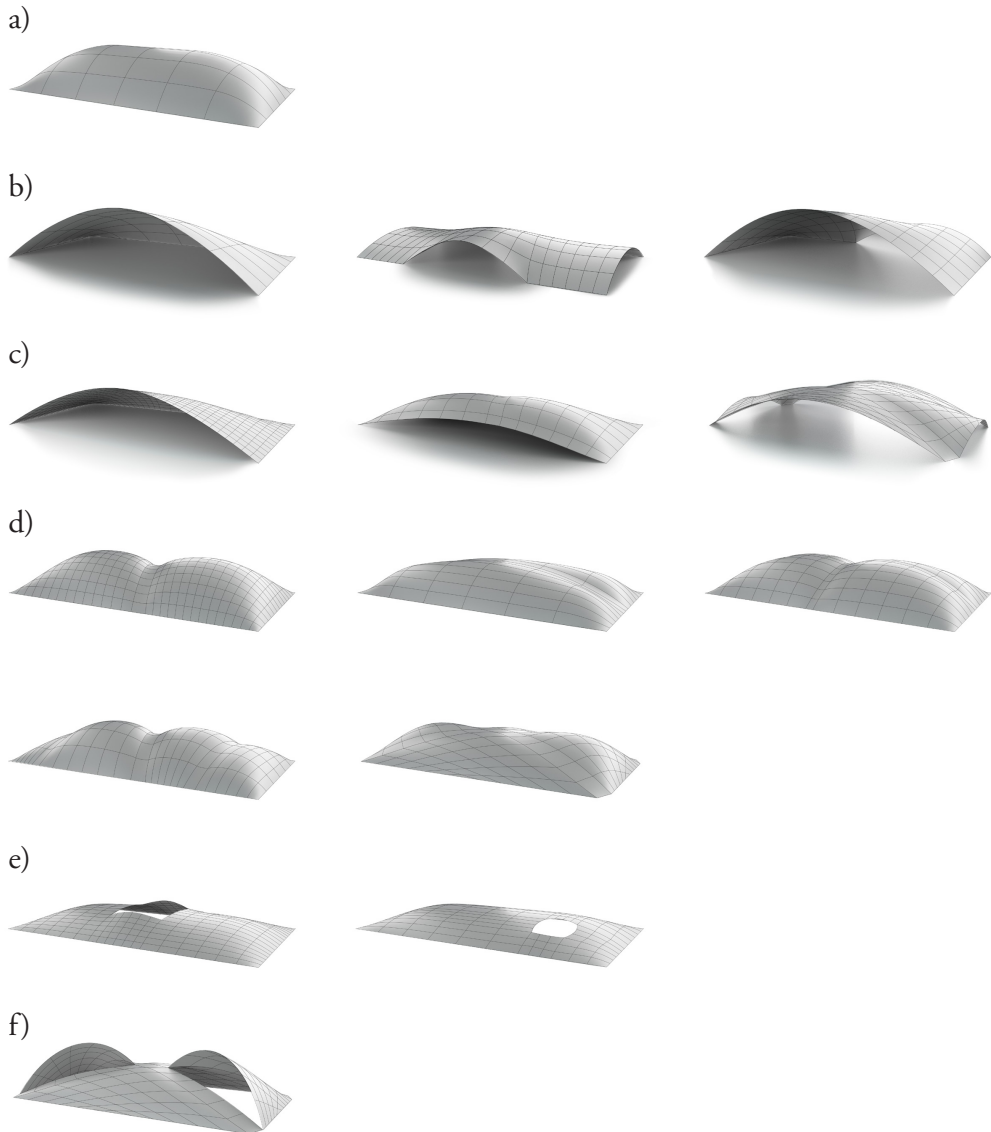


Figure 4.16: Examples with a rectangular initial shape, using multiple patches. a) single patch, fully constrained perimeter. b) multi-patch variants with perimeter openings. c) with stiffened bands and openings. d) with stiffened bands, fully constrained perimeter. e) with holes. f) with holes and stiffened bands.

5 Conclusions

In this thesis research concerning methods and tools suitable for including structural considerations in conceptual design is reported. A literature review and three research papers related to the development of new methods and tools in this research area is included. The main contributions of this thesis to the research field are:

- In Paper A a tool for studying vibration reduction by arrangement of masses is presented.
- The vibration reduction effects of patterns of masses on soil are shown in Paper A.
- Demonstrator tools for form finding by use of the hanging model analogy with IGA are developed, see Paper C and Section 4.2.
- The implementation of NURBS based IGA membrane elements with the dynamic relaxation solver is presented in Paper B. A study of how different choices of damping and mass affect the convergence of the dynamic relaxation method with NURBS based membrane elements is included.
- The advantages of using NURBS based IGA rather than classical finite elements for form finding are presented, see Papers B and C.

The reduction method used to reduce the number of dofs in the tool presented in Paper A made it possible to explore different alternatives quickly and find the most effective patterns, but also patterns that may even amplify the vibrations in the soil. In the paper, this was applied to the site of the new synchrotron research facility, MAX IV. However, tools such as this could be valuable in the planning of our urban environments, which are getting more populated and dense. Being able to get rapid predictions of vibrations in planned areas could allow for cities with reduced noise and vibration problems.

The convergence study with different choices of mass and damping in Paper B was made for a few different geometries. The study was made in order to ensure good performance in the later developed demonstrator tools. The choice of a mass matrix based on the initial stiffness and kinetic damping were implemented in the demonstrator tools for Rhino and Grasshopper.

Numerical form finding with the hanging model analogy is well developed, however, the use of NURBS elements brings some novel additions. It makes it possible to perform the form finding directly in a CAGD software, with geometry that is fully supported by the CAGD programs, in this case Rhino and Grasshopper. The NURBS elements are curved and C^1 continuity between elements can be achieved, which is favourable for form finding since the resulting shapes are often curved and continuous and the employed shell models for verification studies require C^1 . It is possible to perform the form finding with very few elements, rapidly providing previews of what a higher resolution mesh will result in, more or less in real-time. Wrinkling effects present in high resolution models are not observed for low resolution models. Supporting the form finding in Grasshopper means that it can be integrated into larger parametric models allowing for truly complex design explorations in context and simplifying the design process.

5.1 FURTHER RESEARCH

Tools similar to the one presented in Paper A could be useful in urban planning, in order to reduce the noise and vibrations in the built environment. The ability for an engineer to provide feedback to others of the design team in minutes is important, since it means that it can support a creative and collaborative brain-storming session which often is a part of the earliest design phases. To make the tool general, the model reduction process could be automated.

The reduction method used in Paper A works for steady state dynamics, if transient analyses are necessary other methods for reducing the simulation time are required. This could be other model reduction methods, or the use of other methods than FEM.

Form finding can be seen as a first step in a design process. The research has so far primarily dealt with numerical methods, and perhaps the most important further research would be to apply the tools to design projects and real applications, in order to test the tools and to develop their ideas further. The tools could be tested further in case studies where non-experts use the tools, in order to evaluate their usefulness.

The dynamic relaxation method studied in Paper B converges fast for systems where elements are uniformly sized. It could be constructive to study other solution methods, both explicit and implicit to find a method that converges fast for general element geometries. Another promising approach in explicit dynamics is the use of isogeometric collocation, which replaces all of the integration points in an element with a single collocation point, with potential to reduce computational costs.

Recently there have been developments of NURBS based IGA with trimmed patches. The methods are promising in that they simplify the application to complex geometries which are difficult to represent by non-trimmed patches.

6 Summary of appended papers and programs

Three papers have been appended to the thesis, and three tools related to conceptual structural design have been developed. Chapter 4 presents the developed tools and illustrates their use with some examples.

6.1 APPENDED PAPERS

Paper A

Form Finding for Ground Vibration Reduction in an Urban Scale.

Vedad Alic and Kent Persson.

Proceedings of IASS-SLTE Symposium 2014: Shells, Membranes and Spatial Structures: Footprints

Paper A investigates the search of forms in an urban scale that are effective in reducing vibration propagation from external sources, such as highways, high-speed railroads and industrial plants. It describes the implementation of a MATLAB tool for sketching different masses and investigating their effects on vibration reduction.

The author carried out all the simulations, performed the FE modelling in ABAQUS and the subsequent model reductions in MATLAB as well as developed the tool for sketching different arrangements of masses and drawing of conclusions. Other authors assisted in writing the paper and supervising the work.

Paper B

Form Finding with Dynamic Relaxation and Isogeometric Membrane Elements.

Vedad Alic and Kent Persson.

Published in: Computer Methods in Applied Mechanics and Engineering.

doi:10.1016/j.cma.2015.12.009

The use of isogeometric membrane elements together with dynamic relaxation as a means of

form finding is investigated. The applied theories of isogeometric analysis, membrane elements, and dynamic relaxation are briefly presented. Different mass and damping choices are tried and evaluated.

The author implemented the methods, carried out the investigations and wrote the paper. Other authors supported the writing and supervised the research.

Paper C

Using isogeometric elements and dynamic relaxation as a form finding technique.

Vedad Alic and Kent Persson.

Proceedings of IASS 2015 Amsterdam Symposium: Future Visions.

The paper describes the implementation of the Rhinoceros 3D plugin, and possible workflows using isogeometric membrane elements for form finding.

Part of the implementation of the Rhinoceros 3D plug-in was performed by a master's thesis student [77], together with the aid and supervision of the author. The author wrote the paper. Other authors supported the writing and supervised the research.

6.2 DEVELOPED DEMONSTRATOR PROGRAMS

During the work several tools have been developed to try out the methods: A tool for exploring optimal position of masses at the MAX IV site, a form finding plug-in for Rhinoceros 3D and a plug-in for the visual programming environment Grasshopper 3D.

Placing masses To explore different shapes of masses and their effect on mitigating soil wave propagations a tool was developed for sketching shapes of masses on top of soil. Developed by the author.

Rhinoceros 3D plug-in A Rhinoceros 3D [1] plug-in was developed for form finding of efficient shapes for shell structures. Developed by the author and by a master's thesis student [77].

Grasshopper 3D plug-in The Grasshopper 3D [2] plug-in uses the same back end as the Rhinoceros 3D plug-in. Developed by the author.

References

- [1] *Rhinoceros 3D*, <http://www.rhino3d.com/>, online; accessed 2015-10-05.
- [2] *Grasshopper*, <http://www.grasshopper3d.com/>, online; accessed 2015-10-05.
- [3] Landay, J., Myers, B., et al. (2001), *Sketching interfaces: Toward more human interface design*, *Computer* 34(3), 56–64.
- [4] Hsu, W., Liu, B. (2000), *Conceptual design: issues and challenges*, *Computer-Aided Design* 32(14), 849–850.
- [5] Wang, L., Shen, W., Xie, H., Neelamkavil, J., Pardasani, A. (2002), *Collaborative conceptual design—state of the art and future trends*, *Computer-Aided Design* 34(13), 981–996.
- [6] Salter, A., Gann, D. (2003), *Sources of ideas for innovation in engineering design*, *Research Policy* 32(8), 1309–1324.
- [7] Stromberg, L.L., Beghini, A., Baker, W.F., Paulino, G.H. (2012), *Topology optimization for braced frames: combining continuum and beam/column elements*, *Engineering Structures* 37, 106–124.
- [8] Mueller, C.T. (2014), *Computational exploration of the structural design space*, Ph.D. thesis, Massachusetts Institute of Technology.
- [9] Majowiecki, M. (2008), *The Free Form Design (FFD) in steel structural architecture—esthetic values and reliability*, *Steel Construction* 1(1), 3–15.
- [10] Schlaich, M. (2006), *Challenges in Education—Conceptual and Structural Design*, in: *IABSE Symposium Report*, vol. 92, 20–26, International Association for Bridge and Structural Engineering.
- [11] Allen, E., Zalewski, W. (2009), *Form and forces: designing efficient, expressive structures*, John Wiley & Sons.
- [12] Sutherland, I.E. (1964), *Sketch pad a man-machine graphical communication system*, in: *Proceedings of the SHARE design automation workshop*, 6–329, ACM.

- [13] Aish, R., Peters, B., Peters, T., *First Build Your Tools*, Inside Smartgeometry: Expanding the Architectural Possibilities of Computational Design 36–49.
- [14] *Dynamo*, <http://www.autodesk.com/products/dynamo-studio/overview>, online; accessed 2016-01-11.
- [15] Cottrell, J.A., Hughes, T.J., Bazilevs, Y. (2009), *Isogeometric analysis: toward integration of CAD and FEA*, John Wiley & Sons.
- [16] Rolvink, A., Coenders, J., Mueller, C. (2014), *State on the art of computational tools for conceptual structural design*, in: *Proceedings of the IASS-SLTE 2014 Symposium "Shells, Membranes and Spatial Structures: Footprints"*, Brasilia, Brazil, 15-19 September 2014, International Association for Shell and Spatial Structures (IASS).
- [17] Lindemann, J., Sandberg, G., Olsson, K.G. (2004), *An approach to teaching architectural and engineering students utilizing computational mechanics software ForcePAD*, ITcon 9, 219–228.
- [18] Lindemann, J., Dahlblom, O., Sandberg, G. (2001), *ObjectiveFrame-An educational tool for understanding the behaviour of structures*, in: *Applied Virtual Reality in Engineering & Construction Applicatins of Virtual Reality Current Initiatives and Future Challenges AVR II and CONVR*.
- [19] Akesson, D., Lindemann, J. (2015), *A tablet computer application for conceptual design*, Proceedings of the ICE - Engineering and Computational Mechanics 1–8.
- [20] *SAP2000*, <http://www.csiamerica.com/content/sap2000-24-model-alive-watch-learn1/>, online; accessed 2016-01-11.
- [21] *Autodesk ForceEffect*, <https://forceeffect.autodesk.com/>, online; accessed 2016-01-11.
- [22] Olsson, P. (2006), *Conceptual studies in structural design: pointSketch-a based approach for use in early stages of the architectural process*, Chalmers University of Technology.
- [23] *Karamba*, <http://www.karamba3d.com/>, online; accessed 2015-10-05.
- [24] *Kangaroo3d*, <http://www.kangaroo3d.com/>, online; accessed 2015-11-15.
- [25] *Robot Structural Analysis*, <http://www.autodesk.com/products/robot-structural-analysis/overview1>, online; accessed 2016-01-11.
- [26] Christensen, P.W., Klarbring, A. (2008), *An introduction to structural optimization*, vol. 153, Springer Science & Business Media.
- [27] Von Buelow, P. (2008), *Suitability of genetic based exploration in the creative design process*, Digital Creativity 19(1), 51–61.

- [28] Scott, S.D., Lesh, N., Klau, G.W. (2002), *Investigating human-computer optimization*, Proceedings of the SIGCHI conference on Human factors in computing systems Changing our world, changing ourselves - CHI '02 155.
- [29] *structureFIT*, <http://www.caitlinmueller.com/structurefit/>, online; accessed 2016-01-11.
- [30] Culmann, K. (1875), *Die graphische statik*, vol. 2, Meyer & Zeller (A. Reimann).
- [31] Lachauer, L., JUNGJOHANN, H., KOTNIK, T. (2011), *Interactive parametric tools for structural design*, in: *Proceedings of the International Association for Shell and Spatial Structures (IABSE-IASS) Symposium*.
- [32] Block, P., Ochsendorf, J. (2007), *Thrust network analysis: A new methodology for three-dimensional equilibrium*, JOURNAL-INTERNATIONAL ASSOCIATION FOR SHELL AND SPATIAL STRUCTURES 155, 167.
- [33] Adriaenssens, S., Block, P., Veenendaal, D., Williams, C. (2014), *Shell structures for architecture: form finding and optimization*, Routledge.
- [34] Coenders, J., Bosia, D. (2006), *Computational tools for design and engineering of complex geometrical structures: from a theoretical and a practical point of view.*, Rotterdam: Episode publishers.
- [35] Veenendaal, D., Block, P. (2012), *An overview and comparison of structural form finding methods for general networks*, International Journal of Solids and Structures 49(26), 3741–3753.
- [36] Turrin, M., von Buelow, P., Stouffs, R. (2011), *Design explorations of performance driven geometry in architectural design using parametric modeling and genetic algorithms*, Advanced Engineering Informatics 25(4), 656–675.
- [37] Schanz, S., Otto, F., Rasch, B., Bayern, D.W., Stuck, K.V., anlässlich der Preisverleihung des Deutschen Werkbundes Bayern an Frei Otto und Bodo Rasch, A. (2006), *Frei Otto, Bodo Rasch: Finding form: towards on architecture of the minimal; the Werkbund shows Frei Otto, Frei Otto shows Bodo Rasch; exhibition in the Villa Stuck, Munich, on the occasion of the award of the 1992 Deutscher Werkbund Bayern Prize to Frei Otto und Bodo Rasch*, Ed. Menges.
- [38] Ramm, E. (2011), *HEINZ ISLER SHELLS - THE PRIORITY OF FORM*, Journal of the International Association for Shell and Spatial Structures 52(3), 143–154.
- [39] Day, A. (1965), *An introduction to dynamic relaxation(Dynamic relaxation method for structural analysis, using computer to calculate internal forces following development from initially unloaded state)*, The engineer 219, 218–221.

- [40] Barnes, M. (1977), *Form-finding and analysis of tension space structures by dynamic relaxation.*, Ph.D. thesis, City University.
- [41] Schek, H.J. (1974), *The force density method for form finding and computation of general networks*, Computer methods in applied mechanics and engineering 3(1), 115–134.
- [42] Haug, E., Powell, G. (1972), *Analytical shape finding for cable nets*, in: *Proceedings of the 1971 IASS Pacific Symposium Part II on Tension Structures and Space Frames*, 1–5.
- [43] Argyris, J.H., Angelopoulos, T., Bichat, B. (1974), *A general method for the shape finding of lightweight tension structures*, Computer Methods in Applied Mechanics and Engineering 3(1), 135–149.
- [44] *CADenary tool v2*, <http://www.designexplorer.net/newscreens/cadenarytool/cadenarytool.html>, online; accessed 2016-01-11.
- [45] *SmartForm*, <http://www.smart-solutions-network.com/page/introduction-to-smartform>, online; accessed 2015-11-15.
- [46] *RhinoMembrane*, <http://www.ixforten.com/rhinomembrane.htm>, online; accessed 2015-11-15.
- [47] *RhinoVault*, <http://block.arch.ethz.ch/brg/tools/rhinovault>, online; accessed 2016-01-11.
- [48] Philipp, B., Breitenberger, M., Wüchner, R., Bletzinger, K.U. (2014), *Design of architectural membranes with isogeometric elements*, in: *11th World Congress on Computational Mechanics (WCCM XI)*.
- [49] Miki, M., Igarashi, T., Block, P. (2015), *Parametric self-supporting surfaces via direct computation of airy stress functions*, ACM Transactions on Graphics (TOG) 34(4), 89.
- [50] Piegl, L. (1991), *On NURBS: a survey*, IEEE Computer Graphics and Applications (1), 55–71.
- [51] Piegl, L., Tiller, W. (1997), *The NURBS book. 1997*, Monographs in Visual Communication .
- [52] Rogers, D.F. (2000), *An introduction to NURBS: with historical perspective*, Elsevier.
- [53] Cox, M.G. (1972), *The numerical evaluation of B-splines*, IMA Journal of Applied Mathematics 10(2), 134–149.
- [54] De Boor, C. (1972), *On calculating with B-splines*, Journal of Approximation Theory 6(1), 50–62.
- [55] Hughes, T.J., Cottrell, J.A., Bazilevs, Y. (2005), *Isogeometric analysis: CAD, finite elements, NURBS, exact geometry and mesh refinement*, Computer methods in applied mechanics and engineering 194(39), 4135–4195.

- [56] Cirak, F., Ortiz, M., Schroder, P. (2000), *Subdivision surfaces: a new paradigm for thin-shell finite-element analysis*, International Journal for Numerical Methods in Engineering 47(12), 2039–2072.
- [57] Celniker, G., Gossard, D. (1991), *Deformable curve and surface finite-elements for free-form shape design*, in: *ACM SIGGRAPH computer graphics*, vol. 25, 257–266, ACM.
- [58] Terzopoulos, D., Qin, H. (1994), *Dynamic NURBS with geometric constraints for interactive sculpting*, ACM Transactions on Graphics (TOG) 13(2), 103–136.
- [59] Kagan, P., Fischer, A., Bar-Yoseph, P.Z. (2003), *Mechanically based models: Adaptive refinement for B-spline finite element*, International Journal for Numerical Methods in Engineering 57(8), 1145–1175.
- [60] Ottosen, N.S., Petersson, H., Saabye, N. (1992), *Introduction to the finite element method*, Prentice Hall International.
- [61] Bazilevs, Y., Calo, V.M., Cottrell, J.A., Evans, J.A., Hughes, T., Lipton, S., Scott, M., Sederberg, T. (2010), *Isogeometric analysis using T-splines*, Computer Methods in Applied Mechanics and Engineering 199(5), 229–263.
- [62] Kim, H.J., Seo, Y.D., Youn, S.K. (2009), *Isogeometric analysis for trimmed CAD surfaces*, Computer Methods in Applied Mechanics and Engineering 198(37), 2982–2995.
- [63] Holzapfel, G.A. (2000), *Nonlinear solid mechanics*, vol. 24, Wiley Chichester.
- [64] Bathe, K.J. (2006), *Finite element procedures*, Klaus-Jurgen Bathe.
- [65] Craig, R., Kurdila, A. (2006), *Fundamentals of structural dynamics*, Wiley.
- [66] Qu, Z. (2004), *Model order reduction techniques: with applications in finite element analysis*, Springer.
- [67] Kiendl, J., Bletzinger, K.U., Linhard, J., Wüchner, R. (2009), *Isogeometric shell analysis with Kirchhoff–Love elements*, Computer Methods in Applied Mechanics and Engineering 198(49), 3902–3914.
- [68] Chapelle, D., Bathe, K.J. (2010), *The finite element analysis of shells-Fundamentals*, Springer Science & Business Media.
- [69] Bischoff, M., Bletzinger, K.U., Wall, W., Ramm, E. (2004), *Models and Finite Elements for Thin-Walled Structures*, Encyclopedia of computational mechanics .
- [70] Millán, D., Rosolen, A., Arroyo, M. (2011), *Thin shell analysis from scattered points with maximum-entropy approximants*, International Journal for Numerical Methods in Engineering 85(6), 723–751.

- [71] Barnes, M. (1988), *Form-finding and analysis of prestressed nets and membranes*, Computers & Structures **30**(3), 685–695.
- [72] Papadrakakis, M. (1981), *A method for the automatic evaluation of the dynamic relaxation parameters*, Computer methods in applied mechanics and engineering **25**(1), 35–48.
- [73] Underwood, P. (1983), *Dynamic relaxation(in structural transient analysis)*, Computational methods for transient analysis(A 84-29160 12-64). Amsterdam, North-Holland, 1983, 245–265.
- [74] Joldes, G.R., Wittek, A., Miller, K. (2010), *Real-time nonlinear finite element computations on GPU–Application to neurosurgical simulation*, Computer methods in applied mechanics and engineering **199**(49), 3305–3314.
- [75] Persson, P., Persson, K., Sandberg, G. (2014), *Reduction in ground vibrations by using shaped landscapes*, Soil Dynamics and Earthquake Engineering **60**, 31–43.
- [76] Alic, V. (2012), *Good vibrations*, Master’s thesis, Chalmers University of Technology.
- [77] Alexandersson, A. (2015), *Isogeometric analysis in form finding in architecture*, Master’s thesis, Chalmers University of Technology.

Part II

Appended publications

Paper A



Form Finding for Ground Vibration Reduction in an Urban Scale

Vedad ALIC*,
Kent H. PERSSON^a

*Division of Structural Mechanics, Lund University
Box 118, 221 00 Lund, Sweden
vedad.alic@construction.lth.se

^a Division of Structural Mechanics, Lund University

Abstract

Form-finding is traditionally thought of in context of structures whose performance is dependent on their shape, such as grid-shells or cable nets, among others. This paper extends traditional form-finding by investigating the search of forms in an urban scale that are effective in reducing vibration propagation from external sources, such as highways, high-speed railroads and industrial plan. The aim is to lower their negative impact on the built environment. The scale of the urban forms can range from buildings, down to stones or concrete blocks, depending on site conditions (geometry, medium of propagating waves, targeted frequencies).

In this paper a state-of-the-art synchrotron facility, that is located both near a high-way and a city will serve as an example. The facility is located on clay which has resonant frequencies within the range that the facility is sensitive to. It is investigated if further urbanization of the area between the facility and the city can contribute in mitigating vibrations from the external sources, in order to ensure operational conditions for the facility. Forms are investigated numerically by placing out blocks of masses on top of the soil surface, in a tool developed for an iterative study. The vibration levels from external sources are evaluated, with the aim of finding optimal solutions in terms of vibration reduction and suitability as an urban plan.

Results indicate that masses on the ground can be used as a means to mitigate ground vibration, but in order for them to be effective they need to be very heavy. Locating masses in a careful manner can be effective for vibration mitigation, and by combining masses of different densities reduction in a wider frequency range can be reached. Some conclusions from the research were: Forms where masses are applied continuously over the whole area can lead to amplification due to lensing or acting as wave guides, however, all discrete organizations of masses show reductions in vibrations. Density variation for the different masses has greater effect than their position.

Keywords: Conceptual design, form finding, optimization, urban scale, vibration reduction, surface masses, soil dynamics.

1. Introduction

In the architectural design process, a given set of design requirements normally have to be fulfilled. In traditional architectural design the earlier phases of design, assessing the fulfillment of design requirements relies on the insight of the designer and focuses on a limited range of objectives (like functional and aesthetical). For other objectives (like engineering related aspects), the assessment is usually postponed to relatively advanced phases in the process, where a number of relevant aspects of the design may be unexplored, but already limited by decisions taken concerning other objectives. The opposite also holds, if only the engineering aspects are focused upon, functional and aesthetical design requirements may not be fulfilled.

Due to the nature of early stage design the amount of time is very limited. An engineering team cannot come up with a complete solution in this limited time, the focus should instead be on gaining an understanding of the overall behavior, catching interesting phenomena, and highlighting potential critical aspects of the design.

The lack of early stage, project-specific heuristic knowledge, such as experience, intuition, rules of thumb, and precedent examples that can be used as a base for new design needs to be compensated. The methods used should preferably require small investments of consultant time, in order to cope with the unpredictable and

rapidly changing nature of early stage design, excluding traditional time-consuming application of analysis techniques.

Modelling tools utilized in conceptual studies must be capable of interactively modifying the model once it has been created. This is a fundamental aspect in any design activity, where the designer is constantly going forward and backwards, re-elaborating over some particular aspect of the model, or its general layout, or even coming back to a previous solution that had been temporarily abandoned. Supporting an interactive and iterative design process, requires new interaction models and numerical approaches in the tools used.

This paper proposes a method/tool for the search of forms in an urban scale that are effective in reducing vibration propagation from external sources, such as highways, high-speed railroads and industrial plants, in that way lowering their negative impact on the built environment. The scale of the urban forms can range from buildings, down to stones or concrete blocks, depending on site conditions (geometry, medium of propagating waves, targeted frequencies), and in that way the method can be used in collaboration between Architect and Engineering disciplines (collaboration since both engineering and architecture related aspects are being decided upon simultaneously) in cases where vibration pollution in the built society is of concern, which with the continued increase in urban population will be a concern.

The tool is able to predict relative vibration levels at the positions of interest and through an iterative study can lead to urban plans which are good at reducing soil wave propagation, and if care is taken with the design it can also enhance the aesthetic qualities of the site.

1.1. MAX-IV

To illustrate the method it is applied in a case study, at the site of MAX-IV, a new state-of-the-art synchrotron facility in Lund, Sweden. MAX-IV consists of an electron pre-accelerator, a 250 meter long linear accelerator, and two storage rings with 96 and 528 meters circumference respectively. The facility is located northeast of Lund, at the outskirts of a new area, Lund North-East roughly 100 meters southeast of the highway E-22. The instruments that are operating on nano-level scale at MAX-IV are sensitive to vibrations, where a vertical displacements limit of 20-30nm RMS during one second for frequencies above 5Hz and below 100Hz has been set in order to ensure good quality of the measurements. With the facility located closely to the highway and on top of very soft soil measures have been taken to ensure good operation of the facility. The measures include stabilization of the soil underneath the facility (stiffening), and the shaping of the ground topography around the facility in a way that will reduce vibrations, see for instance the study by Persson *et al* [8]. Other more conventional methods for vibration reduction have also been studied, such as open and in-filled trenches.

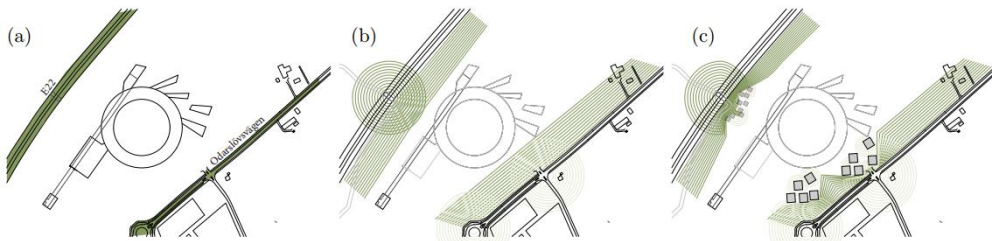


Figure 1: Research idea: (a) roads close to facility (b) vibrations from roads (c) reduced by masses?

Placing out heavy masses on the soil surface between the external sources and the facility, see Figure 1(c), could be seen as a cost effective and maintenance free solution, and as one that is more appropriate in an urban situation than more traditional methods such as trenches. As such, it is of interest to find out if it is a possible method of vibration mitigation, and which configurations are most effective.

2. Heavy masses on the ground

Energy from traffic vibrations is usually concentrated in the frequency range of 5-50Hz, most of it is transmitted as Rayleigh waves close to the soil surface. The principle of operation for resonant mass scatterers (heavy masses on the ground) is based on the fact that any topographic irregularities on the surface cause scattering of incident Rayleigh waves, where some of the energy is reflected back, some is transmitted past the obstacle and some is scattered down into the soil. For masses on the ground the scattering is particularly strong around the natural frequencies of the masses resting on the ground, and as such they have been considered as a viable method of vibration mitigation both numerically, by Ford [2], Petyt and Jones [4], and theoretically by Krylov [5]. Petyt and Jones [4] consider an evaluation point 25 meters from the load, in between which they place different sets of heavy masses and come to the conclusion that in general a heavy mass close to the load works best for their situation. Krylov [5] shows in a 2D analytical model that only 10% of the incoming wave energy is transmitted past a lumped mass around its resonant frequency, the rest of it is either reflected back or propagated as body waves through the half-space medium. The solution should be taken as a very rough estimate as it does not take into account the mass moment of inertia, and models a mass - elastic half-space medium interaction. Recently, Mhanna *et al* [7] performed numerical studies, and verifications with full scale experiments, where they concluded that heavy masses on the ground can potentially lead to reductions of up to 70%. Even though the mentioned studies concerning the wave scattering properties of heavy masses on the ground have been done, the phenomena are not understood well enough to be accounted during design. Furthermore, soil in general, and at MAX-IV consists several sub-surface layers causing reflections and other phenomena which need to be accounted to the specific site. Previous parameter studies by Alic [1] investigated the effects of a heavy mass on the soil surface at the MAX-IV site. Figure 2 shows the geometry for the study.

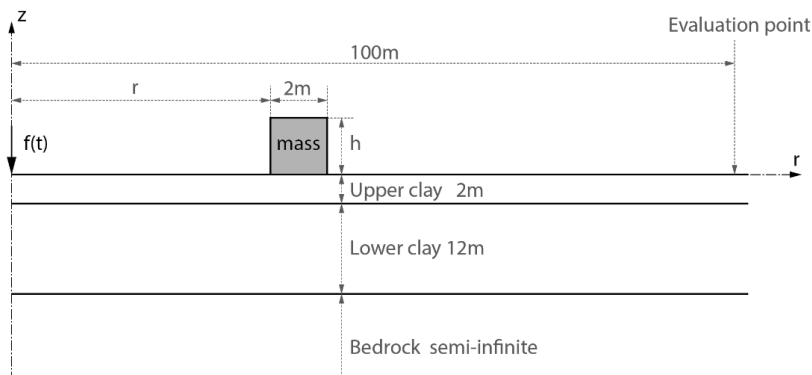


Figure 2: Axisymmetric model with a vertical unit load applied at rotation axis and masses on top of the surface, between the load and the evaluation point.

Figure 3 shows the general effect of a mass on the soil surface, part of the incoming surface wave is scattered down into the half-space which is seen as increased vertical displacements in Figure 3 (left) compared to Figure 3 (right). The scattering leads to smaller vertical displacements in the near-field behind the mass, however, as the bedrock has less damping than the soil, a secondary wave is observed close to the surface further away from the mass, at the far right in Figure 3 (left). This secondary wave was in this case of little concern due to the geometric attenuation of the surface wave.

The study concluded that the mass density showed largest reductions in vibration levels, and the position had some influence, while the height of the mass showed little influence as long as the density was modified to keep the same mass per surface area.

Figure 4 shows that a large reduction around the resonance frequencies can lead to slight amplifications for other frequencies, for example the response with the mass density $\rho = 16211\text{kg/m}^3$ shows reductions around 10Hz compared to the reference model, but an increase around 13-14Hz. The unrealistically high densities can be achieved by using a taller mass with lower density, thereby getting the same mass per surface area. Heavier masses affect a lower frequency range.

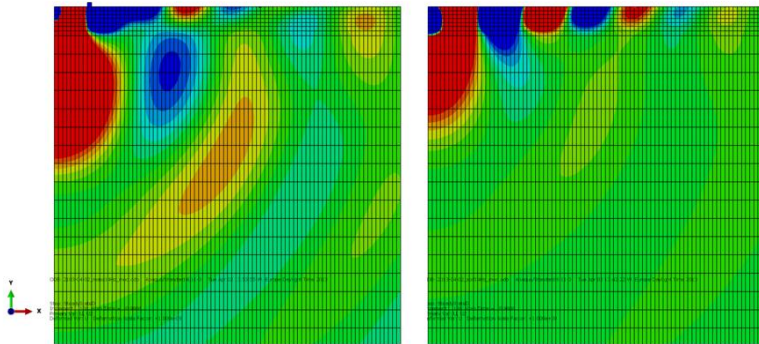


Figure 3: Vertical displacement amplitude of (left) soil model with mass $\rho = 8271\text{kg/m}^3$ and (right) model with no mass, for a prescribed harmonic load with excitation frequency 14Hz and unit amplitude. Surface waves are reduced (left) due to the mass on top of the surface.

Masses with a density around from $\rho = 8271\text{kg/m}^3$ were the most effective, as they showed large reductions in the range 13-15Hz, where the largest vertical displacements are in the reference model. With $\rho = 8271\text{kg/m}^3$ a reduction of almost 30% is achieved, as seen in Figure 5 (left). In Figure 5 (right) amplification vs. mass distance from the load application point is shown. There is little change unless the mass gets close to the load, then negative effects (amplification) are observed, as the mass gets excited by the load.

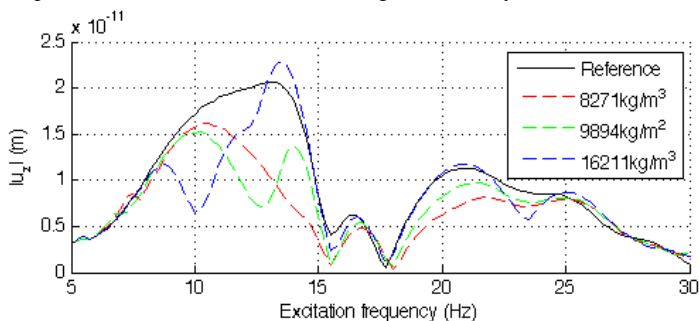


Figure 4: Vertical displacement magnitude response with 3 different densities.

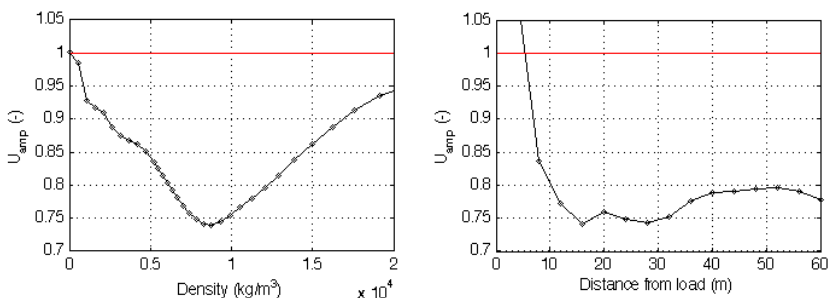


Figure 5: (left) Amplification vs. mass density, for a 2x2 meter mass. (right) Amplification vs. mass position in meters from the load application point, for a 2x2 meter mass with from $\rho = 8271\text{kg/m}^3$.

3. Form Finding Method

The work has been carried out using Finite Element Analysis (FEA) in two (axisymmetric), and three dimensions. Steady state models in the frequency range 5-30Hz have been established with main evaluation points along a line 100 meters from the load application point, which is about the distance from one of the roads to the facility. Unit loading was applied. Once an accurate model was set up masses were placed in between the load application point and the main evaluation points, see Figure 2. The results from the previous two-dimensional study were used to decide for the mass density range and possible mass positions on the soil surface. To aid in the form-finding of patterns a three-dimensional pattern exploration tool was developed, based on the findings from the two-dimensional studies and focused on finding effective and suitable urban patterns for the reduction of the vibration propagations.

3.1. Development of design tool for exploring different patterns

To get a sufficiently accurate model it is necessary to use small elements together with a large domain, leading to great computational costs, however, only a little part of the domain was of interest, namely the green parts on the soil surface in Figure 6. Because of this Guyan [3] reduction with frequency shift together with domain decomposition was applied and all degrees of freedom which were not part of the green parts were condensed away. The reduction method is exact at the angular frequency ω (apart from the approximation in the original dynamic matrices), performing the reduction for each frequency studied allowed for a reduced system with no loss of accuracy. The reduced system is no longer sparse and a large reduction in degrees of freedom is necessary in order for the method to be of benefit. In this case the model was reduced to 11 646 degrees of freedom, which allowed for simulations with a great number of configurations of masses, see Figure 8, where each pixel represents a mass with the size $2 \times 2 \times 2 \text{ m}^3$, and the gray-scale represents the density of each mass, where black is 8271 kg/m^3 and white is no mass at all. Adjacent masses were assembled together to act as a larger geometric entity.

3.2. FE-model

The model used brick elements with quadratic approximation and reduced integration, and infinite elements along the boundary. In order for the 3D model to give accurate results for a steady state analysis in the frequency range of 5-30Hz, a fine mesh with $2 \times 2 \times 2 \text{ m}^3$ elements for the soil (and $2 \times 2 \times 8.8 \text{ m}^3$ for the bedrock) was necessary which resulted in about 2.6 million complex-number degrees of freedom, even though symmetry was used in the x-z plane to bring down the size of the model. The results were evaluated along the green line 100m away from the load application point, see Figure 6.

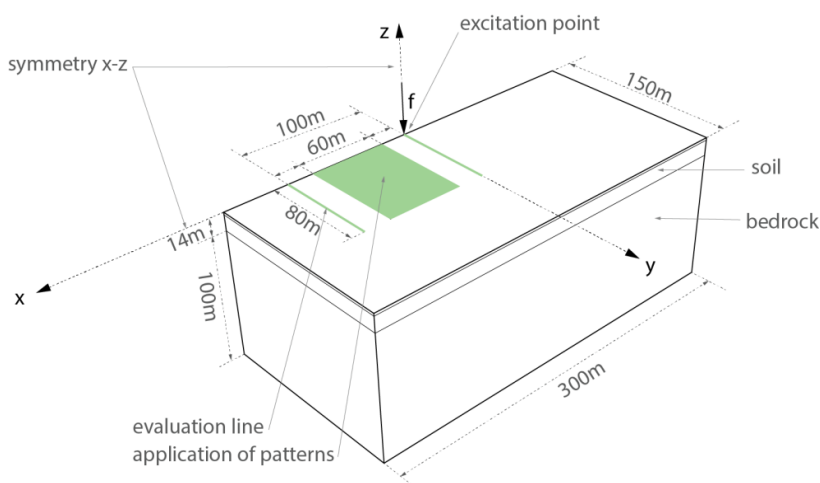


Figure 6: 3D model with the parts that were kept in the reduced model marked in green.

3.3. Materials

Soil as a material is generally treated as highly non-linear and inhomogeneous, however, with the present low magnitude loading and large wavelengths in comparison to grain size it was possible to model the soil and bedrock using homogeneous linear elastic materials. Figure 7 lists the material properties of the upper and lower soil layers and of the bedrock layer. The loss factor includes all attenuation effects (e.g. varying topography of the soil and bedrock). The soil layers are considerably less stiff than the bedrock, and provide higher damping than the bedrock.

-	<i>Upper Clay</i>	<i>Lower Clay</i>	<i>Bedrock</i>
Depth (m)	2	12	-
E (MPa)	215	1136	8800
ν	0.48	0.48	0.4
ρ (Kg/m ³)	2125	2125	2600
Loss factor (%)	14	14	4
c_s (m/s)	185	425	1100
c_p (m/s)	943	2167	2694

Figure 7: Soil and bedrock properties

3.4. RMS evaluation

In order to simplify comparison the root mean square value (RMS) of the vertical displacement magnitudes is used

$$u_{RMS} = \frac{1}{n} \sqrt{(u_1^2 + u_2^2 + u_3^2 + \dots + u_n^2)} \quad (1)$$

Where u_i is the vertical displacement magnitude at each angular frequency ω_i that is part of the steady state analysis, and u_{RMS} is the RMS value of u_i . This is further used to get the amplification as

$$U_{amp} = \frac{u_{RMS,tested}}{u_{RMS,reference}} \quad (2)$$

where $u_{RMS,tested}$ is the RMS value for a tested model with applied mass(es) on the soil surface, and $u_{RMS,reference}$ is for the reference model with no masses applied to it.

4. Results – Parameter study and effective/suitable patterns

4.2. 3D – Tested patterns and results

As the previous 2D parameter studies showed that the mass density was the most important parameter it was the only one that was varied in the pattern studies. The design tool made it possible to digitally sketch different organizations of masses in any paint program, as the sketches were easily imported into the tool. With relatively quick feedback, 10-20 minutes compared to days for the large FE-Model, it was possible to try out many organizations and iteratively (a more interactive/real-time model would be preferred, but the method with current computing power does not allow it) find some patterns which worked better than others. Figure 8 shows some of the types of tested patterns and findings.

The tool made it possible to highlight critical aspects, like the shapes referred to as diagonals and free-form lenses in Figure 8, as well as openings in straight lines. It made it possible to study what type of density variation in terms of position was most effective.

The patterns in Figure 8 are oriented such that the x-axis points downward and y-axis points to the right. The amplification term, U_{amp} , was used to plot the results along a line 100m away from the load, see Figure 6.

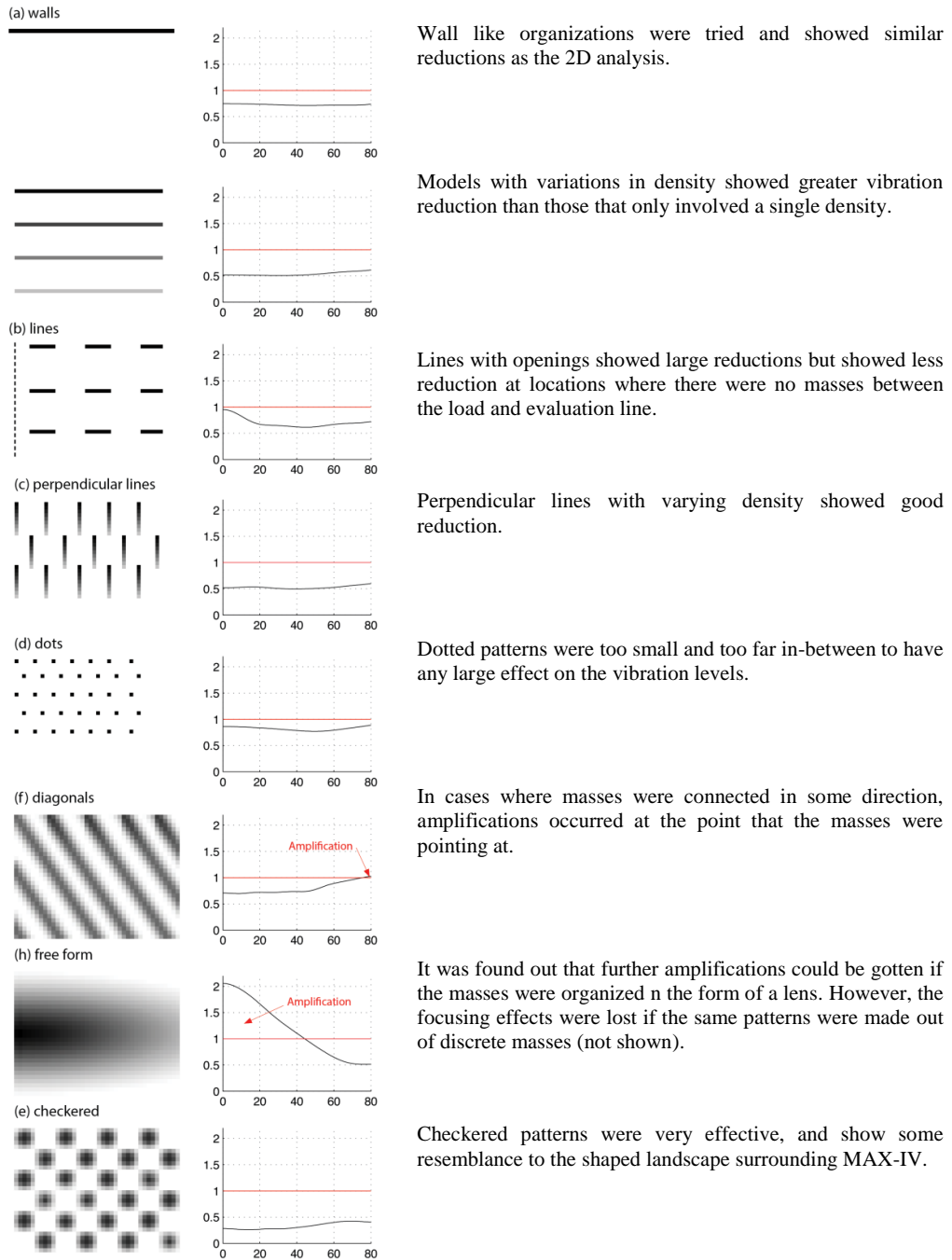


Figure 8: Examples of patterns used in 3D simulations applied on top of the green area in Figure 6, and the corresponding vibration levels in terms of U_{amp} evaluated along a line 100m from the load application point.

5. Conclusions

Two-dimensional results indicate that masses on the ground can be used as a means to mitigate ground vibration, but in order for them to be effective they need to be very heavy. However, due to the nature of being effective around the mass-soil systems resonance frequency they can instead lead to larger vibrations in the soil, if they are excited at frequencies close to their resonant frequencies.

Different organizations of masses were assembled on top of the reduced ground model and steady state analysis was performed in the frequency range between 5-29Hz. Three-dimensional results show that locating masses in a careful manner can be effective for vibration mitigation, and by combining masses of different densities reduction in a wider frequency range can be reached. Some conclusions from the research were: Masses applied continuously over the whole area can lead to amplification due to lensing as seen in Figure 8 (h), or acting as wave guides, Figure 8 (f), however, all discrete masses show reductions in vibrations; Small masses applied with large spacing are ineffective, Figure 8 (d); Straight open paths from the load to the evaluation point lead to little reduction, Figure 8 (b); Density variation for the different masses has a larger effect on vibration reductions than their position.

5.1. Further development

In order for the tool to work in a productive environment the parameter study (2D) and creation of the 3D tool for the specific site (the assembly of the whole model, and the reduction method) could be automated so that the design team can spend time thinking about the urban planning and not the computational method.

References

- [1] Alic, V., Vibration reduction in soil through the use of buildings at the synchrotron radiation facility MAX-IV. Master's Thesis, 2013.
- [2] Ford, R., Inhibiting the transmission of ground-borne vibrations by placing masses on the surface of the ground. *Australian Vibration and Noise Conference 1990: Vibration and Noise measurement Prediction and Control*; Preprints of Papers. Institution of Engineers, Australia, 1990, p. 227.
- [3] Guyan, R.J., Reduction of stiffness and mass matrices. *AIAA journal*, 1965; **3**(2); 380-380.
- [4] Jones, D. and Petyt, M. Ground borne vibrations from passing trains: the effect of masses placed on the ground's surface. *ISVR Technical Memorandum*, 1986.
- [5] Krylov, V. Control of traffic-induced ground vibrations by placing heavy masses on the ground surface, in *Low Frequency Noise, Vibration and Active Control*, 2007; **26**(4); 311-320.
- [6] Maxlab, 2013. *MAX-lab* [online] Available at: <<https://www.maxlab.lu.se/>> [Accessed March 2013]
- [7] Mhanna, M., Shahrour, I., Sadek, M., and Dunez, P. Efficiency of heavy mass technology in traffic vibration reduction: Experimental and numerical investigation. *Computers and Geotechnics*, 2014; **55**; 141-149.
- [8] Persson, P., Persson, K., & Sandberg, G., Reduction in ground vibrations by using shaped landscapes. *Soil Dynamics and Earthquake Engineering*, 2014; **60**; 31-43.

Paper B





Available online at www.sciencedirect.com

ScienceDirect

Comput. Methods Appl. Mech. Engrg. 300 (2016) 734–747

**Computer methods
in applied
mechanics and
engineering**

www.elsevier.com/locate/cma

Form finding with dynamic relaxation and isogeometric membrane elements

Vedad Alic*, Kent Persson

Division of Structural Mechanics, Lund Institute of Technology, Lund University, P.O. Box 118, SE-221 00 Lund, Sweden

Received 11 June 2015; received in revised form 4 December 2015; accepted 10 December 2015

Available online 17 December 2015

Abstract

A method for form finding with dynamic relaxation and Non-Uniform Rational B-Splines (NURBS) based isogeometric membrane elements has been implemented and studied regarding the influence of the discretization and element shape on the form finding. The procedure allows for rapid form finding since NURBS describe the curved geometry well and it is shown that the form-finding can be performed using a coarse mesh. However, to minimize the bending strain energy a fine mesh is needed. Using smaller elements is more advantageous than increasing the degree of the basis functions, keeping the number of integration points few and converging at a lesser number of iterations. Using isogeometric analysis (IGA) simplifies further studies since the form-found shape can be exactly represented with a shell element formulation. The method is suitable to be used in computer aided design environments such as Rhinoceros 3D during design stages, where the form finding can be evaluated together with other studies in a design context.

© 2015 Elsevier B.V. All rights reserved.

Keywords: Structural form finding; Dynamic relaxation; Isogeometric analysis; NURBS; Optimization

1. Introduction

1.1. Form finding

The load carrying capacity of shells and other form-active structures is provided by the shape of the structures, which for a certain load allows the shell to work in a membrane state, using the available material in an optimal way. When determining the shape of such a structure a form finding procedure is typically employed where the objective is to find a shape which minimizes bending, or more generally finds a shape which minimizes the strain energy in the structure [1].

Form finding methods are usually divided into two types. The first is related to pre-stressed structures, whose shapes are analogous to minimal surfaces. The second is the hanging chain and its inverse. As the chain cannot take any bending stresses the resultant shape will be in pure tension, which is generally a much more efficient use of

* Corresponding author.

E-mail address: vedad.alic@construction.lth.se (V. Alic).

material than in bending. Inverting the shape creates an arch in pure compression. The method can be extended to membranes which are physically form-found using hanging cloths, which when inverted gives the shape of a vault in compression. Note that wrinkling of the surface may occur for a hanging model.

1.2. Numerical form finding

Several numerical methods for form finding exist, such as by use of dynamic relaxation [2], the force density method [3], or more recently by use of particle spring systems [4], or the updated reference strategy [5]. The methods were initially developed for the form finding of pre-stressed membrane structures. However, here the dynamic relaxation method will be used for the simulation of hanging cloths. All quantities in the method can be treated as vectors, leading to a low cost for each iteration and making it an efficient solution method [6] which is suitable for interactively exploring different designs in Computer Aided Design (CAD) software.

The hanging cloth may be simulated numerically by membrane finite elements with large displacements and a linear elastic material. By applying a form generating load, usually a uniformly distributed load, the initial geometry deforms into a shape which equilibrates the applied load. The resulting shape is optimal in the sense that forces are transferred mainly by membrane action.

The final shape achieved through form finding as a numerical process for simulating hanging cloth, depends on the initial geometry, the material properties (anisotropy, etc.), and the boundary condition. The relation between the initial and final shape is rather complex, requiring an iterative process of making changes to the initial geometry and evaluating the form-found shape until one which fulfills the specified design criteria is achieved [7]. Just as in the case of the physical hanging model, mesh dependent wrinkles may develop in the numerical model as well when membrane elements are used.

One drawback of many existing methods is that it is necessary to discretize the initial shape which often is described by Non-Uniform Rational B-Splines (NURBS), into structural elements in order to perform the form finding. During design stages this is sometimes unfavorable, since the discretized geometry is difficult to convert back to the initial geometry type. The design process may require many iterations of form finding, design evaluation and conversions between different geometry types before a desired shape is generated resulting in a time consuming process. The discretized geometry may be incompatible with available design software, making it hard to evaluate the form in the architectural context and to further detail it. By employing Isogeometric Analysis (IGA) the form finding and design evaluation can be integrated in design programs resulting in a simplified work flow where conversions between different geometry types are no longer necessary.

1.3. Isogeometric analysis

IGA [8] is an attempt at integrating CAD and Computer Aided Engineering (CAE) by using the same geometrical representation for both environments, typically NURBS, T-Splines or Subdivision Surfaces. Form finding with isogeometric membrane elements makes it possible to integrate the procedure in design software, and to avoid translations from one geometry type to another. NURBS based IGA is well suited since NURBS represent the smooth form found structures with very few control points, making them attractive numerically. A further advantage is that no re-meshing is required for the structural analysis as the form-found geometry can simply be reused with a shell element formulation.

The main part of this work relates to NURBS based IGA membrane elements. However, formulations of structural elements using IGA are plenty, and have been applied for shells [9–11], for beams and plates [12–14]. Recently isogeometric collocation techniques [15] have been used for beams and plates [16–18]. In [19] the Kirchhoff–Love shell model is discretized using polynomial splines over hierarchical T-meshes (PHT-splines). It shows superior performance per degree of freedom compared to cubic NURBS for the Scordelis–Lo roof, Hemispherical shell and Pinched cylinder with diaphragm. Although the method offers advantages in performance and a simple local refinement technique, it requires that the initial NURBS geometry must be able to be refined into bi-cubic NURBS with C^1 over knots in order for the PHT-splines refinement to be applicable, which somewhat limits their application to CAD programs. In [20] an extended isogeometric thin shell formulation based on Kirchhoff–Love theory is presented. Other spline approaches have been used for thin shells, such as those based on subdivision finite elements [21–23]. Subdivision surfaces provide an extension of NURBS to unstructured triangular or quadrilateral meshes [24].

1.4. Objective

Isogeometric analysis has been used together with the updated reference strategy for form finding [25], and isogeometric elements have been used together with dynamic relaxation for the steady-state solution of inflation of spherical shells and square airbags [26]. However, to the authors knowledge isogeometric elements have not been used with dynamic relaxation for form finding by simulation of hanging models. The objective of this paper is to investigate the use of large deformation isogeometric membrane elements with dynamic relaxation as a means of form finding. An overview of dynamic relaxation, isogeometric analysis and membrane kinematics is given in order to perform the investigation.

2. Dynamic relaxation

Dynamic relaxation was first suggested by Day [2] and further adopted to form finding of lightweight and large span structures by Barnes [27,28]. For a thorough discussion on dynamic relaxation see [29] and [30]. The method is suitable for parallelization and has shown good performance on graphics processing units (GPUs) [31]. The study will investigate dynamic relaxation with both critical damping and with kinetic damping. A description of both damping methods is also given.

2.1. Dynamic relaxation with critical damping

The dynamic relaxation method solves static problems by adding fictitious masses, fictitious damping and by using explicit time integration. The equation of motion (EOM) is given by

$$\mathbf{M}\ddot{\mathbf{u}} + \mathbf{C}\dot{\mathbf{u}} + \mathbf{f}^{\text{int}} = \mathbf{f} \quad (1)$$

where \mathbf{f}^{int} is the column matrix of internal forces obtained from Eq. (24), \mathbf{f} is the column matrix of external forces, \mathbf{M} is the mass matrix, \mathbf{C} is the damping matrix, and \mathbf{u} contains the unknown displacements. Since only the static solution is of interest only \mathbf{f} and \mathbf{f}^{int} must represent the physical problem, all other parameters can be chosen freely. To obtain the motion in time the EOM is integrated using central differences giving a set of equations to update the velocities and displacements

$$\dot{\mathbf{u}}^{t_n+h/2} = \frac{(2-ch)}{(2+ch)}\dot{\mathbf{u}}^{t_n-h/2} + 2h\mathbf{M}^{-1}\frac{(\mathbf{f}-\mathbf{f}^{\text{int}})}{(2+ch)} \quad (2)$$

$$\mathbf{u}^{t_n+h} = \mathbf{u}^{t_n} + h\dot{\mathbf{u}}^{t_n+h/2} \quad (3)$$

where \mathbf{M} must be diagonal to preserve the explicit form of the central difference integrator [30]. \mathbf{C} has the form $\mathbf{C} = c\mathbf{M}$, where c is a damping coefficient for the structure, h is the time step. In the first iteration, $t = 0$ and \mathbf{u}^0 is given, then

$$\dot{\mathbf{u}}^{0+h/2} = h\mathbf{M}^{-1}(\mathbf{f}-\mathbf{f}^{\text{int}})/2. \quad (4)$$

To ensure numerical stability and optimal convergence rate the diagonal entries of \mathbf{M} are chosen as suggested in [30] by

$$M_{ii} = \frac{1}{4}\hat{h}^2 \sum_j |K_{ij}| \quad (5)$$

where $\hat{h} = 1.1h$ and the elements of the stiffness matrix K_{ij} are either computed by numerical differentiation of the internal force vector [30] or derived analytically. The damping coefficient c is set to critically damp the lowest eigenmode

$$c = 2\omega_{\min} \quad (6)$$

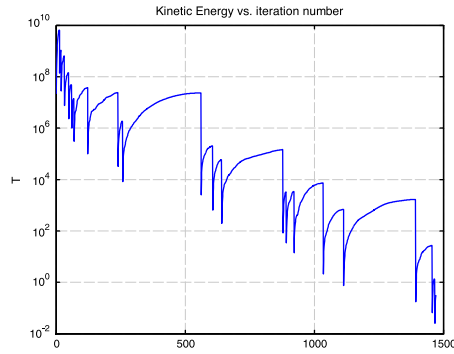


Fig. 1. Example of kinetic damping. The kinetic energy is reset each time a peak is detected.

which is estimated by use of Rayleigh’s principle

$$\omega_{\min}^2 = \frac{\mathbf{u}^T \mathbf{K} \mathbf{u}}{\mathbf{u}^T \mathbf{M} \mathbf{u}}. \tag{7}$$

The dynamic relaxation process is stopped once the norm of the residual is smaller than $\|\mathbf{f} - \mathbf{f}^{\text{int}}\|_2 < \epsilon_{\text{err}}$, where $\|\bullet\|_2$ is the Euclidean norm. In this paper the error is set to $\epsilon_{\text{err}} = \|\mathbf{f}\|_2/10^5$ for the benchmark studies.

2.2. Kinetic damping

An alternative to viscous damping is to use kinetic damping [27], where the total kinetic energy of the system is traced through the motion in time and once a peak is detected the current velocities are set to zero, see Fig. 1. The EOM for kinetic damping is

$$\mathbf{M} \ddot{\mathbf{u}} + \mathbf{f}^{\text{int}} = \mathbf{f} \tag{8}$$

and the set of equations to update the velocities and displacements is simplified

$$\dot{\mathbf{u}}^{t_n+h/2} = \dot{\mathbf{u}}^{t_n-h/2} + h \mathbf{M}^{-1} (\mathbf{f} - \mathbf{f}^{\text{int}}) \tag{9}$$

$$\mathbf{u}^{t_n+h} = \mathbf{u}^{t_n} + h \dot{\mathbf{u}}^{t_n+h/2}. \tag{10}$$

While kinetic damping typically requires more iterations to converge than the critically damped system, it is cheaper per iteration since it is not necessary to formulate \mathbf{K} or update \mathbf{M} . On the other hand it requires a user selection of \mathbf{M} . In this paper two different choices of \mathbf{M} have been tried, and are described in Section 4.1.

3. NURBS based isogeometric analysis

3.1. B-splines and NURBS

IGA was presented by Hughes et al. in an extensive report on NURBS based IGA [8]. NURBS are a further generalization of B-splines, non-interpolating, piecewise polynomial curves, but which unlike B-splines have the ability to represent any conical shape exactly.

Given a knot vector $\Xi = \{\xi_1, \xi_2, \dots, \xi_{n+p+1}\}$, where $\xi_i \in \mathbb{R}$ is the i th knot (parametric coordinate), p is the polynomial order (or degree), and n is the number of basis functions. The B-spline basis functions are constructed recursively using the Cox–de Boor formula starting with piecewise constants (for $p = 0$)

$$N_{i,0}(\xi) = \begin{cases} 1 & \text{if } \xi_i \leq \xi < \xi_{i+1} \\ 0 & \text{otherwise.} \end{cases} \tag{11}$$

For $p = 1, 2, 3, \dots$, recursively

$$N_{i,p}(\xi) = \frac{\xi - \xi_i}{\xi_{i+p} - \xi_i} N_{i,p-1}(\xi) + \frac{\xi_{i+p+1} - \xi}{\xi_{i+p+1} - \xi_i} N_{i+1,p-1}(\xi) \quad (12)$$

for which implementations can be found in [32]. A knot vector is open if its first and last knot values appear $p+1$ times. Basis functions are interpolatory at the ends of open knot vectors $[\xi_1, \xi_{n+p+1}]$ but are in general not interpolatory at interior knots, which distinguishes nodes in finite element analysis and control points in isogeometric analysis.

Using two one-dimensional B-spline basis functions $N_{i,p}(\xi)$, $M_{j,q}(\eta)$, from the knot vectors $\Xi = \{\xi_1, \xi_2, \dots, \xi_{n+p+1}\}$ and $H = \{\eta_1, \eta_2, \dots, \eta_{m+q+1}\}$, of orders p and q and a control point net $\mathbf{B}_{i,j}$ consisting of $n \times m$ points, a B-spline surface is constructed using the tensor product

$$S(\xi, \eta) = \sum_{i=1}^n \sum_{j=1}^m N_{i,p}(\xi) M_{j,q}(\eta) \mathbf{B}_{i,j}. \quad (13)$$

A NURBS surface in \mathbb{R}^3 is constructed from the projection of a B-spline surface which is in \mathbb{R}^4 . The NURBS surface is expressed using the tensor product

$$S(\xi, \eta) = \frac{\sum_{i=1}^n \sum_{j=1}^m N_{i,p}(\xi) M_{j,q}(\eta) w_{i,j} \mathbf{B}_{i,j}}{\sum_{k=1}^n \sum_{l=1}^m N_{k,p}(\xi) M_{l,q}(\eta) w_{k,l}} \quad (14)$$

where the weights $w_{i,j}$ are stored as the fourth component in the control point net $\mathbf{B}_{i,j}(x_{i,j}, y_{i,j}, z_{i,j}, w_{i,j})$. Note that if all the weights are equal the NURBS surface reduces down to a B-spline surface. To get a notation which resembles finite element methodology closer the i, j indices are, adhering to choices in [13], replaced by $A = n(j-1) + i$ leading to the bivariate NURBS basis

$$\tilde{N}_A(\xi, \eta) = \frac{N_{i,p}(\xi) M_{j,q}(\eta) w_{i,j}}{\sum_{k=1}^n \sum_{l=1}^m N_{k,p}(\xi) M_{l,q}(\eta) w_{k,l}} \quad (15)$$

and expressing the surface in Eq. (14) as

$$S = \sum_{A=1}^{nm} \tilde{N}_A \mathbf{B}_A. \quad (16)$$

The tilde is henceforth dropped and the bivariate NURBS basis functions of order p and q are from now on simply referred to as N_A .

3.2. Refinement

The tensor product approach for creating NURBS surfaces or solids confines NURBS to structured meshes, deviation from the tensor product approach can be achieved using trimmed NURBS [33,34], or localized refinement (e.g. T-Splines [35–37]), none of which is considered in this paper. In [38] trimmed boundary representation (B-rep) CAD models are used for IGA and applied to Kirchhoff–Love shells. The approach seems promising and could be applied for form finding with complex initial geometries. However, there are many ways for enriching the NURBS basis without changing the geometry or its parametrization [8]. The mesh can be refined into smaller elements by insertion of new knots (h-refinement). Inserting a duplicate knot reduces the continuity for the bordering elements. Knot insertion thus allows both for control of element size and continuity. The degree of the basis can be increased through order elevation (p-refinement). During order elevation the multiplicity of each knot is raised by one, keeping the same continuity before and after the order elevation.

A third type of refinement (k-refinement) exists, where both the order and continuity are increased. This is done by first applying order elevation and afterwards inserting new knots. As previously stated the refinements do not change the geometry or parametrization.

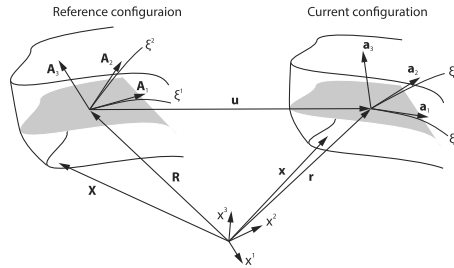


Fig. 2. Membrane kinematics.

3.3. NURBS based IGA membrane element

The dynamic relaxation method is here used with isogeometric membrane elements. If bending is neglected the form found shapes will be in equilibrium with the external loads using only membrane stresses. Hence the primary load carrying of the load applied for the form finding will be with membrane action only.

Membrane kinematics and virtual work. The membrane element is derived following standard procedure, assuming the membrane to be infinitely thin we get [39]

$$\mathbf{X} = \mathbf{R}, \quad \mathbf{x} = \mathbf{r}, \quad \mathbf{r} = \mathbf{R} + \mathbf{u} \tag{17}$$

where \mathbf{X} is the position vector in a three dimensional body, \mathbf{R} is the mid-surface vector, both in the reference configuration, and \mathbf{x} , \mathbf{r} are the corresponding vectors in the current configuration, see Fig. 2. The displacement vector \mathbf{u} relates the reference and current mid-surface vectors. The assumption results in that the Green–Lagrange strains $E_{\alpha\beta}$ are equal to the membrane strains $\epsilon_{\alpha\beta}$

$$E_{\alpha\beta} = \frac{1}{2}(a_{\alpha\beta} - A_{\alpha\beta}) = \epsilon_{\alpha\beta} \tag{18}$$

which are expressed in curvilinear coordinates where the Greek indices range from one to two and Latin from one to three throughout this article. Repeated follow the summation convention. $A_{\alpha\beta}$, and $a_{\alpha\beta}$ are the covariant components of first fundamental form of the surface in reference and current configurations. It is further implied that the transverse strains are zero

$$E_{3i} = E_{i3} = 0. \tag{19}$$

From the equations of virtual work [40] we get the part of the external forces as

$$\delta \Pi^{\text{ext}} = \int_{\Omega^0} t b^i \delta u_i d\Omega^0 \tag{20}$$

where t is the membrane thickness, b^i is the body load, δu_i are the virtual displacements and Ω^0 is the domain of the membrane mid surface in the reference configuration. The virtual work of the internal forces is expressed in terms of the stress resultant tensor and the membrane strains

$$\delta \Pi^{\text{int}} = - \int_{\Omega^0} \mathbf{n} : \delta \epsilon d\Omega^0 \tag{21}$$

where the stress resultant tensor using an isotropic linear elastic constitutive relation can be described as [21]

$$n^{\alpha\beta} = \frac{Et}{1 - \nu^2} \tilde{C}_0^{\alpha\beta\gamma\delta} \epsilon_{\gamma\delta} \tag{22}$$

where

$$\tilde{C}_0^{\alpha\beta\gamma\delta} = \nu A^{\alpha\beta} A^{\gamma\delta} + \frac{1}{2}(1 - \nu)(A^{\alpha\gamma} A^{\beta\delta} + A^{\alpha\delta} A^{\beta\gamma}) \quad (23)$$

in which E is Young's modulus and ν is Poisson's ratio.

For equilibrium we require that

$$\delta II^{\text{ext}} + \delta II^{\text{int}} = 0. \quad (24)$$

which in the paper is fulfilled using the dynamic relaxation method together with isogeometric membrane elements. A standard solution procedure by use of for instance Newton–Raphson iterations is difficult since stiffness matrices generated from membrane elements are not guaranteed to be invertible. The use of the dynamic relaxation method avoids this problem.

For further details see [9], where a Kirchhoff–Love shell element is formulated in NURBS based IGA. By neglecting the bending parts in that formulation one arrives at the equations given here.

Approximation. The approximation is performed using the isogeometric approach where the displacement field is approximated using the same basis functions as the geometry definition. Starting with the mid-surface

$$\mathbf{R}_h = \sum_{A=1}^{nm} N_A \mathbf{B}_A \quad (25)$$

where N_A is the A th basis function associated with the A th control point \mathbf{B}_A . The displacements are discretized using the same basis

$$\mathbf{u}_h = \sum_{A=1}^{nm} N_A \mathbf{u}_A \quad (26)$$

where \mathbf{u}_A is the A th displacement vector. The covariant basis vectors are found by differentiating the surface with respect to the curvilinear coordinates

$$\mathbf{A}_\alpha^h = R_{h,\alpha} = \sum_{A=1}^{nm} N_{A,\alpha} \mathbf{B}_A \quad (27)$$

where $\bullet_{,\alpha}$ denotes differentiation with respect to the curvilinear coordinates, e.g.

$$N_{A,\alpha} = \frac{\partial N_A(\xi, \eta)}{\partial \xi^\alpha}, \quad \xi^1 = \xi, \quad \xi^2 = \eta, \quad \alpha = 1, 2 \quad (28)$$

proceeding in a similar fashion we arrive at the membrane strains as well as the external and internal virtual work. In practice the local support of the NURBS basis is used and implementation is done on element level and necessary integrations are performed numerically.

4. Benchmarking and examples

4.1. Benchmark examples

In the benchmark studies isogeometric membrane elements are used together with the dynamic relaxation method for finding shapes which are in equilibrium with the external applied load, and as bending is omitted by definition the resulting shapes carry the loads using membrane action.

Three initial shapes are used for the benchmarks, one rectangular NURBS surface, and two triangular created by either placing two control points at the same location (collapsing edge), or by placing one control point in-line with each other (co-linear edges), see Fig. 3. K-refinement (by performing order elevation to a given degree p , and then inserting new knots with multiplicity one, getting C^{p-1} continuity) is applied and the number of iterations required to converge is studied with critical damping and with kinetic damping, see Fig. 4. The material properties are taken as $t = 0.05$ m, $E = 17$ GPa, $\nu = 0.3$, and a pressure load of $4.05 \cdot 10^7$ N/m² is applied to the initial configuration.

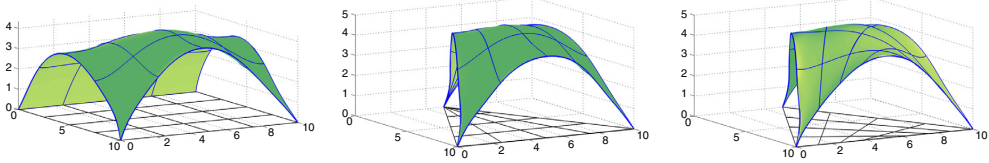


Fig. 3. Benchmarking examples, 4 elements per side with quintic basis and C^4 continuity, (left) rectangular shape, ten meters by ten meters (middle) triangular shape with collapsing edge (left) triangular shape with co-linear edges.

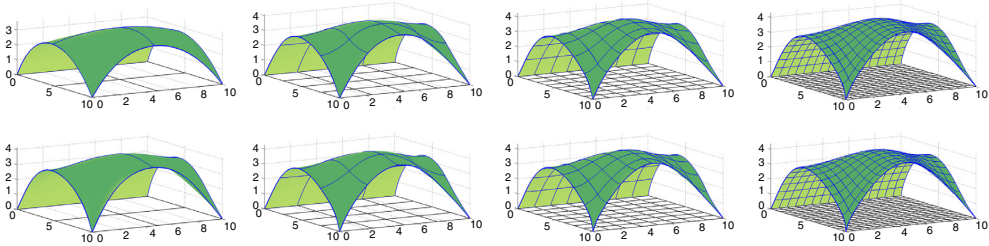


Fig. 4. Refinement, top shows quadratic basis ($p = q = 2$) and bottom shows quartic basis ($p = q = 4$), both with C^{p-1} . From left to right: 2×2 elements, 4×4 elements, 8×8 elements, 16×16 elements.

For the kinetic damping two different choices for the mass matrix have been applied. The first choice is by taking the mass matrix as $\mathbf{M} = \mathbf{I}\rho$, where \mathbf{I} is the identity matrix (of right size) and ρ is either $2.1e9$ kg, $32 \cdot 2.1e9$ kg or $128 \cdot 2.1e9$ kg for the square, triangular (collapsed edge) and triangular (co-linear edges) respectively. The values were found through trial and error, being the smallest possible without causing any instability. The second choice of mass matrix for the kinetic damping was based on the initial stiffness matrix \mathbf{K}_0 , where similarly to Eq. (5) we have

$$\tilde{M}_{ii} = \frac{1}{4} \hat{h}^2 \sum_j |K_{ij}| \tag{29}$$

where now K_{ij} are the elements of \mathbf{K}_0 . The geometric stiffness was accounted for by summing the three degrees of freedom related to a control point and multiplying by four

$$M_{ii} = 4(\tilde{M}_{ii} + \tilde{M}_{ii+1} + \tilde{M}_{ii+2}); \quad M_{ii+1} = M_{ii}; \quad M_{ii+2} = M_{ii}; \quad i = 1, 4, 7, \dots, n_{\text{dof}} - 2 \tag{30}$$

where n_{dof} is the number of degrees of freedom.

Since the membrane elements only provide in plane stiffness, Eq. (5) needs to be modified to avoid numerical issues due to diagonal entries being close to zero. In the paper any diagonal entry M_i which is smaller than $\max(\mathbf{M})/3$ is set to $\max(\mathbf{M})/3$.

The basis functions for the membrane elements need to be in the Hilbert space H^1 , which is true for the rectangular shape, and the triangular shape created with the co-linear edges. This is, however, not the case for the triangular shape with control points that share the same physical coordinates (collapsed edge). This was remedied by taking the sum of the basis functions with a common control point [41].

4.2. Hausdorff distance

To determine the error in shape between different form found surfaces the Hausdorff distance is used [42]. The Hausdorff distance measures the maximum of the largest distance for any point on one surface to the closest point on a reference surface. The Hausdorff distance has to be calculated twice by letting each surface be the reference surface since the two distances are in general not equal. The Hausdorff distance $d_H(S, S')$ between two surfaces S and S' is

defined as

$$d_H(\mathcal{S}, \mathcal{S}') = \max \left\{ \max_{\mathbf{p} \in \mathcal{S}} \min_{\mathbf{p}' \in \mathcal{S}'} d(\mathbf{p}, \mathbf{p}'), \max_{\mathbf{p}' \in \mathcal{S}'} \min_{\mathbf{p} \in \mathcal{S}} d(\mathbf{p}, \mathbf{p}') \right\} \quad (31)$$

where \mathbf{p} and \mathbf{p}' are points on \mathcal{S} and \mathcal{S}' , and $d(\mathbf{p}, \mathbf{p}') = \|\mathbf{p} - \mathbf{p}'\|_2$.

A mean distance d_m can be defined in a similar way

$$d_m(\mathcal{S}, \mathcal{S}') = \frac{1}{|\mathcal{S}|} \int_{\mathcal{S}} \min_{\mathbf{p}' \in \mathcal{S}'} \|\mathbf{p} - \mathbf{p}'\|_2 d\mathcal{S} \quad (32)$$

where $|\mathcal{S}|$ is the area of \mathcal{S} . The mean distance is not symmetric, i.e. $d_m(\mathcal{S}, \mathcal{S}') \neq d_m(\mathcal{S}', \mathcal{S})$. Whenever the mean distance is used \mathcal{S}' represents the surface with the finest discretization (unless otherwise stated, i.e. p5h16, where p5 means that the degree is 5 and h16 means that there are 16 elements along one side of the geometry, that is 256 elements in total), and \mathcal{S} being the surface that is compared.

4.3. Strain energy

The form finding procedure minimizes the bending part of the strain energy in the structure for the applied load. It is, however, not possible to reach zero bending strain energy since it depends on the discretization (and degree of the basis functions). The bending part of the strain energy is thus used as a metric to compare the results of the numerical studies. The strain energy is calculated as

$$U = \frac{1}{2} \mathbf{u}^T \mathbf{K} \mathbf{u} \quad (33)$$

where \mathbf{u} is the displacement vector of the structure and the stiffness \mathbf{K} is calculated using linear isogeometric Kirchhoff–Love elements [9]. The strain energy can be split into a bending U_b , and a membrane part U_m , where the bending part is calculated as [21]

$$U_b = \frac{1}{2} \int_{\Omega} \frac{Et^3}{12(1-\nu^2)} \kappa_{\alpha\beta} C_0^{\alpha\beta\gamma\delta} \kappa_{\gamma\delta} d\Omega \quad (34)$$

where $\kappa_{\alpha\beta}$ are the bending strains. The strain energy is calculated on a further refined structure by insertion of new knots. The refined models have 48×48 elements. The same load that was used for the form finding was applied to get the displacements of the refined discretization.

The strain energy was only calculated for triangular shape with co-linear edges since several basis functions for the triangular shape with the collapsed edge are not in H^2 [43].

4.4. Numerical studies

Rectangular initial shape. In Fig. 5 (Left column) the number of iterations required for the square shape to converge using either critical or kinetic damping is shown. For most cases the critically damped model converges on fewer iterations than the model with kinetic damping. For meshes with polynomial degree $p = 5$ there were convergence problems compared to the ones with lower degrees, and are excluded from Fig. 5. The bottom left subfigure (rectangular shape, constant mass) of Fig. 5 with $p = 5$ included is shown in Fig. 6. In Fig. 4 the results from models with quadratic and quartic basis functions, divided into 2, 4, 8, or 16 elements per side are shown. Visually it is only possible to notice differences between the most coarse meshes (to the left in the figures) and the ones with finer mesh.

In Fig. 7 (Left) the Hausdorff and mean distances from all the tested rectangular models to the finest rectangular model (p5h16) are shown. The coarsest model (p2h2) has a Hausdorff distance of over 1m, and is visually very different from the finer models, as shown in Fig. 4, top left image. The mean distances for all except the coarsest mesh (p2h2) are close to or less than 0.1m. In Fig. 8 (Left) the bending and strain energy for each model with the rectangular initial shape is shown. The bending part of the strain energy is small only for solutions with a fine mesh.

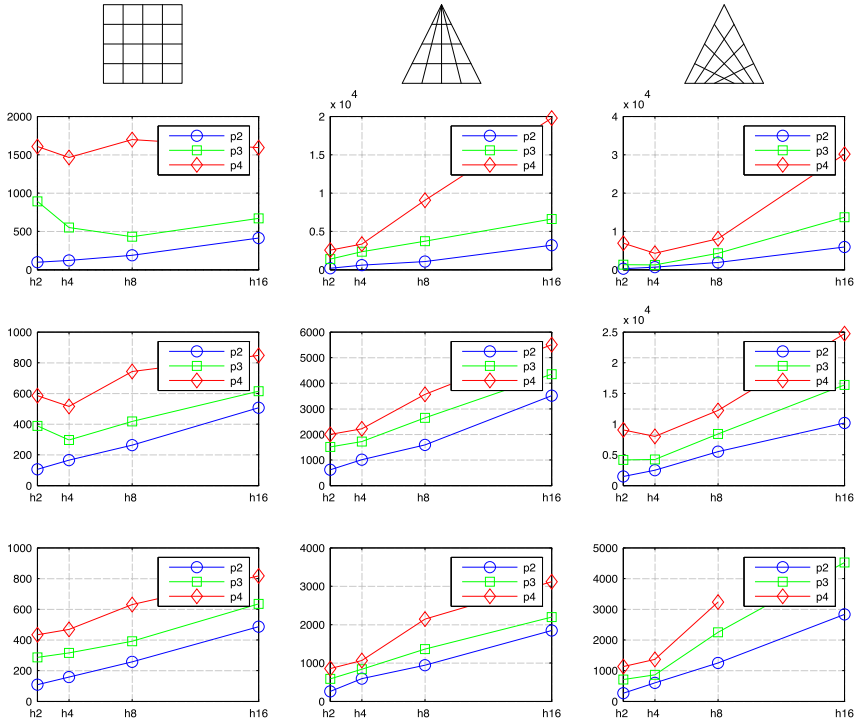


Fig. 5. Number of iterations to converge vs. number of elements per side. (Left column) Rectangular shape. (Middle column) Triangular shape with collapsed edge. (Right column) Triangular with co-linear edges. (Top to bottom) Critically damped, kinetic damping with constant mass matrix, kinetic damping with mass matrix from initial stiffness.

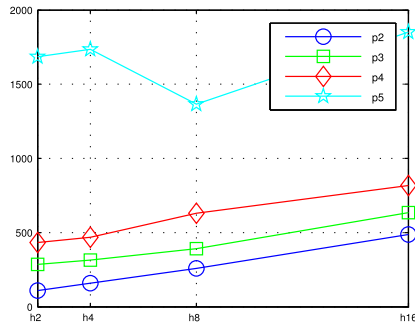


Fig. 6. Bottom left subplot of Fig. 5 with degree 5 mesh results included. The number of iterations required for convergence with degree 5 mesh is much larger.

Triangular initial shapes. Fig. 5 (Middle column) shows the number of iterations required for the initial form with collapsed edge to converge using critical or kinetic damping. Identical refinements have been applied as was made for the square shape. The model with quartic basis functions and 16 elements per side (p4h16) with kinetic damping and mass matrix from initial stiffness failed to converge, seen in the bottom right subfigure of Fig. 5. In Fig. 5 (Right column) the number of iterations to converge for the triangular shape with co-linear edges is found. Fig. 7 (Right)

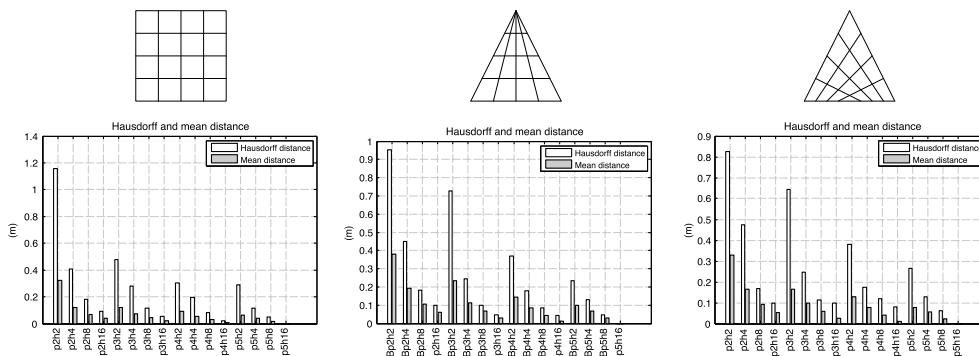


Fig. 7. Hausdorff and mean distances. (Left column) Rectangular shape. (Middle column) Triangular shape with collapsed edge. (Right column) Triangular with co-linear edges. All meshes are compared to the finest one (p5h24) with 24×24 elements and quintic basis.

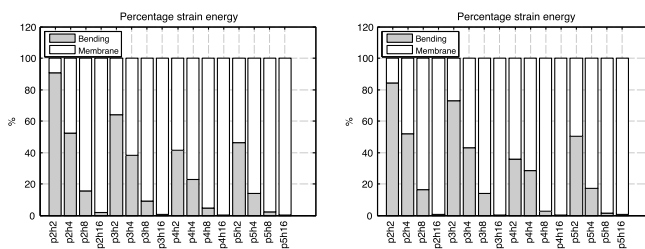


Fig. 8. Percentage of bending and membrane strain energy for (Left) Rectangular shape. (Right) Triangular with co-linear edges.

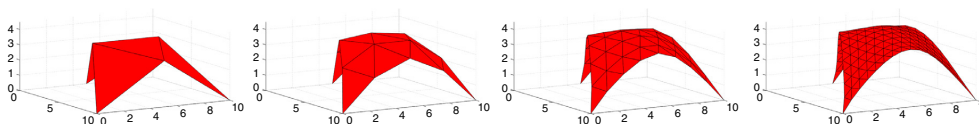


Fig. 9. Triangular shape with membrane finite elements, with 2, 4, 8, and 16 elements per side.

shows the Hausdorff and mean distances for the triangular shape (co-linear edges) compared to the finest model (p5h16). The Hausdorff distances are more than 0.5 m for some coarse discretizations. The mean distance is below 0.2 m for all except (p2h2). Fig. 8 (Right) shows the bending and strain energy for each model with the triangular (co-linear edges) initial shape. This is in agreement with the rectangular shape. The bending part of the strain energy is small only for solutions with many elements.

Fig. 7 (Middle) shows the Hausdorff and mean distances for the triangular shape (collapsed edges).

In order to compare the performance of the dynamic relaxation method with isogeometric elements, the form-finding was also performed on the triangular shape with triangular membrane finite elements [44]. The Hausdorff distance for the solutions with FE was calculated with the finest triangular IGA shape (p5h16) as reference. Discretizations of 2, 4, 8, 16, 32 and 64 elements per side were studied, see Fig. 9. The mean distance falls below 0.2 m only for discretizations with 32 side elements or more, see Fig. 11.

The number of iterations to converge for triangular shape with finite elements is shown in Fig. 10.

5. Conclusions and further work

The rectangular shape IGA elements with quadratic basis functions converge at about the same number of iterations to converge as the triangular shape with triangular finite elements. The number of iterations to converge is much larger

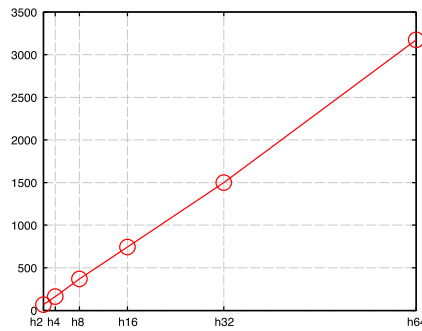


Fig. 10. Number of iterations required for the triangular membrane finite elements to converge using kinetic damping.

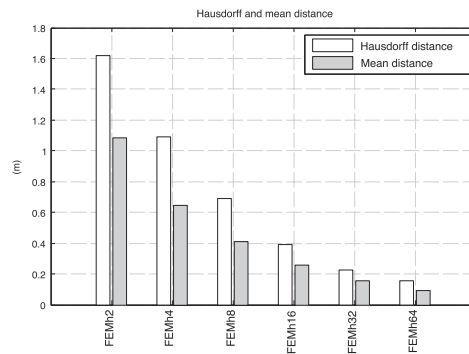


Fig. 11. Hausdorff and mean distance for the FEM triangular shape using 2, 4, 8, 16, 32, and 64 elements per side. All are compared to the finest isogeometric triangular shape with co-linear edges (p5h16) with 16×16 elements and quintic basis.

for the triangular shapes with isogeometric elements, where the mesh in the physical space no longer has a uniform size, the effect is greatest for the triangular discretizations with co-linear edges where the elements are the smallest. By applying some type of local refinement, e.g. T-Splines or trimmed NURBS, it would be possible to generate meshes of more uniform size for triangular, and other kinds of shapes.

Increasing the degree of the basis functions requires a larger number of iterations to converge. Since the numerical quadrature requires more integration points for a higher degree of the basis it requires longer computational time per iteration. Most of the time in the dynamic relaxation loop is spent evaluating stresses at integration points and as such it is good to keep the degree of the basis low. Increasing the degree of the basis to quintic leads to convergence difficulties.

The distance measures where the mean distance was below 0.2 m for all discretizations except the coarsest, which indicates that exploiting higher order NURBS basis functions allows for form-finding with very few elements, making the method attractive for form finding in the design stages. In such situations a coarse mesh can be used for design experiments and, then later can be refined to determine a form-found shape that is more optimal in terms of strain energy. Using the regular finite elements for design experiments would require a finer mesh, Fig. 7 shows that it is not until 32 by 32 finite elements are used that the mean distance falls below 0.2 m.

The use of NURBS based isogeometric elements simplifies verification studies, since it is straightforward to further discretize the form found shape into smaller elements and to evaluate the structure using IGA Kirchhoff–Love shells to check for a near membrane state of stress.

The use of membrane elements for form finding can lead to wrinkling of the surfaces when fine meshes are used due to compressive stresses and a lack of bending stiffness. Some of the benchmarking geometries used in the paper

show wrinkling for fine meshes of 64×64 elements or finer. This has not been further studied in the paper, since the problem is not specifically related to the use of isogeometric elements.

Mass matrix selection for dynamic relaxation with kinetic damping should be investigated further. In this study it was set through trial and error and selected in a way which allowed for the finest mesh to converge. For the coarser meshes smaller values in the mass matrix may result in fewer iterations for the procedure to converge. It is possible to use a critically damped structure as described here, but it is much more costly per iteration since it requires the evaluation of a tangent stiffness matrix, which in a sense loses the advantages of the explicit method, both in terms of efficiency and simplicity. A promising approach is to use kinetic damping and update the mass matrix after a stability criteria [30], or after every n iterations based on the tangent stiffness. It removed convergence difficulties seen in the bottom right subfigure of Fig. 5, where the mass matrix was updated every 100th iteration.

Further, the integration of CAE into CAD allows for continuous evaluation of the form found structures within a design context. It is possible to keep working with the geometry after the form finding and adding architectural details and to use the models for other types of studies, such as, daylight, energy, and evaluation within an architectural context, and to use the model for rendering/visualization. The integration also allows for the initial shapes to be much easier to model and modify in CAD than in most CAE software.

Acknowledgment

This work was supported by the Swedish strategic research programme eSENCE. The support is gratefully acknowledged.

References

- [1] K.-U. Bletzinger, R. Wüchner, F. Daoud, N. Camprubi, Computational methods for form finding and optimization of shells and membranes, *Comput. Methods Appl. Mech. Engrg.* 194 (30) (2005) 3438–3452.
- [2] A. Day, An introduction to dynamic relaxation (dynamic relaxation method for structural analysis, using computer to calculate internal forces following development from initially unloaded state), *Engineer* 219 (1965) 218–221.
- [3] H.-J. Schek, The force density method for form finding and computation of general networks, *Comput. Methods Appl. Mech. Engrg.* 3 (1) (1974) 115–134.
- [4] A. Kilian, J. Ochsendorf, Particle-spring systems for structural form finding, *J. Int. Assoc. Shell Spat. Struct.* 148 (2005) 77.
- [5] K.-U. Bletzinger, E. Ramm, A general finite element approach to the form finding of tensile structures by the updated reference strategy, *Int. J. Space Struct.* 14 (2) (1999) 131–145.
- [6] G.R. Joldes, A. Wittek, K. Miller, An adaptive dynamic relaxation method for solving nonlinear finite element problems. application to brain shift estimation, *Int. J. Numer. Methods Biomed. Eng.* 27 (2) (2011) 173–185.
- [7] E. Ramm, Shape finding of concrete shell roofs, *J. Int. Assoc. Shell Spat. Struct.* 45 (1) (2004) 29–39.
- [8] T.J. Hughes, J.A. Cottrell, Y. Bazilevs, Isogeometric analysis: CAD, finite elements, NURBS, exact geometry and mesh refinement, *Comput. Methods Appl. Mech. Engrg.* 194 (39) (2005) 4135–4195.
- [9] J. Kiendl, K.-U. Bletzinger, J. Linhard, R. Wüchner, Isogeometric shell analysis with Kirchhoff–Love elements, *Comput. Methods Appl. Mech. Engrg.* 198 (49) (2009) 3902–3914.
- [10] J. Kiendl, Y. Bazilevs, M.-C. Hsu, R. Wüchner, K.-U. Bletzinger, The bending strip method for isogeometric analysis of Kirchhoff–Love shell structures comprised of multiple patches, *Comput. Methods Appl. Mech. Engrg.* 199 (37) (2010) 2403–2416.
- [11] D. Benson, Y. Bazilevs, M.-C. Hsu, T. Hughes, A large deformation, rotation-free, isogeometric shell, *Comput. Methods Appl. Mech. Engrg.* 200 (13) (2011) 1367–1378.
- [12] J. Cottrell, A. Reali, Y. Bazilevs, T. Hughes, Isogeometric analysis of structural vibrations, *Comput. Methods Appl. Mech. Engrg.* 195 (41) (2006) 5257–5296.
- [13] J.A. Cottrell, T.J. Hughes, Y. Bazilevs, *Isogeometric Analysis: Toward Integration of CAD and FEA*, John Wiley & Sons, 2009.
- [14] C.H. Thai, H. Nguyen-Xuan, N. Nguyen-Thanh, T.-H. Le, T. Nguyen-Thoi, T. Rabczuk, Static, free vibration, and buckling analysis of laminated composite Reissner–Mindlin plates using NURBS-based isogeometric approach, *Internat. J. Numer. Methods Engrg.* 91 (6) (2012) 571–603.
- [15] F. Auricchio, L.B. Da Veiga, T. Hughes, A. Reali, G. Sangalli, Isogeometric collocation methods, *Mathe. Models Methods Appl. Sci.* 20 (11) (2010) 2075–2107.
- [16] A. Reali, H. Gomez, An isogeometric collocation approach for Bernoulli–Euler beams and Kirchhoff plates, *Comput. Methods Appl. Mech. Engrg.* 284 (2015) 623–636.
- [17] J. Kiendl, F. Auricchio, L.B. da Veiga, C. Lovadina, A. Reali, Isogeometric collocation methods for the Reissner–Mindlin plate problem, *Comput. Methods Appl. Mech. Engrg.* 284 (2015) 489–507.
- [18] L.B. da Veiga, C. Lovadina, A. Reali, Avoiding shear locking for the Timoshenko beam problem via isogeometric collocation methods, *Comput. Methods Appl. Mech. Engrg.* 241 (2012) 38–51.
- [19] N. Nguyen-Thanh, J. Kiendl, H. Nguyen-Xuan, R. Wüchner, K. Bletzinger, Y. Bazilevs, T. Rabczuk, Rotation free isogeometric thin shell analysis using pht-splines, *Comput. Methods Appl. Mech. Engrg.* 200 (47) (2011) 3410–3424.

- [20] N. Nguyen-Thanh, N. Valizadeh, M. Nguyen, H. Nguyen-Xuan, X. Zhuang, P. Areias, G. Zi, Y. Bazilevs, L. De Lorenzis, T. Rabczuk, An extended isogeometric thin shell analysis based on Kirchhoff–Love theory, *Comput. Methods Appl. Mech. Engrg.* 284 (2015) 265–291.
- [21] F. Cirak, M. Ortiz, P. Schroder, Subdivision surfaces: a new paradigm for thin-shell finite-element analysis, *Internat. J. Numer. Methods Engrg.* 47 (12) (2000) 2039–2072.
- [22] F. Cirak, M. Ortiz, Fully c_1 -conforming subdivision elements for finite deformation thin-shell analysis, *Internat. J. Numer. Methods Engrg.* 51 (7) (2001) 813–833.
- [23] F. Cirak, M.J. Scott, E.K. Antonsson, M. Ortiz, P. Schröder, Integrated modeling, finite-element analysis, and engineering design for thin-shell structures using subdivision, *Comput.-Aided Des.* 34 (2) (2002) 137–148.
- [24] F. Cirak, Q. Long, *Advances in Subdivision Finite Elements for Thin Shells*, Springer, 2010.
- [25] B. Philipp, M. Breitenberger, R. Wuchner, K.-U. Bletzinger, Design of architectural membranes with isogeometric elements, in: 11th World Congress on Computational Mechanics, WCCM XI, 2014.
- [26] L. Chen, N. Nguyen-Thanh, H. Nguyen-Xuan, T. Rabczuk, S.P.A. Bordas, G. Limbert, Explicit finite deformation analysis of isogeometric membranes, *Comput. Methods Appl. Mech. Engrg.* 277 (2014) 104–130.
- [27] M. Barnes, Form-finding and analysis of prestressed nets and membranes, *Comput. Struct.* 30 (3) (1988) 685–695.
- [28] M. Barnes, Form-finding and analysis of tension space structures by dynamic relaxation (Ph.D. thesis), City University, 1977.
- [29] M. Papadrakakis, A method for the automatic evaluation of the dynamic relaxation parameters, *Comput. Methods Appl. Mech. Engrg.* 25 (1) (1981) 35–48.
- [30] P. Underwood, Dynamic relaxation (in structural transient analysis), in: *Computational Methods for Transient Analysis* (A 84-29160 12-64), North-Holland, Amsterdam, 1983, pp. 245–265.
- [31] G.R. Joldes, A. Wittek, K. Miller, Real-time nonlinear finite element computations on GPU—application to neurosurgical simulation, *Comput. Methods Appl. Mech. Engrg.* 199 (49) (2010) 3305–3314.
- [32] L. Piegl, W. Tiller, *The NURBS Book*, in: *Monographs in Visual Communication*, 1997.
- [33] H.-J. Kim, Y.-D. Seo, S.-K. Youn, Isogeometric analysis for trimmed CAD surfaces, *Comput. Methods Appl. Mech. Engrg.* 198 (37) (2009) 2982–2995.
- [34] R. Schmidt, R. Wüchner, K.-U. Bletzinger, Isogeometric analysis of trimmed NURBS geometries, *Comput. Methods Appl. Mech. Engrg.* 241 (2012) 93–111.
- [35] Y. Bazilevs, V.M. Calo, J.A. Cottrell, J.A. Evans, T. Hughes, S. Lipton, M. Scott, T. Sederberg, Isogeometric analysis using t-splines, *Comput. Methods Appl. Mech. Engrg.* 199 (5) (2010) 229–263.
- [36] M.A. Scott, M.J. Borden, C.V. Verhoosel, T.W. Sederberg, T.J. Hughes, Isogeometric finite element data structures based on Bézier extraction of t-splines, *Internat. J. Numer. Methods Engrg.* 88 (2) (2011) 126–156.
- [37] M.R. Dörfel, B. Jüttler, B. Simeon, Adaptive isogeometric analysis by local h-refinement with t-splines, *Comput. Methods Appl. Mech. Engrg.* 199 (5) (2010) 264–275.
- [38] M. Breitenberger, A. Apostolatos, B. Philipp, R. Wüchner, K.-U. Bletzinger, Analysis in computer aided design: Nonlinear isogeometric b-rep analysis of shell structures, *Comput. Methods Appl. Mech. Engrg.* 284 (2015) 401–457.
- [39] M. Bischoff, K.-U. Bletzinger, W. Wall, E. Ramm, Models and finite elements for thin-walled structures, *Encyclopedia Comput. Mech.* (2004).
- [40] K.-J. Bathe, *Finite Element Procedures*, Klaus-Jurgen Bathe, 2006.
- [41] T. Takacs, B. Jüttler, Existence of stiffness matrix integrals for singularly parameterized domains in isogeometric analysis, *Comput. Methods Appl. Mech. Engrg.* 200 (49) (2011) 3568–3582.
- [42] N. Aspert, D. Santa Cruz, T. Ebrahimi, Mesh: measuring errors between surfaces using the Hausdorff distance, in: *ICME*, vol. 1, 2002, pp. 705–708.
- [43] T. Takacs, B. Jüttler, H_2 regularity properties of singular parameterizations in isogeometric analysis, *Graph. Models* 74 (6) (2012) 361–372.
- [44] B. Tabarrok, Z. Qin, Nonlinear analysis of tension structures, *Comput. Struct.* 45 (5) (1992) 973–984.

Paper C





*Proceedings of the International Association for Shell and Spatial Structures (IASS)
Symposium 2015, Amsterdam
Future Visions
17 - 20 August 2015, Amsterdam, The Netherlands*

Using isogeometric elements and dynamic relaxation as a form finding technique

Vedad ALIC*, Kent PERSSON^a

*Division of Structural Mechanics
Faculty of Engineering, Lund University
P.O. Box 118, SE-221 00 Lund, Sweden
vedad.acli@construction.lth.se

^aDivision of Structural Mechanics, Lund University

Abstract

In this paper, the use of NURBS based isogeometric analysis for form finding and further design of form found structures is presented. The form finding is performed with non-linear isogeometric membrane elements together with dynamic relaxation [1]. The method has previously been tested on simple geometries in a computational environment, and is here further integrated in a Computer Aided Design program, Rhinoceros 3D where the method is evaluated for complex geometries in a design scenario. The form found shape is further studied and it is shown how the membrane and bending utilization can be plotted on the shape by making refinements to the mesh without affecting the geometry. Finally the form finding is employed on some complex geometries to show the possibilities of using coarse NURBS meshes for form finding.

Keywords: Form finding, isogeometric analysis, dynamic relaxation, design tool, NURBS, CAD.

1. Introduction

The load carrying capacity of shells and other form-active structures is provided by the shape of the structures. In order to find an efficient form of such structures several methods exist such as, dynamic relaxation [2], the force density method [11], or more recent ones such as thrust network analysis [4] and particle spring systems [7]. One drawback of many existing methods is that it is necessary to discretize the initial geometry into structural elements in order to perform the form finding. During design stages this is sometimes unfavourable, because after the discretization it is difficult to convert back to the initial geometry type, and the design process may require many iterations of form finding and evaluation (going between different geometry types) before a desired shape is generated. By employing isogeometric analysis using Non-Uniform Rational B-Splines (NURBS) the conversion between geometry types can be avoided and an integration of design and analysis can be achieved, where all computations are performed using the design geometry, or at the very least an analysis

model which is automatically created from the design geometry. A further advantage of form finding with isogeometric membrane elements is that no re-meshing is required for the structural analysis as the form found geometry can simply be reused with a shell element formulation for the subsequent analyses.

The paper describes a design process where isogeometric membrane elements with dynamic relaxation is used as a form finding method for shapes with minimal bending. Some advantages and drawbacks of the method are discussed. To test the integration of design and analysis the method is implemented in a Rhinoceros 5 plug-in.

2. Form finding with dynamic relaxation

A form finding process with isogeometric membrane elements has been implemented. It has been previously shown that the form finding can be performed with few elements [1], and makes the method suitable for design exploration. However, for the form finding to result in a good shape in terms of mechanical performance a discretization with smaller elements needs to be used. To find the static equilibrium of the membrane elements and the applied load dynamic relaxation is used [5]. The dynamic relaxation method solves static problems by simulating a dynamic problem with fictitious masses and fictitious damping. An advantage of the dynamic relaxation method is that it is an explicit method where only the internal forces need to be computed, there is no need to calculate the stiffness matrix, thus it is a vectorised method which is efficient and well suited for parallelization. For more information on the dynamic relaxation implementation with isogeometric membrane elements see [1], where different choices of mass matrix and damping were tried out in order to find appropriate choices.

3. NURBS based Isogeometric Analysis

To explain the advantages of NURBS based form finding and analysis of shell structures a brief introduction to NURBS and isogeometric analysis is given. NURBS are used by many practicing designers, for instance in the software Rhinoceros 5 [9]. The mathematical properties of NURBS surfaces make them suitable for representing curved geometries such as shells and membranes with very few control points.

NURBS are a generalization of B-splines, non-interpolating, piecewise polynomial curves, with the ability to represent any conical shapes such as circles exactly. A B-spline curve $C(\xi)$ is defined by its polynomial degree p , a knot vector $\Xi = \{\xi_1, \xi_2 \dots \xi_{n+p+1}\}$, and a set of n control points $\mathbf{B}_i = (x_i, y_i, z_i)$. The knot vector contains non decreasing values and divides the parametric space into intervals known as knot spans, the first and last values in the knot vector are repeated $p + 1$ times. If an internal knot is repeated r times it is said to have a multiplicity of r , and the continuity of the basis functions at a repeated knot is C^{p-r} . Each control point has an associated basis function which is non-zero in $p + 1$ knot spans, which is known as local support. The local support of the NURBS basis, where a change at some part of the geometry only has a local effect, makes them highly intuitive and predictable. The curve is computed by a summation of the basis functions multiplied by the control points

$$C(\xi) = \sum_{i=1}^n N_{i,p}(\xi) \mathbf{B}_i \quad (1)$$

where the i :th basis function $N_{i,p}$ is constructed recursively, for the formulas see *Piegl et al.* [10]. The basis functions are only interpolatory at the ends of the knot vector, and at knots with multiplicity $r = p$, leading to C^0 continuity. The number of knots does not coincide with the number of control points or basis functions.

A B-spline surface is defined using the tensor product approach, where another set of basis functions $M_{j,q}(\eta)$ of degree q , with the knot vector $H = \{\eta_1, \eta_2, \dots, \eta_{m+q+1}\}$, with m control points in the second direction and the control point net $\mathbf{B}_{i,j}$ is used

$$S(\xi, \eta) = \sum_{i=1}^n \sum_{j=1}^m N_{i,p}(\xi) M_{j,q}(\eta) \mathbf{B}_{i,j}. \quad (2)$$

To extend the B-spline surface to a NURBS surface each control point is extended with a weight, $\mathbf{B}_{i,j} = (x_{i,j}, y_{i,j}, z_{i,j}, w_{i,j})$ and we get the NURBS surface

$$S(\xi, \eta) = \frac{\sum_{i=1}^n \sum_{j=1}^m N_{i,p}(\xi) M_{j,q}(\eta) w_{i,j} \mathbf{B}_{i,j}}{\sum_{k=1}^n \sum_{l=1}^m N_{k,p}(\xi) M_{l,q}(\eta) w_{k,l}}. \quad (3)$$

Geometrically this can be explained that a NURBS surface in R^3 is a projection of B-Spline surface in R^4 . If all weights are equal the NURBS surface is reduced to a B-Spline surface. In NURBS based isogeometric analysis (IGA) the basis functions chosen to represent the geometry are also used to approximate the unknown solution fields, for instance, the unknown displacements. For more information on IGA see the extensive report by *Hughes et al.* [5] on NURBS based IGA.

An attractive property of B-Splines for design and analysis is that the represented geometry is invariant during refinements and is represented exactly irrespective of the mesh being coarse or refined. There are three types of refinements possible for B-Splines/NURBS based IGA. The first is the same as for finite elements, namely making the elements smaller (h-refinement), which is done by performing so called knot insertion, whereby new knot values are inserted into the knot vector without affecting the geometry. The elements in NURBS based IGA are defined by the knot spans, and thus by introducing new knots one also introduces new elements. As for finite elements it is possible to increase the degree the basis functions (p-refinement). A new type of refinement is possible with B-splines/NURBS where if the degree is first raised and then the elements made smaller (k-refinement) it is possible to get basis functions with continuous derivatives across element borders. The refinement possibilities make NURBS suitable for form finding where a coarse mesh can be used initially to explore shapes in near real time and a finer one can be used afterward to get a better approximation.

The tensor product nature of NURBS surfaces, seen in Eq. (3), constrains standard isogeometric analysis with NURBS to 4-sided surfaces. Possible ways of getting around this is by use of T-Splines [3], or trimmed NURBS [8], but is out of the scope of this paper.

A NURBS based isogeometric Kirchhoff-Love shell element was first presented by *Kiendl et al.* [6]. It is used in this paper, and the membrane elements in the paper are formulated by neglecting the bending stiffness of the shell elements. A small deformations version of the shell element is used after the form finding in a static analysis to compute displacements, stresses and strain energies.

4. Design process

The ability to perform form finding with very few elements is favourable in design situations as it allows the designer to quickly explore alternative shapes. Figure 1 illustrates some of the advantages of a design process with isogeometric elements. It is split into three parts, an exploration of different form found shapes, followed by a final accurate form finding, and after that a verification part with further studies.

In the form finding exploration the first step is to define an initial shape, boundary conditions, material parameters and applied loads (typically the self-weight). Once this is done the form found shape is computed with a coarse mesh. An evaluation of the shape follows, where the shape is evaluated in terms of architectural and engineering criteria, such as structural performance, daylight, acoustics, limitations on the shape (height, span), and so on. To fulfil the criteria it is often necessary to change initial parameters such as the initial geometry, boundary conditions, loads before the form finding process is iterated. Using a coarse mesh allows for quick exploration of different shapes which geometrically are often similar to the same shapes that have been form found with a finer discretization [1]. Figure 1 a) shows a few design explorations of a simple geometry with a uniformly distributed load. Variations of the boundary conditions and geometry generates different shapes, all approximated with a coarse mesh.

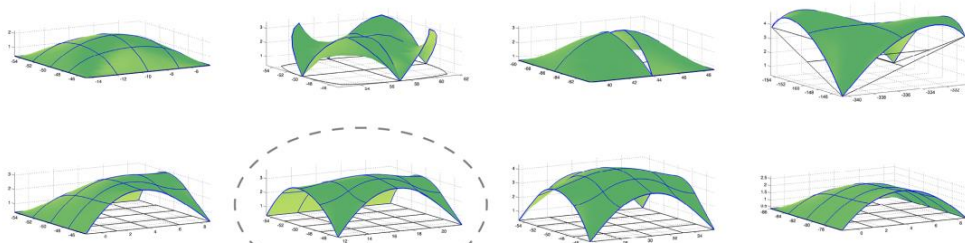
Once the form found shape fulfils necessary design and engineering criteria, it can be further refined and ran through the form finding process once again, in order to obtain a more optimal shape. As shown in Figure 1 b) there is visually very little difference between the coarse and fine meshes used for the form finding, however, the difference can be large in terms of mechanical performance. This second form finding can be done using the same initial geometry, or from the results of the form finding with the coarse mesh can be used as the initial shape for the finer mesh in order to save computation time.

The form finding procedure reduces the bending part of the strain energy in the structure for the applied load. How well the bending strain energy is reduced depends on the discretization, i.e. how small the elements are and the degree of their basis functions. To compute the bending strain energy after the form finding it is necessary to first perform a further discretization to smaller elements, this is a straightforward procedure with NURBS based IGA since the geometry is always exactly represented. Doing the same refinement with finite elements which only approximate a geometry and often make use of flat elements would be very difficult and time consuming. Figure 1 c) shows the displacements (left) and percentage bending strain energy (right) in the chosen structure. A form finding with an even finer mesh would further reduce the bending strain energy.

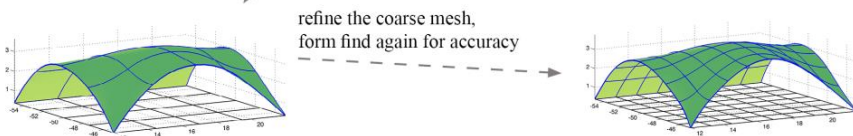
A near optimal shape shows very little bending strain energy in a plot like the one shown in Figure 1 c). A shape that is modified from its optimal form may show high bending strain energy in the plot, this also provides information about the amount of material that is needed at different parts in the structure.

Implementing the form finding process with isogeometric elements in a Computer Aided Design software (CAD) can help with this design process and has several other benefits listed in the next section.

a) design exploration stage



b) refined form finding



c) verification

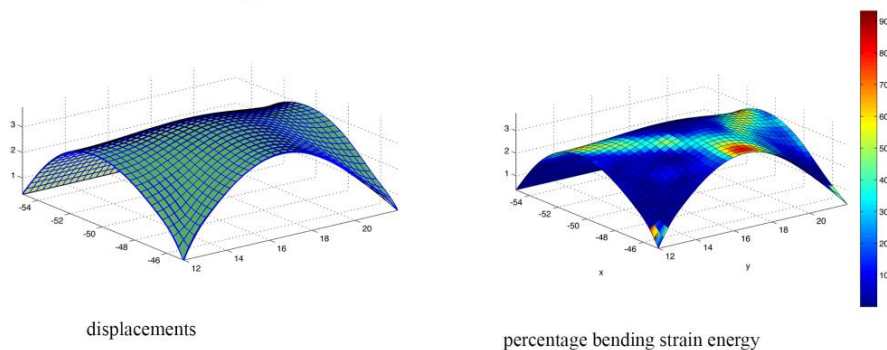


Figure 1: Design process with a) a form finding exploration step, b) a final form finding with a finer mesh, and c) further studies on a linear elastic model with a refined mesh after the form finding has been performed. The NURBS based geometry makes it straightforward to make further refinements without changing the geometry as necessary.

5. Integration of design and analysis, and modelling aspects

A Rhinoceros 3D V.5 [9] plugin by the authors and an ongoing master's thesis project is in development to integrate isogeometric form finding in a design software. The tool is currently at the very early stages. The interface consists of a tabbed docking panel where initial geometries, materials, and boundary conditions can be set up, and where the form finding can be performed.

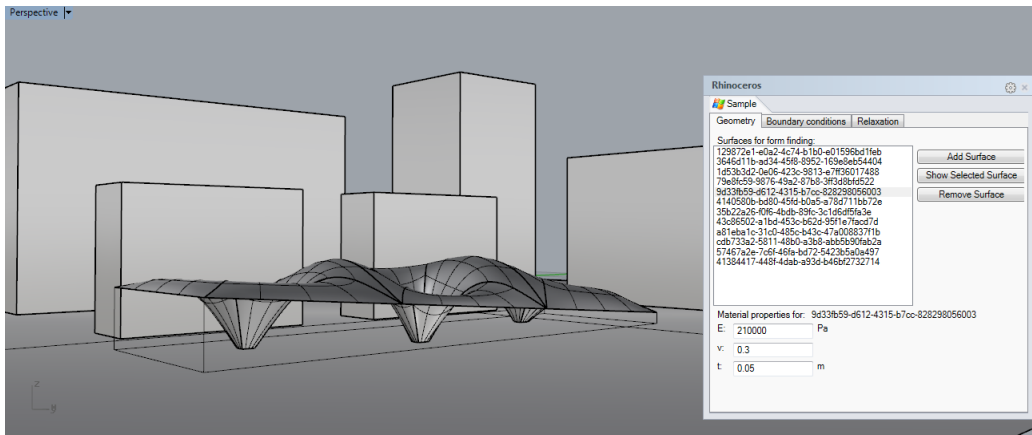


Figure 2: Displaying the user interface for the form finding tool in Rhinoceros 5.

The form finding can be performed with multiple patches which are connected. The limitations at the moment are that the edges of bordering patches have to have compatible discretizations, meaning that they need to have identical curves on the edges which border each other. In this way each patch is treated as a “super” element. By modelling the coarsest possible geometry the refinements to smaller elements can be handled by the plugin. The limitations must be kept in mind while modelling the initial geometry, if for instance modelling a hole it must be modelled following “patch” modelling techniques. Implementing T-Splines or trimmed NURBS for the form finding could simplify the creation of suitable models for the form finding. Using a CAD environment simplifies the modelling of the initial geometry compared finite element software. The form finding process typically requires several iterations to fulfil both architectural design and engineering criteria's, this requires modifications to the initial geometry and is simple to do in a CAD software, where unlike FE-software an iterative workflow is important.

Integrating the process into Rhinoceros simplifies several parts which are often included in the design process. The form finding can be performed within the architectural context, and thus simplifies considerations related to the surrounding buildings, such as shading and reflections, etc. Having the form found shapes in the design software and having them be the complete curved geometry description can make it easy to do architectural renderings to present to clients, further detailing can be performed after the form finding since the geometry is still NURBS. Another advantage of CAD tools is that they often include geometry diagnostics tools, such as curvature and edge analysis.

6. Design examples

In this section some examples are included to show the method applied to more complex geometries. Figure 3 shows the form finding of connected circular shapes, with the introduction of some openings. Figure 4 shows a free form shape with holes. The geometry consist of 9 patches where all the connecting boundaries are matching.

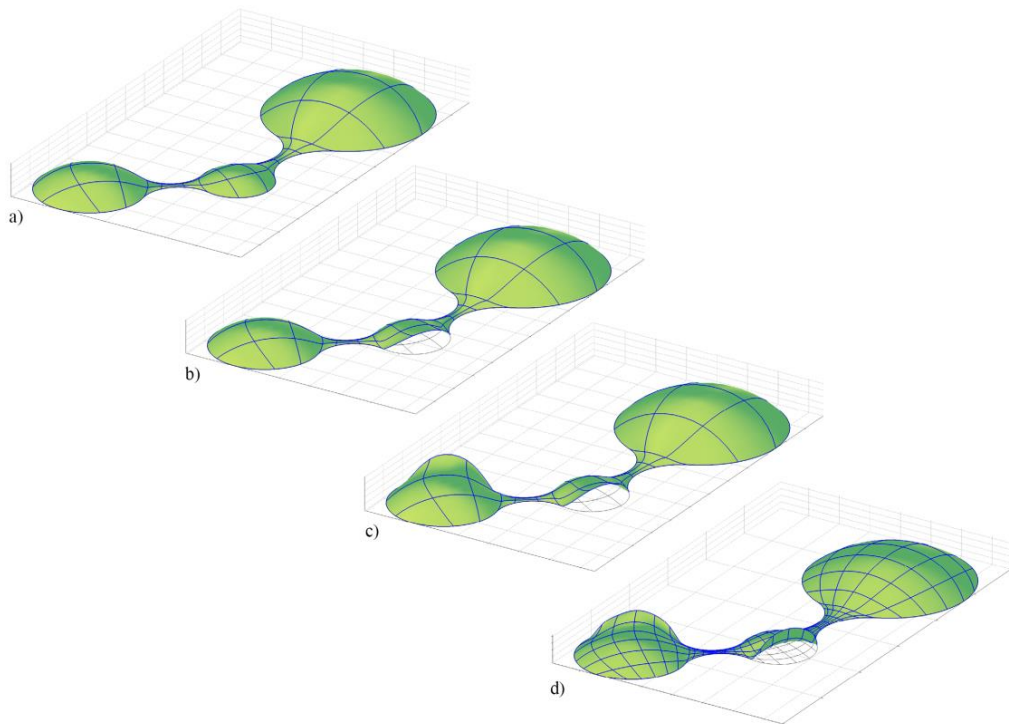


Figure 3: Connected circular forms with openings.

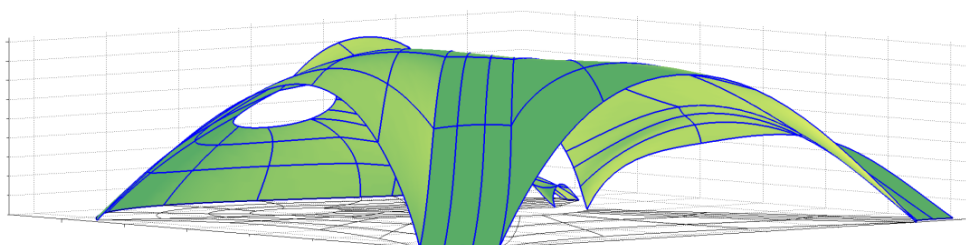


Figure 4: Free form shape with holes

7. Conclusions

The use of isogeometric membrane elements for form finding of structures with minimal bending has been presented. The form finding can be performed with few elements, and as such can be used in an interactive fashion. An advantage over other methods is that it is straightforward to do further discretisation after the form finding in order to perform other studies. A plugin for Rhinoceros 3D which is in the very early stages has been described. The tool allows for form finding within context and simplifies modelling of the initial geometries, however, using standard NURBS based IGA sets limitations on how to model the geometry in CAD software. Further work could include implementation of IGA with trimmed NURBS, or T-Splines.

References

- [1] Alic V and Persson K., Isogeometric elements in the dynamic relaxation method. *Proceedings of 27th Nordic Seminar on Computational Mechanics* 2014, 256-259.
- [2] Barnes M. R., Form finding and analysis of tension structures by dynamic relaxation. *International journal of space structures*, 1999, 14(2), 89-104.
- [3] Bazilevs Y., Calo V. M., Cottrell J. A., Evans J. A., Hughes T. J. R., Lipton S., ... and Sederberg T. W., Isogeometric analysis using T-splines. *Computer Methods in Applied Mechanics and Engineering*, 2010, 199(5), 229-263.
- [4] Block P., and Ochsendorf J. Thrust network analysis: A new methodology for three-dimensional equilibrium. *JOURNAL-INTERNATIONAL ASSOCIATION FOR SHELL AND SPATIAL STRUCTURES*, 2007, 155, 167.
- [5] Hughes T. J., Cottrell J. and Bazilevs Y., Isogeometric analysis: Cad, finite elements, nurbs, exact geometry and mesh refinement. *Computer methods in applied mechanics and engineering* 194 (39) 2005, 4135–4195.
- [6] Kiendl J., Bletzinger K. U., Linhard J. and Wüchner R., Isogeometric shell analysis with Kirchhoff–Love elements. *Computer Methods in Applied Mechanics and Engineering*, 2009, 198(49), 3902-3914.
- [7] Kilian A., and Ochsendorf J. Particle-spring systems for structural form finding. *Journal-International Association for Shell and Spatial Structures*, 2005, 148, 77.
- [8] Kim H. J., Seo Y. D., and Youn, S. K., Isogeometric analysis for trimmed CAD surfaces. *Computer Methods in Applied Mechanics and Engineering*, 2009, 198(37), 2982-2995.
- [9] McNeel R., Rhinoceros 3D. <http://www.rhino3d.com/> Retrieved 2009, Jan, 15.
- [10] Piegl L. A., and Tiller W., *The NURBS book* (Monographs in visual communication), 1996.
- [11] Schek H. J., The force density method for form finding and computation of general networks. *Computer methods in applied mechanics and engineering*, 1974, 3(1), 115-134.